

Supporting Information

Stereoisomeric Homo- and Hetero-Binuclear Iridium(III) Complexes with 3-Oxidopicolinate Bridging Ligand and Their Application in OLEDs

Kochan Sathyaseelan Bejoymohandas,^[a] Andrea Baschieri,^[a] Francesco Reginato,^[b] Stefano Toffanin,^[b] Mario Prosa,^{*[b]} Elisa Bandini,^[a] Andrea Mazzanti,^[c] and Filippo Monti ^{*[a]}

[a] Institute for Organic Synthesis and Photoreactivity (ISOF), National Research Council of Italy (CNR), Via Piero Gobetti 101, I-40129 Bologna (Italy)

[b] Institute of Nanostructured Materials (ISMN), National Research Council of Italy (CNR), Via Piero Gobetti 101, I-40129 Bologna (Italy)

[c] Department of Industrial Chemistry "Toso Montanari", University of Bologna, Via Piero Gobetti 85, I-40129 Bologna (Italy)

Table of contents

Content	Page
Survey of binuclear iridium(III) complexes already reported in literature	S2 – S6
Experimental procedures	S6 – S13
NMR spectra of all the investigated complexes	S13 – S48
Correlation between experimental NMR data and DFT-computed ones	S49 – S50
NOE experiments on complexes BY1 and BY2	S51 – S58
Electrochemical data	S59
TD-DFT triplet excitations for all complexes in NTO basis	S60 – S70
Relaxed triplet geometries of the binuclear complexes	S71
Emission spectra in PMMA matrix	S72
OLED data (CIE coordinates and external quantum efficiencies)	S72 – S73
References	S73 – S74

Table S1. Binuclear iridium(III) complexes reported in literature, classified based on the presence of identical or different cyclometalating ligands on the two iridium centres (*i.e.*, homo- or hetero-binuclear complexes, column 3) and the properties of the bridging ligand. The photophysical properties of the complexes are also reported.

Entry	Publication year	Homo or hetero binuclear	Bridge structural properties			Photophysical properties			Literature references
			Short or long	Type	π conjugation	Emission maximum	Photoluminescence quantum yield	Lifetime (ns)	DOI
1	1988	Homo	Short	Symm.	NO	525		1130	10.1021/ac980234p
2	2001	Homo	Long	Asymm.	YES	646	0.006	65	10.1021/ic000212x
3	2001	Homo	Long	Symm.	YES	631	0.007	69	10.1021/ic000212x
4	2003	Homo	Long	Symm.	YES	608	0.094	390	10.1039/ b300704a
5	2003	Homo	Long	Symm.	YES	606	0.175	411	10.1039/ b300704a
6	2004	Homo	Short	Symm.	YES	665	0.04	2000	10.1039/ b404101c
7	2005	Homo	Long	Symm.	YES	578	0.006	2774	10.1039/b508063k
8	2005	Homo	Long	Symm.	YES	546	0.117	15000	10.1039/b508063k
9	2006	Homo	Short	Symm.	YES	620	0.003	6	10.1021/ic061009q
10	2006	Homo	Long	Symm.	YES	600			10.1021/ic061009q
11	2006	Homo	Long	Symm.	YES	600			10.1021/ic061009q
12	2007	Homo	Short	Symm.	YES	654	0.006	49	10.1021/ic700494e
13	2007	Homo	Short	Symm.	YES	654	0.005	44	10.1021/ic700494e
14	2007	Homo	Short	Symm.	YES	654	0.006	47	10.1021/ic700494e
15	2008	Homo	Long	Symm.	YES	632	0.27	140	10.1021/ic701788d
16	2008	Homo	Long	Symm.	YES	633	0.27	144	10.1021/ic701788d
17	2009	Hetero	Long	Asymm.	YES	607	0.3	3200	10.1039/b821161b
18	2010	Homo	Long	Symm.	NO	588	0.009	400	10.1002/chem.201000600
19	2010	Homo	Long	Symm.	NO	521	0.007	1200	10.1002/chem.201000600
20	2010	Homo	Short	Symm.	YES	615	0.03	22	10.1002/ejic.201000275
21	2011	Homo	Short	Asymm.	YES	582	0.025		10.1039/c1cc11254f
22	2011	Homo	Long	Symm.	YES	594	0.091	400	10.1039/c1cc13733f
23	2011	Homo	Long	Symm.	YES	557	0.15	1200	10.1039/c1cc13733f
24	2011	Homo	Short	Symm.	YES	538	0.17	90	10.1021/ic200704s
25	2011	Homo	Short	Symm.	YES	477	0.05	150	10.1021/ic200704s
26	2012	Homo	Short	Symm.	YES	541	0.58	4000	10.1002/anie.201105212
27	2012	Homo	Short	Symm.	YES	647	0.14	620	10.1039/c2dt30836c
28	2012	Homo	Short	Symm.	YES	541	0.24	720	10.1039/c2dt30836c
29	2013	Homo	Long	Symm.	YES	606	0.13	630	10.1002/chem.201202827
30	2013	Homo	Short	Symm.	YES	600			10.1039/c3sc52301b
31	2013	Homo	Short	Symm.	YES	715			10.1021/ic400478d

32	2014	Homo	Short	Symm.	YES	568	0.11	290	10.1021/cs500296s
33	2014	Homo	Short	Symm.	YES	500	0.38	1280	10.1021/cs500296s
34	2014	Homo	Short	Symm.	YES	521	0.71	1450	10.1002/anie.201407475
35	2014	Homo	Short	Symm.	YES	523	0.88	1440	10.1002/anie.201407475
36	2014	Homo	Short	Symm.	YES	644	0.37	47	10.1039/c4cc01799d
37	2014	Homo	Long	Symm.	YES	692	0.26	38	10.1039/c4cc01799d
38	2014	Homo	Short	Symm.	YES	622	0.65	760	10.1039/c4cc01808
39	2014	Homo	Short	Symm.	YES	625	0.65	730	10.1039/c4cc01808
40	2014	Homo	Long	Symm.	YES	486			10.1016/j.orgel.2014.08.014
41	2015	Homo	Short	Symm.	YES	591	0.0018	72	10.1016/j.biomaterials.2015.06.014
42	2015	Homo	Short	Symm.	YES	591	0.0032	117	10.1016/j.biomaterials.2015.06.014
43	2015	Homo	Short	Symm.	YES	513	0.0057	151	10.1016/j.biomaterials.2015.06.014
44	2015	Homo	Short	Symm.	YES	529	0.015	124	10.1016/j.biomaterials.2015.06.014
45	2015	Homo	Short	Symm.	YES	612	0.31	180	10.1039/c5cc04850h
46	2015	Homo	Long	Symm.	YES	627	0.24	170	10.1039/c5cc04850h
47	2015	Homo	Long	Symm.	YES	582	0.336	521	10.1039/c5tb00251f
48	2015	Homo	Long	Symm.	YES	579	0.187	531	10.1039/c5tb00251f
49	2015	Homo	Long	Symm.	YES	580	0.234	607	10.1039/c5tb00251f
50	2015	Homo	Long	Symm.	YES	581	0.217	380	10.1039/c5tb00251f
51	2015	Homo	Long	Symm.	YES	580	0.194	579	10.1039/c5tb00251f
52	2015	Homo	Long	Symm.	YES	579	0.185	642	10.1039/c5tb00251f
53	2015	Homo	Long	Symm.	YES	581	0.098	533	10.1039/c5tb00251f
54	2015	Homo	Long	Symm.	YES	542	0.09	10000	10.1016/j.poly.2015.04.011
55	2016	Homo	Short	Symm.	YES	603	0.36	200	10.1021/acsami.6b12446
56	2016	Homo	Short	Symm.	YES	603	0.43	190	10.1021/acsami.6b12446
57	2016	Homo	Short	Symm.	YES	580	0.68	480	10.1021/acsami.6b12446
58	2016	Homo	Short	Symm.	YES	580	0.68	410	10.1021/acsami.6b12446
59	2016	Homo	Short	Symm.	YES	552	0.94	440	10.1039/c6dt00881j
60	2016	Homo	Short	Symm.	YES	544	1	550	10.1039/c6dt00881j
61	2016	Homo	Short	Symm.	YES	526	1	590	10.1039/c6dt00881j
62	2016	Homo	Short	Symm.	YES	517	0.88	590	10.1039/c6dt00881j
63	2016	Homo	Short	Symm.	YES	568	0.88	570	10.1039/c6dt00881j
64	2016	Homo	Short	Symm.	YES	570	0.91	590	10.1039/c6dt00881j
65	2016	Homo	Short	Symm.	YES	528	1	360	10.1039/c6dt00881j
66	2016	Homo	Short	Symm.	YES	572	0.94	4000	10.1039/c6dt00881j
67	2016	Homo	Short	Symm.	YES	606	0.61	180	10.1021/acs.inorgchem.5b02625
68	2016	Homo	Short	Symm.	YES	607	0.49	180	10.1021/acs.inorgchem.5b02625
69	2016	Homo	Short	Symm.	YES	436			10.1021/acs.inorgchem.6b00527
70	2016	Homo	Short	Symm.	YES	492		69	10.1021/acs.inorgchem.6b00527
71	2016	Homo	Short	Symm.	YES	626	0.88	1070	10.1364/OE.24.015757
72	2016	Homo	Short	Symm.	NO	575	0.18	4830	10.1038/srep22458
73	2016	Homo	Short	Symm.	NO	490	0.07	4590	10.1038/srep22458
74	2016	Homo	Long	Symm.	YES	465			10.1016/j.tet.2016.09.012

75	2016	Homo	Long	Symm.	NO	468			10.1016/j.tet.2016.11.008
76	2016	Homo	Long	Symm.	NO	468			10.1016/j.tet.2016.11.009
77	2017	Homo	Short	Symm.	YES	587	0.2	970	10.1039/c7cc00769h
78	2017	Homo	Short	Symm.	YES	609	0.24	670	10.1039/c7tc04066k
79	2017	Homo	Short	Symm.	NO	604	0.021	26	10.1016/j.jlumin.2016.09.033
80	2017	Homo	Short	Symm.	NO	595	0.024	2820	10.1016/j.jlumin.2016.09.033
81	2017	Homo	Short	Symm.	YES	565			10.1039/c6nj02890j
82	2017	Homo	Short	Symm.	YES	570			10.1039/c6nj02890j
83	2017	Homo	Long	Symm.	YES	575		254	10.1039/c7nj01423f
84	2017	Homo	Short	Symm.	YES	489	0.0023	34	10.1021/acs.organomet.6b00887
85	2017	Homo	Short	Symm.	YES	493	0.0023	51	10.1021/acs.organomet.6b00887
86	2017	Homo	Short	Symm.	YES	514	0.0003	1	10.1021/acs.organomet.6b00887
87	2017	Homo	Short	Symm.	YES	513	0.0003	1	10.1021/acs.organomet.6b00887
88	2017	Homo	Short	Symm.	NO	455	0.009	767	10.1016/j.poly.2017.05.017
89	2017	Homo	Short	Symm.	NO	568	0.99		10.1134/S1070363217060147
90	2017	Homo	Short	Symm.	NO	521	0.98		10.1134/S1070363217060147
91	2017	Homo	Short	Symm.	NO	598	0.021		10.1134/S1070363217060147
92	2017	Homo	Long	Symm.	YES	587	0.95		10.1134/S1070363217060159
93	2017	Homo	Long	Symm.	YES	523	0.96		10.1134/S1070363217060159
94	2017	Hetero	Long	Symm.	YES	527	0.79		10.1134/S1070363217060159
95	2017	Hetero	Long	Symm.	YES	561	0.76		10.1134/S1070363217060159
96	2017	Homo	Long	Asymm.	NO	571	0.062	250	10.1016/j.snb.2016.12.147
97	2018	Homo	Long	Symm.	YES	699	0.007	1410	10.1016/j.dyepig.2017.09.061
98	2018	Homo	Long	Symm.	YES	700	0.0122	1420	10.1016/j.dyepig.2017.09.061
99	2018	Homo	Long	Symm.	YES	583	0.024	3570	10.1021/acs.inorgchem.8b00789
100	2018	Homo	Long	Symm.	YES	576	0.003	1990	10.1021/acs.inorgchem.8b00789
101	2018	Homo	Long	Symm.	YES	608	0.025	1470	10.1021/acs.inorgchem.8b00789
102	2018	Homo	Long	Symm.	YES	578	0.22	53300	10.1021/acs.inorgchem.8b00789
103	2018	Homo	Long	Symm.	YES	619	0.045	1920	10.1021/acs.inorgchem.8b00789
104	2018	Homo	Short	Symm.	YES	530	0.092	1740	10.1016/j.jorganchem.2018.09.022
105	2018	Homo	Short	Symm.	YES	608	0.065	1300	10.1016/j.jorganchem.2018.09.022
106	2018	Homo	Long	Symm.	NO	440	0.38		10.1016/j.tet.2017.12.018
107	2018	Homo	Long	Symm.	NO	483	0.19		10.1016/j.tet.2017.12.018
108	2018	Homo	Short	Symm.	YES	576	0.62	1890	10.1039/c8ra00265g
109	2019	Homo	Short	Symm.	NO	479	0.97	5412	10.1149/2.0161906jss
110	2019	Homo	Short	Symm.	YES	598	0.33		10.1149/2.0161906jss
111	2019	Homo	Long	Symm.	YES	536	0.62	2890	10.1002/ejic.201801367
112	2019	Hetero	Long	Symm.	YES	593	0.16	2010	10.1002/ejic.201801367
113	2019	Homo	Long	Symm.	YES	600	0.27	1670	10.1002/ejic.201801367
114	2019	Homo	Short	Symm.	YES	722	0.15	1270	10.1016/j.jlumin.2019.02.045
115	2019	Homo	Short	Symm.	NO	534	0.57	730	10.1039/c9tc04556b
116	2019	Homo	Short	Asymm.	NO	534	0.5	830	10.1039/c9tc04556b
117	2019	Homo	Short	Asymm.	NO	585	0.31	210	10.1039/c9tc04556b

118	2019	Homo	Short	Symm.	YES	575	0.95	440	10.1021/acs.jpcclett.9b03002
119	2019	Homo	Short	Symm.	NO	585	0.01	190	10.1007/s11243-019-00368-6
120	2019	Homo	Short	Symm.	NO	583	0.02	110	10.1007/s11243-019-00368-6
121	2019	Homo	Short	Symm.	NO	578	0.01	360	10.1007/s11243-019-00368-6
122	2019	Homo	Short	Symm.	NO	579	0.01	320	10.1007/s11243-019-00368-6
123	2019	Homo	Short	Symm.	NO	580	0.01	370	10.1007/s11243-019-00368-6
124	2019	Homo	Short	Symm.	NO	581	0.01	350	10.1007/s11243-019-00368-6
125	2020	Homo	Long	Symm.	YES	530			10.1021/acsabm.0c00784
126	2020	Homo	Short	Symm.	YES	599	0.45	220	10.1016/j.cej.2019.123505
127	2020	Homo	Short	Symm.	YES	601	0.35	170	10.1016/j.cej.2019.123505
128	2020	Homo	Short	Symm.	YES	613	0.3	130	10.1016/j.cej.2019.123505
129	2020	Homo	Short	Symm.	YES	617	0.28	130	10.1016/j.cej.2019.123505
130	2020	Homo	Short	Symm.	YES	654	0.64	220	10.1016/j.cej.2019.123505
131	2020	Homo	Short	Symm.	YES	651	0.78	240	10.1016/j.cej.2019.123505
132	2020	Homo	Short	Asymm.	YES				10.1002/chem.202002351
133	2020	Homo	Short	Symm.	YES	564	0.1	2100	10.1039/d0dt01964j
134	2020	Homo	Short	Symm.	YES	574	0.16	4010	10.1039/d0dt01964j
135	2020	Homo	Short	Symm.	YES	569	0.17	6700	10.1039/d0dt01964j
136	2020	Homo	Short	Symm.	YES	698			10.1016/j.dyepig.2019.107855
137	2020	Homo	Short	Symm.	YES	643			10.1016/j.dyepig.2019.107855
138	2020	Homo	Short	Symm.	YES	709	0.01	13	10.1016/j.jlumin.2019.116847
139	2020	Homo	Short	Symm.	YES	710	0.009	22	10.1016/j.jlumin.2019.116847
140	2020	Homo	Short	Symm.	YES	707	0.009	19	10.1016/j.jlumin.2019.116847
141	2020	Homo	Short	Symm.	YES	714	0.035	2900	10.1021/acs.jpcclett.0c01276
142	2021	Homo	Short	Symm.	NO	541	0.035		10.1039/d1dt03579g
143	2021	Homo	Short	Symm.	NO	538	0.044		10.1039/d1dt03579g
144	2021	Homo	Short	Symm.	NO	548	0.024		10.1039/d1dt03579g
145	2021	Homo	Short	Symm.	NO				10.1039/d1dt03579g
146	2021	Homo	Long	Symm.	YES	590	0.003	1420	10.1039/d1dt02176a
147	2021	Homo	Short	Symm.	YES	600	0.003	2490	10.1039/d1dt02176a
148	2021	Homo	Short	Symm.	YES	642	0.8	1310	10.1021/acs.inorgchem.0c03251
149	2021	Homo	Short	Symm.	YES	595	0.53	1230	10.1016/j.inoche.2021.108667
150	2021	Homo	Short	Symm.	YES	575	0.59	1420	10.1016/j.inoche.2021.108667
151	2021	Homo	Long	Symm.	YES	712	0.002	5	10.1016/j.jorganchem.2020.121628
152	2021	Homo	Short	Symm.	YES	635	0.12	1510	10.1021/acs.jpcc.1c05037
153	2021	Homo	Short	Symm.	YES	632	0.15	3120	10.1021/acs.jpcc.1c05037
154	2022	Homo	Short	Symm.	YES	560	0.036		10.1002/anie.202202098
155	2022	Homo	Long	Symm.	YES	585	0.034	2710	10.1039/d2dt02104h
156	2022	Homo	Long	Symm.	YES	602	0.0065	300	10.1039/d2dt02104h
157	2022	Homo	Short	Symm.	YES	560	0.85	4500	10.1039/d1tc05271c
158	2022	Homo	Long	Symm.	NO	643	0.72	1890	10.1016/j.jorganchem.2021.122202
159	2022	Homo	Long	Symm.	YES	478	0.06	115	10.3390/molecules27186003
160	2022	Homo	Long	Symm.	YES	543	0.44	1800	10.1021/acs.organomet.1c00617

161	2022	Homo	Long	Symm.	YES	597	0.68	2300	10.1021/acs.organomet.1c00617
162	2022	Hetero	Long	Symm.	YES	528	0.58	2000	10.1021/acs.organomet.1c00617
163	2023	Homo	Short	Symm.	YES	547	0.72	1890	10.1039/d2tc03539a
164	2023	Homo	Short	Symm.	YES	620	0.038	73	10.1002/aoc.6964
165	2023	Hetero	Long	Symm.	YES	550	0.3	1700	10.1039/d3dt00901g

Experimental procedures

Materials and physical measurements. Varian Inova (600 MHz for ^1H , 564.3 MHz for ^{19}F , and 150.8 MHz for ^{13}C) and Agilent 500 MHz spectrometers were used to record the ^1H , ^{13}C , ^{19}F , COSY, HMBC and HSQC NMR spectra of the iridium(III) complexes in CDCl_3 solution. Chemical shifts (δ) are reported in ppm relative to residual solvent signals for ^1H and ^{13}C NMR (^1H NMR: 7.26 ppm for CDCl_3 ; ^{13}C NMR: 77.0 ppm for CDCl_3) or relative to internal standard as chemical shift reference for ^{19}F NMR (-163 ppm for C_6F_6). $^{13}\text{C}\{^1\text{H}\}$ NMR spectra were acquired with ^1H broad band decoupled mode. Coupling constants (J) are given in Hz. The signals splitting is abbreviated as follows: s = singlet; d = doublet; t = triplet; dd = doublet of doublets; td = triplet of doublets; m = multiplet. Exact mass was performed by a Waters Xevo G2-XS QToF with an ESI-APCI source.

Magnesium sulphate (anhydrous), 2-ethoxyethanol, sodium carbonate, sodium hydroxide, iridium(III) chloride hydrate $\text{IrCl}_3 \cdot x(\text{H}_2\text{O})$, 2-(2,4-difluorophenyl)pyridine (**dfppy**), 2-phenylbenzothiazole (**pbt**) were employed in the synthesis of the iridium(III) complex. These chemicals were purchased from Merck Aldrich and were used without any further purification. The synthesis of the iridium dimer complex $[(\text{C}^{\wedge}\text{N})_2\text{Ir}(\mu\text{-Cl})]_2$ was carried out by a standard procedure proposed by Watts *and co.*¹ using $\text{IrCl}_3 \cdot x \text{H}_2\text{O}$ and cyclometalating ligands in a mixture of 2-ethoxyethanol and water. Celite 545 filter aid (treated with sodium carbonate, flux c{Garces, 2002, 3464-3471}alcined, Merck Aldrich Co) was used to filter the reaction crude. Thin-layer chromatography (TLC) was used to monitor the reaction progress (silica gel 60 F254, Merck Co.) and the spots were observed under UV light at 254 and 365 nm. Silica column chromatography was performed using silica gel (230–400 mesh, Merck Co.). Aluminium oxide 90 active neutral 0.063-0.200 mm (70 - 230 mesh ASTM) was used for Alumina column separations. Unless otherwise specified, all other reagents are of analytical grade and used as received from Merck Aldrich, CARLO ERBA Reagents, AlfaAesar and Tokyo chemical industries.

NMR spectra of previously reported compounds were in agreement with those of the authentic samples and/or available literature data.

Synthesis of μ -dichloro-bridged iridium(III) dimer complex

$[(\text{dfppy})_2\text{Ir}(\mu\text{-Cl})]_2$. $\text{IrCl}_3 \cdot x(\text{H}_2\text{O})$ (406 mg, 1.35 mmol) and 2-(2,4-difluorophenyl)pyridine (**dfppy**) (500 mg, 2.61 mmol) were dissolved in 30 mL of 2-ethoxyethanol and water (8:2) mixture and refluxed at 140 °C for 24 h. After the solution was cooled, the addition of 70 mL of H_2O gave a yellow precipitate

that was filtered and washed with diethyl ether. The crude product was used for the next reaction without further purification (yield: 78 %).

[(pbt)₂Ir(μ-Cl)]₂. IrCl₃·x(H₂O) (367 mg, 1.23 mmol) and 2-phenylbenzothiazole (**pbt**) (500 mg, 2.36 mmol) were dissolved in 30 mL of 2-ethoxyethanol and water (8:2) mixture and refluxed at 140 °C for 24 h. After the solution was cooled, the addition of 70 mL of H₂O gave an orange precipitate that was filtered and washed with diethyl ether. The crude product was used for the next reaction without further purification (yield: 85 %).

General procedure for the synthesis of mononuclear iridium(III) complexes.

A mixture of 250 mg of the corresponding dimer [(C^N)₂Ir(μ-Cl)]₂, 2.6 equivalents of 3-hydroxy picolinic acid and 11 equivalents of sodium carbonate was stirred overnight in a mixture (7:3) of dichloromethane and ethanol (40 mL) at 70 °C under nitrogen atmosphere. The solvent was removed by evaporation under reduced pressure. The crude product obtained was poured into water and extracted with ethyl acetate (3 × 50 mL). The combined organic layer was dried over magnesium sulphate (anhydrous). The solvent was removed under reduced pressure to give a crude residue, that was purified by using silica gel column chromatography with dichloromethane/methanol in 9:1 ratio as eluent, giving the desired complex as yellow powder. All purified samples were recrystallized and vacuum-dried before conducting all analysis.

(*dfppy*)₂Ir(*pic3OH*) (**B**).² Results: 220 mg, 0.309 mmol, yield = 75 %. **¹H NMR** (500 MHz, CDCl₃) δ 13.58 (s, 1H), 8.68 (d, *J* = 8.3 Hz, 1H), 8.31 (d, *J* = 11.1 Hz, 1H), 8.25 (d, *J* = 8.3 Hz, 1H), 7.81 (tt, *J* = 7.7, 1.9 Hz, 2H), 7.48 (m, 1H), 7.44 (m, 1H), 7.28 (m, 2H), 7.23 (t, *J* = 7.9 Hz, 1H), 7.04 (t, *J* = 6.3 Hz, 1H), 6.52 – 6.45 (m, 1H), 6.45 – 6.38 (m, 1H), 5.79 (dd, *J* = 8.7, 2.3 Hz, 1H), 5.58 (dd, *J* = 8.6, 2.4 Hz, 1H); **¹³C NMR** (126 MHz, CDCl₃) δ 177.4 (C), 165.7 (d, *J* = 7.0 Hz, C), 164.2 (m, 2C), 162.2 (m, 2C), 160.7 (C), 160.1 (m, 2C), 152.0 (d, *J* = 7.4 Hz, C), 149.7 (d, *J* = 7.8 Hz, C), 148.6 (CH), 148.0 (CH), 139.6 (CH), 138.4 (CH), 138.3 (CH), 134.3 (C), 130.0 (CH), 128.2 (m, C), 127.9 (m, C), 127.3, 123.4 (d, *J* = 19.8 Hz, CH), 122.8 (d, *J* = 19.1 Hz, CH), 122.6 (CH), 122.5 (CH), 114.6 (t, *J* = 3.3 Hz, CH), 114.5 (t, *J* = 3.6 Hz, CH), 98.4 (t, *J* = 26.8 Hz, CH), 97.9 (t, *J* = 26.7 Hz, CH); **¹⁹F NMR** (470 MHz, CDCl₃) δ -107.0 (q, *J* = 9.1 Hz), -107.8 (q, *J* = 9.5 Hz), -109.8 (t, *J* = 11.6 Hz), -110.2 (t, *J* = 11.6 Hz).

(*pbt*)₂Ir(*pic3OH*) (**Y**). Results: 240 mg, 0.319 mmol, yield = 83 %. **¹H NMR** (500 MHz, CDCl₃) δ 13.63 (s, 1H), 8.43 (d, *J* = 8.2 Hz, 1H), 7.86 (d, *J* = 8.1 Hz, 2H), 7.73 (d, *J* = 9.3 Hz, 1H), 7.68 (d, *J* = 7.8 Hz, 1H), 7.51 (t, *J* = 7.8 Hz, 1H), 7.47 – 7.38 (m, 2H), 7.38 – 7.29 (m, 2H), 7.25 – 7.20 (m, 1H), 7.05 (t, *J* = 7.9 Hz, 1H), 6.98 (t, *J* = 7.4 Hz, 1H), 6.91 (t, *J* = 6.8 Hz, 1H), 6.78 – 6.68 (m, 2H), 6.56 (d, *J* = 7.8 Hz, 1H), 6.30 (d, *J* = 9.1 Hz, 1H), 6.19 (d, *J* = 10.3 Hz, 1H); **¹³C NMR** (126 MHz, CDCl₃) δ 182.0 (C), 179.3 (C), 177.7 (C), 160.1 (C), 149.9 (C), 149.8 (C), 148.5 (C), 146.8 (C), 141.2 (C), 140.6 (C), 140.0 (CH), 136.0 (C), 134.6 (CH), 134.1 (CH), 131.7 (C), 131.2 (1 C, 1CH), 130.9 (CH), 129.5 (CH), 128.4 (CH), 127.4 (CH), 126.8 (CH), 126.3 (CH), 126.0 (CH), 125.8 (CH), 125.1 (CH), 123.1 (CH), 122.4 (CH), 122.3 (CH), 121.7 (CH), 120.8 (CH), 117.9 (CH).

General procedure for the synthesis of binuclear iridium(III) complexes

Mononuclear iridium(III) complex **B** or **Y** and 0.6 equivalents of μ -chloro bridged iridium(III) dimer $[(\text{pbt})_2\text{Ir}(\mu\text{-Cl})]_2$ or $[(\text{dfppy})_2\text{Ir}(\mu\text{-Cl})]_2$ was dissolved in 20 mL of dichloromethane and kept for stirring under nitrogen atmosphere. 3 mL of NaOH in absolute ethanol (0.05 N) was added dropwise. Stirring was continued at room temperature for about 48h. The reaction progress was continuously monitored with silica TLC using basified diethyl ether (with a few drops of triethylamine) as eluent. After observing a considerable amount of product formation from the TLC (both the starting materials will have zero R_f under elution conditions), the crude reaction mixture was concentrated under vacuum to eliminate all solvents. The crude was further dissolved in dichloromethane and passed through Celite 545 followed by a quick wash column with neutral alumina (with 10 cm packing height) to remove any unreacted chloro-bridged dimers. The resulting solution was concentrated and subjected to column chromatography separation with basified silica gel using diethyl ether as the sole eluent.

$(\text{pbt})_2\text{Ir}(\text{pic3O})\text{Ir}(\text{pbt})_2$ (**YY**). Synthesized in accordance with general procedure using **Y** (25 mg, 0.033 mmol) and μ -chloro bridged iridium(III) dimer $[(\text{pbt})_2\text{Ir}(\mu\text{-Cl})]_2$ (25.89 mg, 0.019 mmol). The desired product **YY** ($R_f = 0.32$) was obtained as an orange powder. Results: 42.1 mg, 0.030 mmol, yield = 92 %. **¹H NMR** (500 MHz, CDCl_3) δ 8.09 (d, $J = 8.2$ Hz, H_{25}), 7.94 (d, $J = 8.2$ Hz, H_4), 7.85 (d, $J = 7.2$ Hz, H_{28}), 7.77 (dd, $J = 8.3, 4.9$ Hz, $\text{H}_{17} + \text{H}_9$), 7.67 – 7.57 (m, $\text{H}_5 + \text{H}_{29} + \text{H}_{21} + \text{H}_{20} + \text{H}_{13} + \text{H}_{12}$), 7.20 (t, $J = 7.2$ Hz, H_3), 7.14 (t, $J = 7.0$ Hz, H_{27}), 7.10 (dd, $J = 8.9, 1.5$ Hz, H_{35}), 6.99 (t, $J = 7.1$ Hz, H_{11}), 6.94 (dd, $J = 4.6, 1.4$ Hz, H_{33}), 6.89 – 6.78 (m, $\text{H}_{22} + \text{H}_{19} + \text{H}_{26} + \text{H}_{30} + \text{H}_6 + \text{H}_{34}$), 6.73 (t, $J = 7.3$ Hz, H_{14}), 6.67 – 6.56 (m, $\text{H}_7 + \text{H}_2 + \text{H}_{31} + \text{H}_{23}$), 6.47 (td, $J_T = 7.4, J_D = 1.4$ Hz, H_{15}), 6.39 – 6.31 (m, $\text{H}_1 + \text{H}_{24} + \text{H}_{10} + \text{H}_8$), 6.18 (dd, $J = 7.3, 4.2$ Hz, $\text{H}_{16} + \text{H}_{32}$), 5.83 (t, $J = 7.2$ Hz, H_{18}); **¹³C NMR** (126 MHz, CDCl_3) δ 181.8 (C), 180.7 (C), 179.4 (C), 178.8 (C), 175.9 (C), 169.7 (C), 150.7 (C), 150.7 (C), 150.2 (C), 150.2 (C), 150.1 (C), 149.2 (C), 148.7 (C), 147.0 (C), 141.8 (C), 141.8 (C), 141.2 (C), 140.7 (C), 136.3 (CH), 135.5 (CH), 135.0 (CH), 134.8 (CH), 134.4 (C), 134.2 (CH), 134.1 (CH), 131.4 (C), 131.2 (C), 130.8 (CH), 130.8 (C), 130.6 (CH), 130.5 (C), 130.0 (CH), 130.0 (CH), 128.0 (CH), 127.5 (CH), 127.2 (CH), 126.8 (CH), 126.4 (CH), 126.0 (CH), 125.8 (CH), 125.7 (CH), 125.6 (CH), 125.2 (CH), 125.2 (CH), 124.8 (CH), 124.7 (CH), 122.3 (CH), 121.8 (CH), 121.7 (CH), 121.3 (CH), 121.1 (CH), 120.9 (CH), 120.8₅ (CH), 120.8 (CH), 120.5 (CH), 120.0 (CH), 119.7 (CH), 119.0 (CH). **HRMS** (ESI-QTOF) ($[\text{M}]^+$): m/z calcd for $(\text{C}_{58}\text{H}_{35}\text{Ir}_2\text{N}_5\text{O}_3\text{S}_4+\text{Na})^+$: 1386.0773; found: 1386.0811.

$(\text{dfppy})_2\text{Ir}(\text{pic3O})\text{Ir}(\text{dfppy})_2$ (**BB**). Synthesized in accordance with general procedure using **B** (25 mg, 0.035 mmol) and μ -chloro bridged iridium(III) dimer $[(\text{dfppy})_2\text{Ir}(\mu\text{-Cl})]_2$ (25.60 mg, 0.021 mmol). Two products were isolated as yellow powder, namely **BB1** ($R_f = 0.21$) and **BB2** ($R_f = 0.16$).

BB1. Results: 14.0 mg, 0.010 mmol, yield = 31 %. **¹H NMR** (500 MHz, CDCl_3) δ 8.63 (dd, $J = 5.7, 0.9$ Hz, H_{19}), 8.51 (dd, $J = 5.7, 0.9$ Hz, H_{13}), 8.33 (d, $J = 8.6$ Hz, H_4), 8.30 (d, $J = 8.3$ Hz, H_{22}), 8.27 – 8.21 (m, $\text{H}_{10} + \text{H}_7 + \text{H}_{16}$), 7.86 (t, $J = 7.8$ Hz, H_3), 7.82 (t, $J = 7.8$ Hz, H_{21}), 7.75 (t, $J = 7.5$ Hz, $\text{H}_{15} + \text{H}_9$), 7.61 (dd, $J = 5.7, 0.9$ Hz, H_1), 7.20 (dd, $J = 8.9, 1.5$ Hz, H_{25}), 7.07 – 7.02 (m, $\text{H}_{20} + \text{H}_2$), 7.00 – 6.88 (m, $\text{H}_{26} + \text{H}_{27} + \text{H}_8 + \text{H}_{14}$), 6.47 – 6.41 (m, 1H), 6.38 – 6.30 (m, 2H), 6.30 – 6.23 (m, 1H), 5.70 (dd, $J = 8.7, 2.4$ Hz, 1H), 5.64 (dd, $J = 8.9, 2.4$ Hz, 1H), 5.53 (dd, $J = 8.9, 2.3$ Hz, 1H), 5.48 (dd, $J = 8.6, 2.4$ Hz, 1H); **¹³C**

NMR (126 MHz, CDCl₃) δ 175.6 (C), 169.7 (C), 166.3 (d, *J* = 6.7 Hz, C), 166.1 (d, *J* = 7.2 Hz, C), 165.3 (d, *J* = 6.7 Hz, C), 164.4 (m, 2C), 164.1 (d, *J* = 12.9 Hz, C), 163.7 (dd, *J* = 12.5, 2.5 Hz, C), 162.4 – 161.8 (m, 2C), 161.7 (dd, *J* = 12.5, 2.5 Hz, C), 160.2 (dd, *J* = 12.9, 2.8 Hz, C), 159.9 (t, *J* = 12.1 Hz, C), 153.8 (d, *J* = 7.2 Hz, C), 152.3 (d, *J* = 7.2 Hz, C), 151.2 (d, *J* = 7.2 Hz, C), 149.3 (d, *J* = 7.3 Hz, C), 148.3 (CH), 148.1₂ (CH), 148.0₇ (CH), 148.0 (CH), 138.1 (CH), 137.8 (CH), 137.7 (CH), 137.6 (CH), 136.8 (CH), 136.5 (CH), 132.1 (C), 129.1 (CH), 128.7 (m, C), 128.5 (m, C), 128.1 (m, C), 127.7 (m, C), 123.5 (d, *J* = 20.1 Hz, CH), 122.7 (m, 3CH), 122.1 (CH), 122.0 (CH), 121.4 (CH), 121.3 (CH), 114.9 (m, 2CH), 114.4 (dd, *J* = 17.2, 2.5 Hz, CH), 114.2 (dd, *J* = 17.2, 2.6 Hz, CH), 97.9 (t, *J* = 27.2 Hz, CH), 97.4 (t, *J* = 27.1 Hz, CH), 97.1 (m, 2CH); **¹⁹F NMR** (470 MHz, CDCl₃) δ -107.3 (q, *J* = 9.3 Hz), -108.1 (q, *J* = 9.2 Hz), -108.5 (q, *J* = 9.4 Hz), -109.1 (q, *J* = 9.4 Hz), -110.1 (t, *J* = 11.4 Hz), -110.4 (t, *J* = 11.5 Hz), -111.0 (t, *J* = 11.2 Hz, 2F). **HRMS** (ESI-QTOF) ([M]⁺): *m/z* calcd for (C₅₀H₂₇F₈Ir₂N₅O₃+Na)⁺: 1304.1115; found: 1304.1096.

BB2. Results: 16.5 mg, 0.012 mmol, yield = 36 %. **¹H NMR** (500 MHz, CDCl₃) δ 8.78 (d, *J* = 5.7 Hz, H₁₉), 8.76 (d, *J* = 5.9 Hz, H₇), 8.69 (d, *J* = 6.7 Hz, H₁₃), 8.28 (d, *J* = 8.3 Hz, H₁₀), 8.25 (d, *J* = 8.3 Hz, H₂₂), 8.21 (d, *J* = 8.4 Hz, H₄), 8.16 (d, *J* = 8.3 Hz, H₁₆), 7.85 (t, *J* = 7.9 Hz, H₉), 7.77 – 7.69 (m, H₂₁+ H₁₅ + H₃), 7.44 (d, *J* = 6.7 Hz, H₁), 7.30 (t, *J* = 7.3 Hz, H₈), 7.18 (dd, *J* = 8.9, 1.5 Hz, H₂₅), 7.11 – 7.05 (m, H₁₄ + H₂₀), 7.00 – 6.95 (m, H₂₆), 6.93 – 6.98 (m, H₂ + H₂₇), 6.48 – 6.40 (m, 1H), 6.39 – 6.29 (m, 2H), 6.29 – 6.21 (m, 1H), 5.67 (dd, *J* = 8.7, 2.4 Hz, 1H), 5.63 (td, *J* = 8.4, 2.3 Hz, 2H), 5.55 (dd, *J* = 8.7, 2.3 Hz, 1H); **¹³C NMR** (126 MHz, CDCl₃) δ 175.4 (C), 169.7 (C), 166.0 – 165.9 (m, 2C), 165.4 (d, *J* = 7.2 Hz, C), 164.8 (d, *J* = 7.2 Hz, C), 164.5 (d, *J* = 12.9 Hz, C), 164.1 (d, *J* = 12.9 Hz, C), 163.8 (d, *J* = 13 Hz, C), 162.4 – 161.7 (m, 3C), 160.3 – 159.8 (m, 2C), 153.5 (d, *J* = 6.5 Hz, C), 152.5 (d, *J* = 7.2 Hz, C), 151.0 (d, *J* = 7.0 Hz, C), 149.4 (d, *J* = 7.2 Hz, C), 148.0 (CH), 147.9₄ (CH), 147.9₆ (CH), 147.8 (CH), 138.1 (CH), 137.9 (CH), 137.8 (CH), 137.7 (CH), 136.8 (CH), 136.3 (CH), 132.4 (C), 129.1 (CH), 128.8 (m, C), 128.4 (m, C), 128.2 (m, C), 127.7 (m, C), 123.4 (d, *J* = 18.8 Hz, CH), 123.0 – 122.6 (m, 3CH), 121.9 (CH), 121.8 (CH), 121.2 (CH), 121.0 (CH), 115.1 – 114.8 (m, 2CH), 114.3 (dd, *J* = 9.6, 2.8 Hz, CH), 114.2 (dd, *J* = 9.6, 2.8 Hz, CH), 98.1 – 97.0 (m, 4CH); **¹⁹F NMR** (470 MHz, CDCl₃) δ -107.2 (q, *J* = 9.1 Hz), -108.3 (q, *J* = 9.1 Hz), -108.5 (q, *J* = 9.9 Hz), -109.2 (q, *J* = 9.5 Hz), -109.9 (t, *J* = 11.6 Hz), -110.5 (t, *J* = 11.6 Hz), -111.0 (t, *J* = 11.2 Hz), -111.2 (t, *J* = 11.6 Hz). **HRMS** (ESI-QTOF) ([M]⁺): *m/z* calcd for (C₅₀H₂₇F₈Ir₂N₅O₃+Na)⁺: 1304.1115; found: 1304.1096.

(*dfppy*)₂Ir(*pic*3O)Ir(*pbt*)₂, **BY**. Synthesized in accordance with general procedure using **B** (25 mg, 0.035 mmol) and μ-chloro bridged iridium(III) dimer [(*pbt*)₂Ir(μ-Cl)]₂ (27.30 mg, 0.021 mmol). Two products were isolated as orange powder, namely **BY1** (R_f = 0.26) and **BY2** (R_f = 0.13)

BY1. Results: 17.2 mg, 0.013 mmol, yield = 37 %. **¹H NMR** (500 MHz, CDCl₃) δ 8.30 (d, *J* = 8.4 Hz, H₄), 8.26 (d, *J* = 8.2 Hz, H₂₁), 8.10 (d, *J* = 8.3 Hz, H₁₀), 8.02 (d, *J* = 8.1 Hz, H₁₃), 7.96 (d, *J* = 8.3 Hz, H₂₄), 7.89 – 7.81 (m, H₁₆ + H₃), 7.77 (dd, *J* = 4.9, 0.8 Hz, H₇), 7.65 (dd, *J* = 7.6, 0.8 Hz, H₁₇), 7.60 (dd, *J* = 7.7, 0.8 Hz, H₂₅), 7.58 – 7.53 (m, H₁ + H₉), 7.39 – 7.30 (m, H₁₅ + H₂₃), 7.12 (dd, *J* = 8.9, 1.3 Hz, H₂₉), 7.06 (t, *J* = 7.7 Hz, H₂₂), 6.90 – 6.80 (m, H₁₈ + H₂ + H₁₄ + H₃₀), 6.77 – 6.72 (m, H₃₁ + H₂₆), 6.64 (t, *J* = 7.5 Hz, H₁₉), 6.51 (t, *J* = 7.5 Hz, H₂₇), 6.46 (d, *J* = 8.1 Hz, H₂₀), 6.41 – 6.35 (m, H₁₂), 6.35 – 6.26 (m, H₂₈ + H₈ + H₅), 5.68 (dd, *J* = 8.8, 2.3 Hz, H₁₁), 5.46 (dd, *J* = 8.6, 2.4 Hz, H₆); **¹³C NMR** (126 MHz, CDCl₃) δ

181.4 (C), 180.0 (C), 175.8 (C), 170.7 (C), 166.0 (d, $J = 6.7$ Hz, C), 164.3 (d, $J = 12.4$ Hz, C), 164.1 (d, $J = 7.2$ Hz, C), 162.3 (d, $J = 8.4$ Hz, C), 162.1 (d, $J = 12.1$ Hz, C), 160.1 (dd, $J = 12.0, 8.0$ Hz, C), 154.3 (d, $J = 6.6$ Hz, C), 153.2 (d, $J = 7.0$ Hz, C), 150.8 (C), 150.7 (C), 148.5 (C), 148.4 (CH), 147.2 (CH), 146.5 (C), 141.7 (C), 141.6 (C), 137.7 (CH), 137.3 (CH), 135.9 (CH), 135.6 (CH), 135.0 (CH), 134.9 (CH), 132.7 (C), 131.5 (C), 131.4 (C), 130.3 (CH), 130.1 (CH), 128.5 (CH), 128.1 (C), 127.8 (C), 127.5 (CH), 127.4 (CH), 126.0 (CH), 125.9 (CH), 124.7 (CH), 124.6 (CH), 123.0 (d, $J = 19.7$ Hz, CH), 122.4 (d, $J = 19.0$ Hz, CH), 122.2 (2 CH), 122.1 (CH), 121.6 (CH), 121.1 (CH), 121.0 (CH), 120.5 (CH), 120.4 (CH), 114.5 (dd, $J = 17.5, 3.3$ Hz, CH), 114.2 (dd, $J = 17.0, 2.3$ Hz, CH), 97.7 (t, $J = 27.0$ Hz, CH), 97.1 (t, $J = 26.6$ Hz, CH); **^{19}F NMR** (470 MHz, CDCl_3) δ -107.9 (q, $J = 9.5$ Hz), -108.6 (q, $J = 9.5$ Hz), -110.5 (t, $J = 11.6$ Hz), -110.8 (t, $J = 11.6$ Hz). **HRMS** (ESI-QTOF) ($[\text{M}]^+$): m/z calcd for $(\text{C}_{54}\text{H}_{31}\text{F}_4\text{Ir}_2\text{N}_5\text{O}_3\text{S}_2+\text{Na})^+$: 1346.0956; found: 1346.0992.

BY2. Results: 19.0 mg, 0.014 mmol, yield = 41 %. **^1H NMR** (500 MHz, CDCl_3) δ 8.65 (d, $J = 5.7$ Hz, H₇), 8.56 (d, $J = 8.8$ Hz, H₂₁), 8.40 (d, $J = 8.3$ Hz, H₁₃), 8.19 (d, $J = 8.1$ Hz, H₁₀), 8.10 (d, $J = 8.4$ Hz, H₄), 7.95 – 7.86 (m, H₂₄ + H₁₆), 7.72 (t, $J = 8.7$ Hz, H₉), 7.65 (dd, $J = 7.7, 0.9$ Hz, H₁₇), 7.60 – 7.43 (m, H₂₅ + H₃ + H₂₃ + H₂₂ + H₁₅), 7.31 (t, $J = 7.8$ Hz, H₁₄), 7.18 (dd, $J = 9.0, 1.4$ Hz, H₂₉), 7.09 (t, $J = 7.3$ Hz, H₈), 6.90 – 6.83 (m, H₁ + H₁₈ + H₃₀), 6.73 (t, $J = 7.7$ Hz, H₂₆), 6.68 (dd, $J = 4.6, 1.4$ Hz, H₃₁), 6.63 (t, $J = 7.7$ Hz, H₁₉), 6.54 (t, $J = 7.5$ Hz, H₂₇), 6.45 – 6.35 (m, H₂₀ + H₂₈ + H₁₂), 6.33 – 6.25 (m, H₅), 6.07 (t, $J = 7.3$ Hz, H₂), 5.62 (dd, $J = 8.8, 2.4$ Hz, H₁₁), 5.55 (dd, $J = 8.6, 2.4$ Hz, H₆); **^{13}C NMR** (101 MHz, CDCl_3) δ 181.5 (C), 180.1 (C), 175.3 (C), 170.8 (C), 165.5 (d, $J = 7.0$ Hz, C), 164.5 (d, $J = 7.4$ Hz, C), 164.1 (C), 162.2 (C), 162.0 (C), 160.1 (C), 154.3 (d, $J = 6.3$ Hz, C), 153.4 (d, $J = 6.4$ Hz, C), 150.9 (C), 150.6 (C), 148.5 (C), 148.0 (CH), 147.4 (CH), 146.8 (C), 141.7₅ (C), 141.7 (C), 137.8 (CH), 137.4 (CH), 136.0 (CH), 135.9 (CH), 135.0 (CH), 134.9 (CH), 132.7 (C), 132.0 (C), 131.7 (C), 130.2 (CH), 130.0 (CH), 128.5 (CH), 128.2 (C), 127.6 (C), 127.0 (CH), 126.9 (CH), 126.2 (CH), 125.9 (CH), 124.9 (CH), 124.5 (CH), 122.9 (d, $J = 19.5$ Hz, CH), 122.7 (d, $J = 17.9$ Hz, CH), 122.5 (CH), 122.2 (CH), 121.9 (CH), 121.4 (CH), 121.0 (CH), 120.9 (CH), 120.8 (2 CH), 114.4 (CH), 114.3 (CH), 97.6 (CH), 97.1 (CH); **^{19}F NMR** (470 MHz, CDCl_3) δ -107.8 (q, $J = 9.5$ Hz), -108.7 (q, $J = 9.5$ Hz), -110.3 (t, $J = 11.2$ Hz), -110.7 (t, $J = 11.6$ Hz). **HRMS** (ESI-QTOF) ($[\text{M}]^+$): m/z calcd for $(\text{C}_{54}\text{H}_{31}\text{F}_4\text{Ir}_2\text{N}_5\text{O}_3\text{S}_2+\text{Na})^+$: 1346.0956; found: 1346.0992.

$(\text{pbt})_2\text{Ir}(\text{pic}3\text{O})\text{Ir}(\text{dfppy})_2$ (**YB**). Synthesized in accordance with general procedure using **Y** (25 mg, 0.033 mmol) and 0.6 equivalent of μ -chloro bridged iridium(III) dimer $[(\text{dfppy})_2\text{Ir}(\mu\text{-Cl})]_2$ (24.07 mg, 0.019 mmol). Two products were isolated as yellow powder, namely **YB1** ($R_f = 0.20$) and **YB2** ($R_f = 0.15$).

YB1. Results: 18.0 mg, 0.013 mmol, yield = 41 %. **^1H NMR** (500 MHz, CDCl_3) δ 8.47 (d, $J = 5.5$ Hz, H₂₃), 8.28 (d, $J = 8.4$ Hz, H₂₆), 8.17 (d, $J = 8.5$ Hz, H₂₀), 8.02-7.97 (m, H₄ + H₁₇), 7.89 (d, $J = 8.3$ Hz, H₉), 7.83 (d, $J = 8.1$ Hz, H₁₂), 7.80 (t, $J = 7.8$ Hz, H₂₅), 7.69 (d, $J = 7.6$ Hz, H₁₃), 7.64 - 7.57 (m, H₁₉ + H₅), 7.45 (t, $J = 7.7$ Hz, H₃), 7.34 (t, $J = 7.7$ Hz, H₁₁), 7.12 (d, $J = 8.9$ Hz, H₃₁), 7.09 – 7.01 (m, H₂₉ + H₂), 6.95 – 6.90 (m, H₁₄ + H₃₀), 6.87 – 6.79 (m, H₂₄ + H₁₀ + H₆), 6.71 (t, $J = 7.5$ Hz, H₁₅), 6.61 (t, $J = 7.5$ Hz, H₇), 6.51 – 6.46 (m, H₁₆ + H₁), 6.34 – 6.18 (m, H₁₈ + H₈ + 2H), 5.66 (dd, $J = 8.9, 1.8$ Hz, 1H), 5.46 (dd, $J = 8.8, 1.8$ Hz, 1H); **^{13}C NMR** (101 MHz, CDCl_3) δ 182.3 (C), 179.3 (C), 175.3 (C), 168.8 (C), 165.8 (d, $J = 6.6$ Hz, C), 165.0 (d, $J = 6.7$ Hz, C), 163.7 (d, $J = 13.2$ Hz, C), 161.8 (d, $J = 6.7$ Hz, C), 161.7 (d, $J =$

66.5 Hz, C), 159.8 (d, $J = 13$ Hz, C), 151.8 (d, $J = 7.8$ Hz, C), 150.4 (C), 150.2 (C), 150.1, (d, $J = 7.6$ Hz, C) 149.9 (C), 149.8 (C), 148.1 (CH), 147.9 (CH), 141.1 (C), 140.5 (C), 137.4 (CH), 137.0 (2 CH), 136.0 (CH), 134.3 (CH), 134.1 (CH), 134.0 (C), 132.0 (C), 131.2 (C), 131.1 (CH), 130.7 (CH), 128.7 (m, C), 128.6 (m, C), 128.5 (CH), 128.0 (CH), 127.6 (CH), 126.2 (CH), 125.9 (CH), 125.1 (CH), 124.8 (CH), 123.0 (CH), 122.4 (d, $J = 18.6$ Hz, CH), 122.3₅ (d, $J = 18.7$ Hz, CH), 122.3 (CH), 121.8 (CH), 121.4 (CH), 121.3 (CH), 121.2 (CH), 120.2 (CH), 118.6 (CH), 115.0 (dq, $J = 17.1, 2.8$ Hz, 2 CH), 97.0 (t, $J = 27.2$ Hz, CH), 96.9 (t, $J = 27.0$ Hz, CH); **¹⁹F NMR** (470 MHz, CDCl₃) δ -108.9 (q, $J = 9.4$ Hz), -109.6 (q, $J = 9.4$ Hz), -111.4 (t, $J = 11.3$ Hz), -111.6 (t, $J = 11.2$ Hz). **HRMS** (ESI-QTOF) ([M]⁺): m/z calcd for (C₅₄H₃₁F₄Ir₂N₅O₃S₂+Na)⁺: 1346.0956; found: 1346.0992.

YB2. Results: 19.5 mg, 0.014 mmol, yield = 44 %. **¹H NMR** (500 MHz, CDCl₃) δ 8.62 – 8.58 (m, H₂₃ + H₉), 8.37 (d, $J = 5.7$ Hz, H₁₇), 8.16 (d, $J = 8.3$ Hz, H₂₆), 8.03 (d, $J = 8.4$ Hz, H₂₀), 7.95 (d, $J = 8.1$ Hz, H₁₂), 7.84 (d, $J = 9.4$ Hz, H₄), 7.72 – 7.68 (m, H₁₀ + H₁₃), 7.65 – 7.52 (m, H₂₅ + H₁₁ + H₅), 7.47 – 7.38 (m, H₁₉ + H₃), 7.16 (t, $J = 7.8$ Hz, H₂), 7.11 (dd, $J = 9.0, 1.3$ Hz, H₃₁), 7.04 (dd, $J = 4.6, 1.3$ Hz, H₂₉), 6.96 – 6.91 (m, H₃₀ + H₁₄), 6.81 (d, $J = 7.4$ Hz, H₆), 6.76 – 6.68 (m, H₂₄ + H₁₅), 6.63 (td, $J = 7.6, 1.2$ Hz, H₁₄), 6.54 (t, $J = 6.6$ Hz, H₁₈), 6.46 (d, $J = 7.5$ Hz, H₁₆), 6.33 – 6.20 (m, H₈ + H₁ + 2H), 5.64 (dd, $J = 8.9, 2.4$ Hz, 1H), 5.60 (dd, $J = 8.9, 2.4$ Hz, 1H); **¹³C NMR** (101 MHz, CDCl₃) δ 182.2 (C), 179.4 (C), 175.1 (C), 168.8 (C), 165.5 (d, $J = 6.7$ Hz, C), 165.2 (d, $J = 6.9$ Hz, C), 163.7 (d, $J = 13.1$ Hz, C), 161.7 (m, 2C), 159.8 (m, 2C), 151.7 (d, $J = 6.9$ Hz, C), 150.2₃ (C), 150.2 (C), 150.1, (C), 150.0₆ (C) 150.0 (C), 147.9 (CH), 147.6 (CH), 141.2 (C), 140.5 (C), 137.4 (2 CH), 137.2 (CH), 136.0 (CH), 134.3 (CH), 134.1 (CH), 131.9 (C), 131.8 (C), 131.1 (CH), 130.6 (CH), 128.9 (m, C), 128.5 (m, C), 128.5 (CH), 127.6 (CH), 126.9 (CH), 126.3 (CH), 125.9 (CH), 125.5 (CH), 124.5 (CH), 122.8 (2 CH), 122.4 (d, $J = 18.8$ Hz, 2 CH), 121.7 (CH), 121.2 (2 CH), 121.0 (CH), 120.7 (CH), 118.4 (CH), 115.0 (d, $J = 17.1$ Hz, 2 CH), 97.9 (dt, $J_T = 27.2, J_D = 9.5$ Hz, CH); **¹⁹F NMR** (470 MHz, CDCl₃) δ -108.9 (q, $J = 9.5$ Hz), -109.7 (q, $J = 9.5$ Hz), -111.3 (t, $J = 11.6$ Hz), -111.5 (t, $J = 11.2$ Hz). **HRMS** (ESI-QTOF) ([M]⁺): m/z calcd for (C₅₄H₃₁F₄Ir₂N₅O₃S₂+Na)⁺: 1346.0956; found: 1346.0992.

Electrochemistry

Voltammetric experiments were performed using a Metrohm AutoLab PGSTAT 302N electrochemical workstation in combination with the NOVA 2.0 software package. All the measurements were carried out at room temperature in acetonitrile solutions (if not otherwise stated) with a sample concentration of approx. 0.5 mM and using 0.1 M tetrabutylammonium hexafluorophosphate (electrochemical grade, TBAPF₆) as the supporting electrolyte. Oxygen was removed from the solutions by bubbling argon. All the experiments were carried out using a three-electrode setup (BioLogic VC-4 cell, volume range: 1–3 mL) using a glassy carbon working electrode (having an active surface disk of 1.6 mm in diameter), the Ag/AgNO₃ redox couple (0.01 M in acetonitrile, with 0.1 M TBAClO₄ supporting electrolyte) as the reference electrode and a platinum wire as the counter electrode. At the end of each measurement, ferrocene was added as the internal reference. Osteryoung square-wave voltammograms (OSWV) were recorded with scan rate of 125 mV s⁻¹, a SW amplitude of ± 20 mV, and a frequency of 25 Hz. Cyclic voltammograms (CV) were recorded at 100 mV s⁻¹.

Computational details

Density functional theory (DFT) calculations were carried out using the B.01 revision of the Gaussian 16 program package³ in combination with the M06 global-hybrid meta-GGA exchange-correlation functional.^{4,5} The fully relativistic Stuttgart/Cologne energy-consistent pseudopotential with multi-electron fit was used to replace the first 60 inner-core electrons of the iridium metal centre (*i.e.*, ECP60MDF) and it was combined with the associated triple-z basis set (*i.e.*, cc-pVTZ-PP basis).⁶ On the other hand, the Pople 6-31G(d,p) basis was adopted for all other atoms.^{7,8} All of the compounds were fully optimized without symmetry constraints, both in the ground state (S_0) and in their lowest triplet states (T_1), by using the polarizable continuum model (PCM) to simulate acetonitrile solvation effects.⁹⁻¹¹ Frequency calculations were always used to confirm that every stationary point found by geometry optimizations was actually a minimum on the corresponding potential-energy surface (no imaginary frequencies). Time-dependent DFT calculations (TD-DFT),^{12,13} carried out at the same level of theory used for geometry optimizations, were employed to map the excited-state scenario of the investigated molecules in their optimized S_0 geometry. Natural transition orbitals (NTOs) transformations were adopted to obtain a clear and compact orbital representation for the electronic transition density matrix in the case of complex multi-configurational excitations.¹⁴ To investigate the nature of the triplet states, geometry optimizations and frequency calculations were performed at the spin-unrestricted UM06 level of theory, imposing a spin multiplicity of 3; the ground-state minimum-energy geometry was used as initial guess for T_1 . In order to model $^1\text{H-NMR}$ chemical shift and to compare them with the experimental ones, the previously optimized ground-state structures were submitted to a GIAO calculations in chloroform using the optimized procedure described by Rablen *and co.*;¹⁵ in detail, the specially parametrized WP04 functional was adopted in combination with the previously described basis set for iridium and the cc-pVDZ basis set for all other atoms. All the pictures showing molecular-orbitals and spin-density surfaces were created using GaussView 6.¹⁶

Photophysical measurements

The spectroscopic investigations were carried out in spectrofluorimetric-grade acetonitrile. The absorption spectra were recorded with Perkin-Elmer Lambda 950 spectrophotometer. For the photoluminescence experiments, the sample solutions were placed in fluorimetric Suprasil quartz cuvettes (10.00 mm) and dissolved oxygen was removed by bubbling argon for 30 minutes. The uncorrected emission spectra were obtained with Edinburgh Instruments FLS920 spectrometer equipped with a Peltier-cooled Hamamatsu R928 photomultiplier tube (spectral window: 185–850 nm). Osram XBO xenon arc lamp (450 W) was used as the excitation light source. The corrected spectra were acquired by means of a calibration curve, obtained by using an Ocean Optics deuterium–halogen calibrated lamp (DH-3plus-CAL-EXT). The photoluminescence quantum yields (PLQYs) in solution were obtained from the corrected spectra on a wavelength scale (nm) and measured according to the approach described by Demas and Crosby,¹⁷ using an air-equilibrated water solution of quinine sulfate in 1 N H_2SO_4 (PLQY = 0.546)¹⁸ as reference. The emission lifetimes (τ) were measured through the time-correlated single photon counting (TCSPC) technique using a HORIBA Jobin Yvon IBH FluoroHub

controlling a spectrometer equipped with a pulsed NanoLED ($\lambda_{\text{exc}} = 373 \text{ nm}$) as the excitation source and a red-sensitive Hamamatsu R-3237-01 PMT (185–850 nm) as the detector. The analysis of the luminescence decay profiles was accomplished with the DAS6 Decay Analysis Software provided by the manufacturer, and the quality of the fit was assessed with the χ^2 value close to unity and with the residuals regularly distributed along the time axis. To record the 77 K luminescence spectra, samples were put in quartz tubes (2 mm inner diameter) and inserted into a special quartz Dewar flask filled with liquid nitrogen. The poly(methyl methacrylate) (PMMA) films containing 1% (w/w) of the complex were obtained by drop casting and the thickness of the films was not controlled. Solid-state PLQY values were calculated by corrected emission spectra obtained from an Edinburgh FLS920 spectrometer equipped with a barium sulfate coated integrating sphere (diameter of 4 in.) following the procedure described by Würth *et al.*¹⁹ Experimental uncertainties are estimated to be $\pm 8\%$ for τ determinations, $\pm 10\%$ for PLQYs, $\pm 2 \text{ nm}$ and $\pm 5 \text{ nm}$ for absorption and emission peaks, respectively.

OLED fabrication and characterization

Materials: PEDOT:PSS (CleviosTM, P VP Al 4083) was purchased from Heraeus, PVK (average M_n 25000-50000) was purchased from Sigma Aldrich, OXD-7 (purity grade > 99 %) was purchased from Ossila. All chemicals were used as received without further purification.

Device fabrication and characterization: Solution-processed OLEDs were fabricated on patterned ITO-coated glasses (1 inch square), which were previously cleaned in sequential sonicating baths (for 15 min) of deionized water, acetone and isopropanol and further treated in an oxygen plasma cleaner for 5 minutes at 200 W.

The OLEDs structure was: Glass/ITO (150 nm)/PEDOT:PSS (40 nm)/PVK:OXD-7:x (60 nm)/LiF (0.6 nm)/Al (80 nm)

PEDOT:PSS was spin coated at room temperature followed by an annealing at 150°C for 15 minutes to remove residual solvent from the polymeric layer. Solutions of PVK:OXD-7:binuclear complex (66.6:30:3.3 wt %) in chloroform (PVK concentration: 10 mg/mL) were stirred at room temperature for at least 4 h and then spin coated inside a nitrogen-filled glove box to obtain a 60 nm thick layer. To complete the device fabrication, LiF and Al were deposited sequentially using a thermal evaporator without breaking vacuum (approx. 3×10^{-6} Torr). Shadow masks were used to obtain device with an active area of 31 mm².

The current-voltage (I-V) characteristics of OLEDs were recorded in dark conditions inside a glovebox using a standard SUSS probe station coupled to a B1500A Agilent semiconductor device analyser.

The optical output was measured from the glass side of the device by using a silicon photodiode (sensitivity of 0.49 A W⁻¹ at 766 nm). EL spectra, CIE coordinates and luminance were measured by using a commercial CS2000 Konica Minolta spectroradiometer.

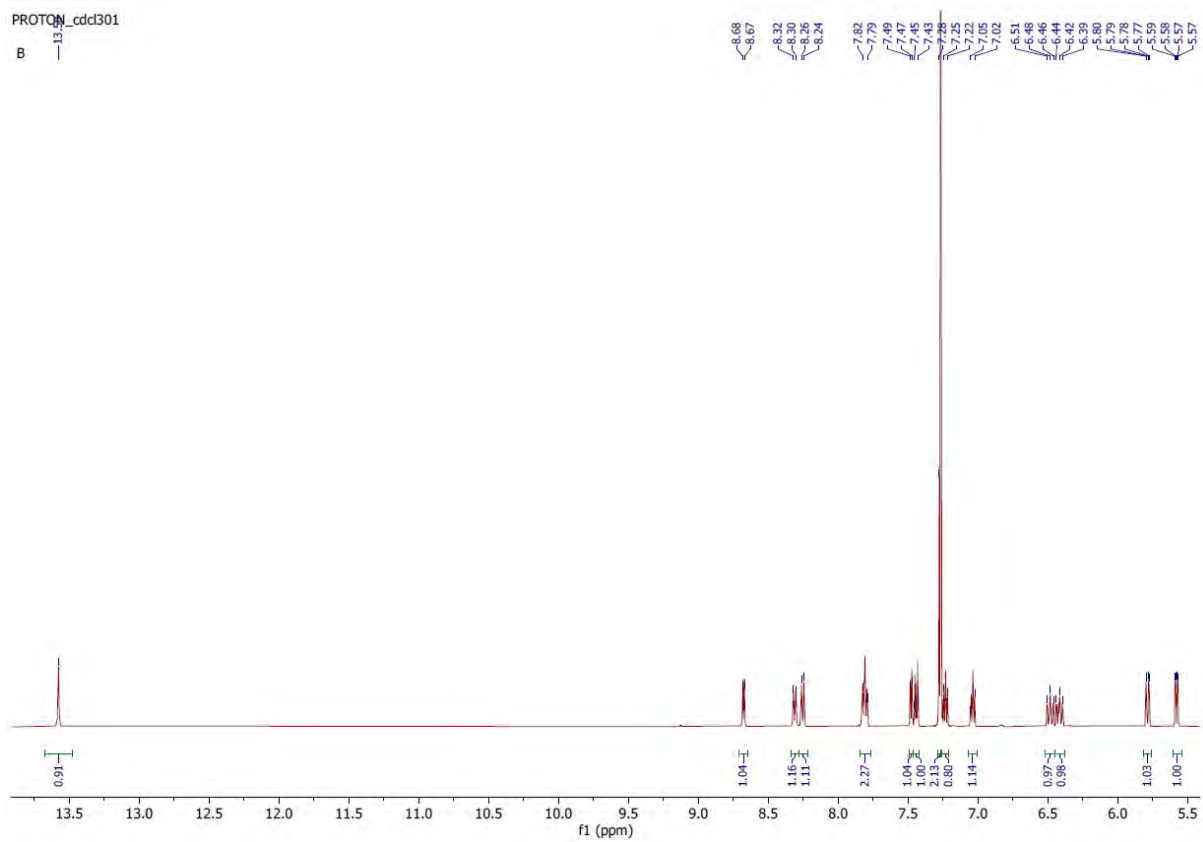
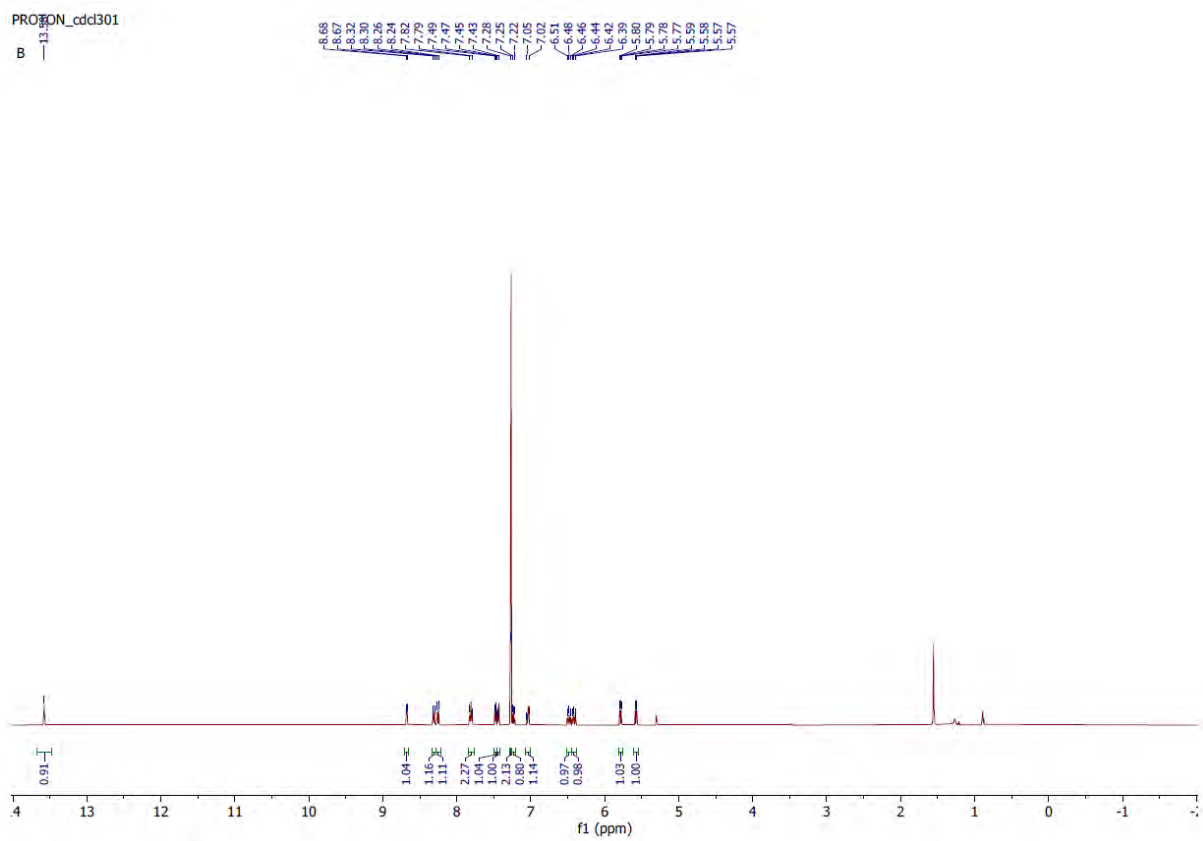


Figure S1a. ¹H NMR spectrum of complex B.

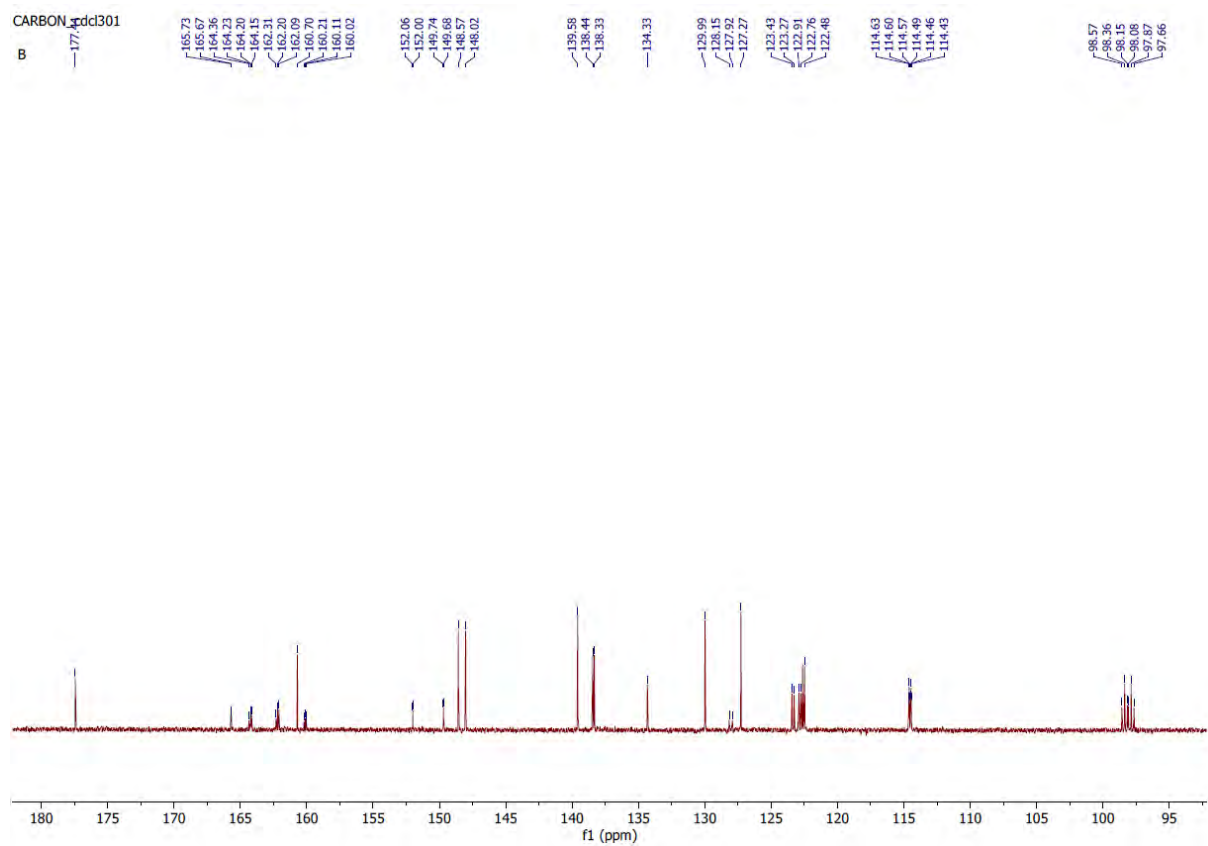
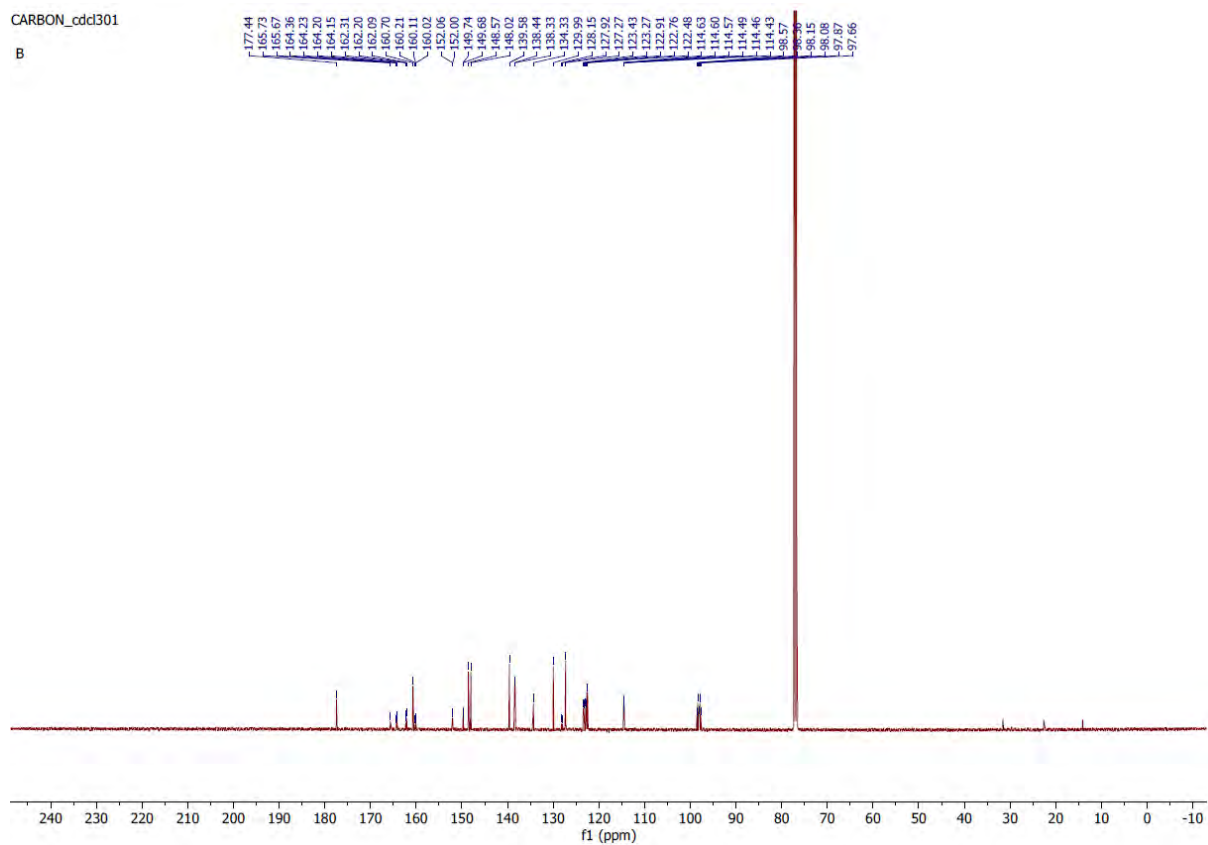


Figure S1b. ^{13}C NMR spectrum of complex **B**.

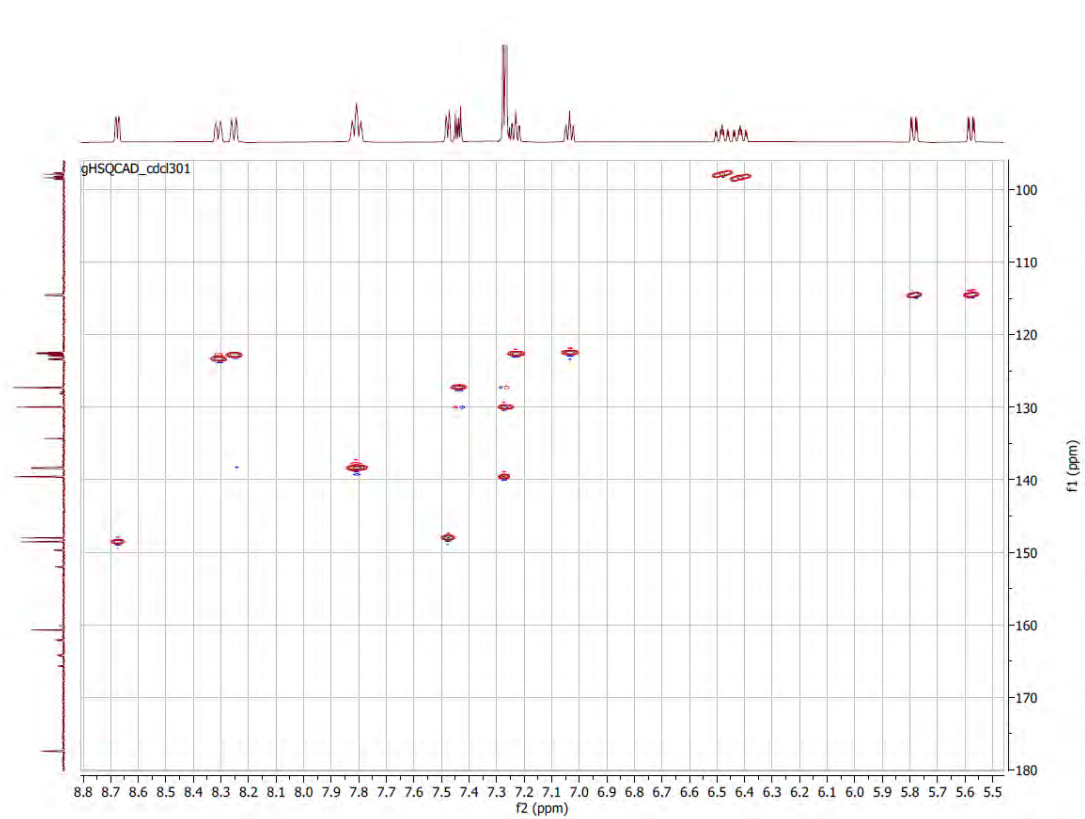


Figure S1c. HSQC spectrum of complex B.

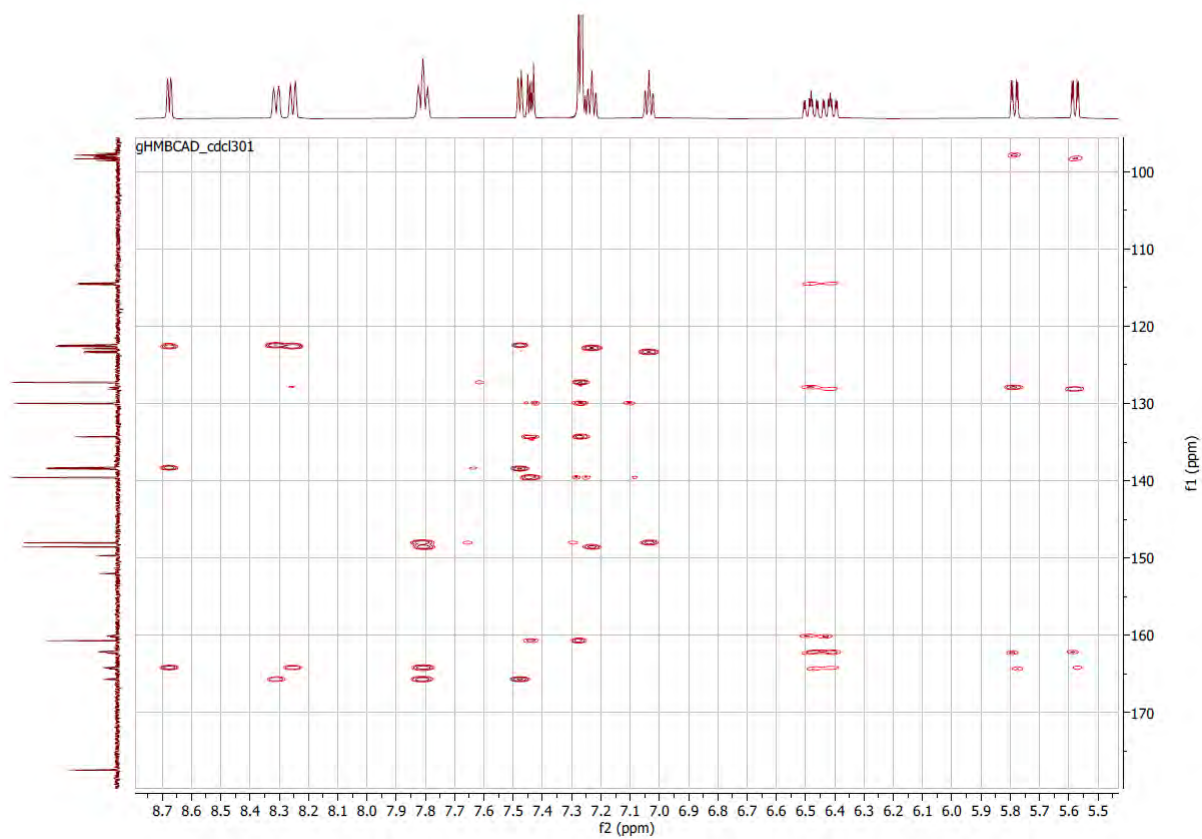


Figure S1d. HMBC spectrum of complex B.

19F_FTpicOH_20210705

B

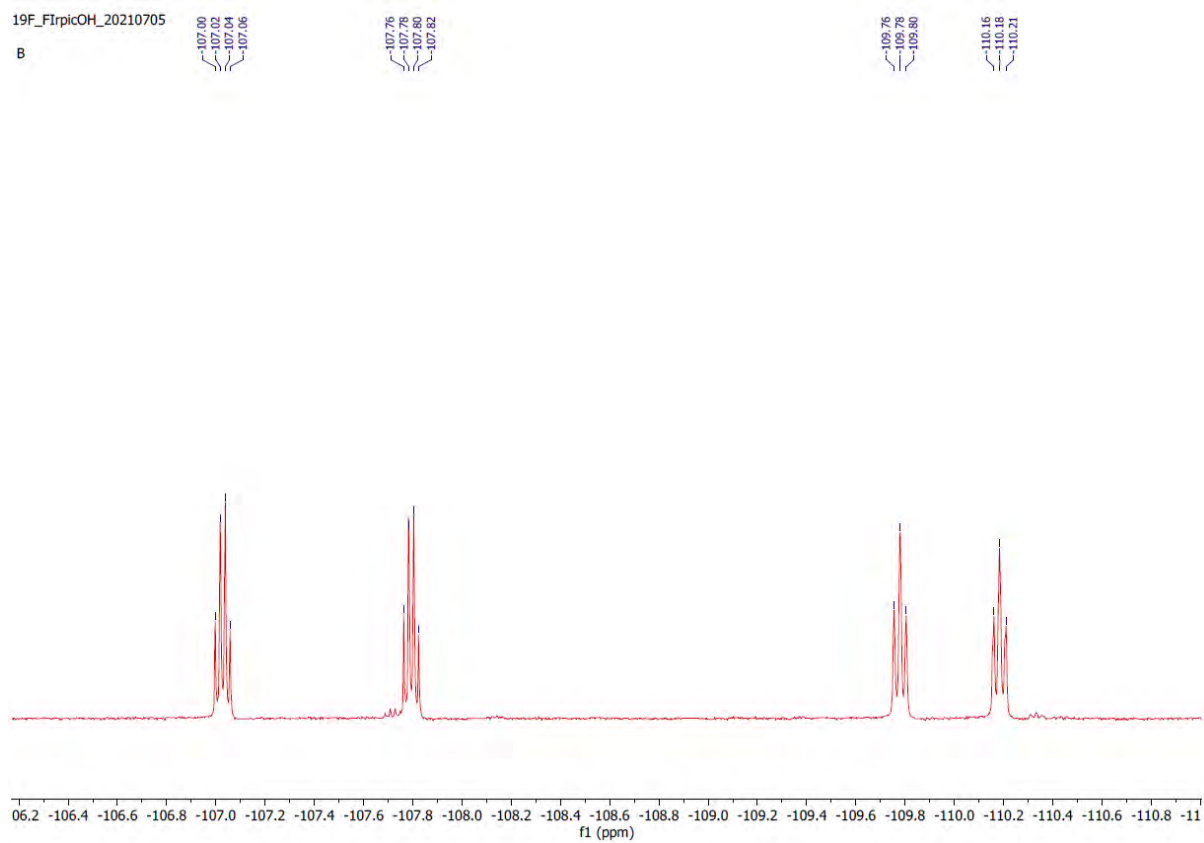


Figure S1e. ^{19}F NMR spectrum of complex **B**.

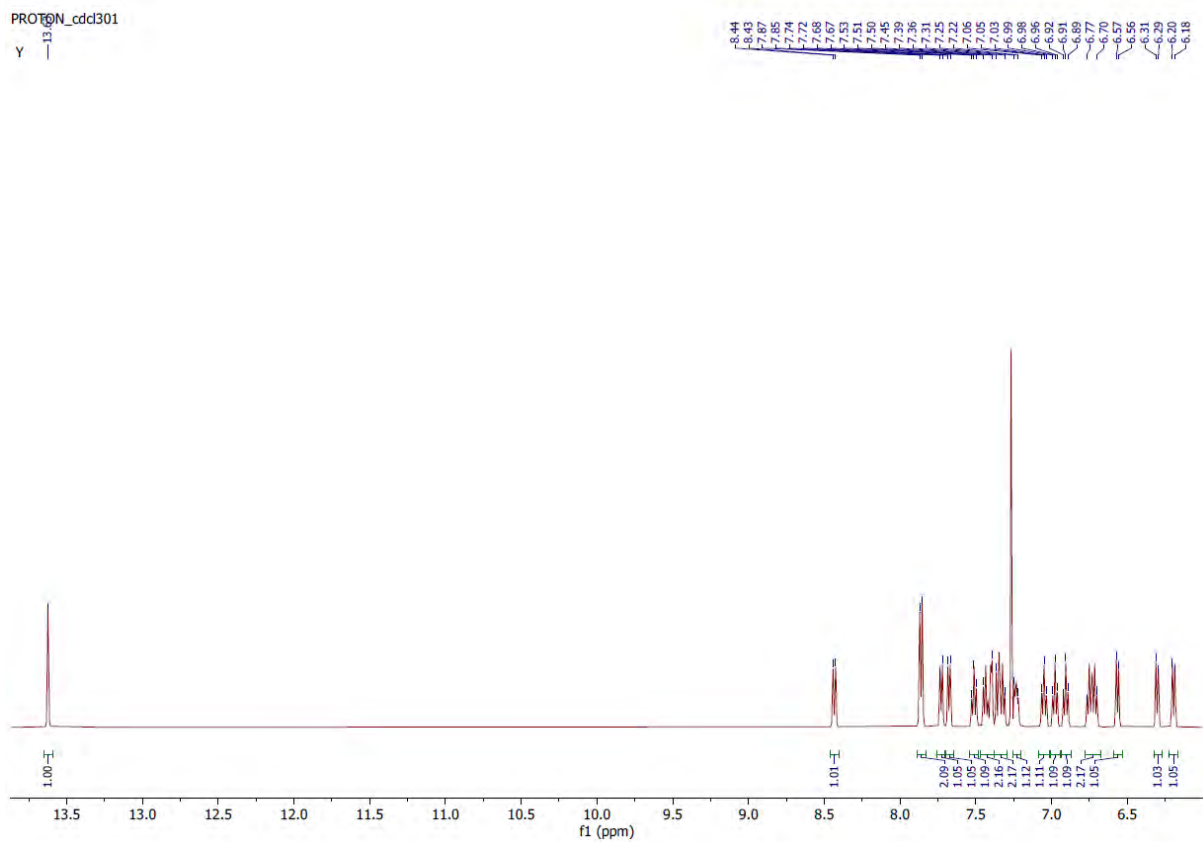
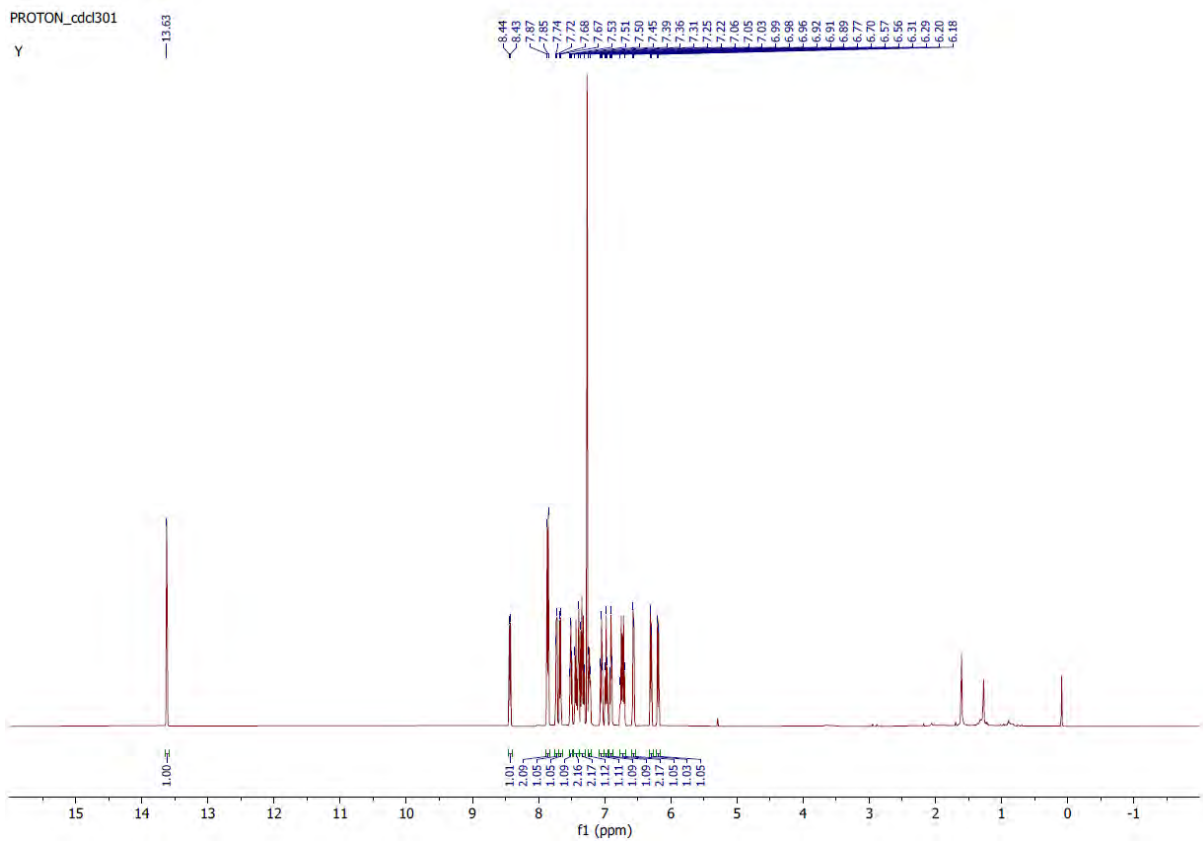


Figure S2a. ¹H NMR spectrum of complex Y.

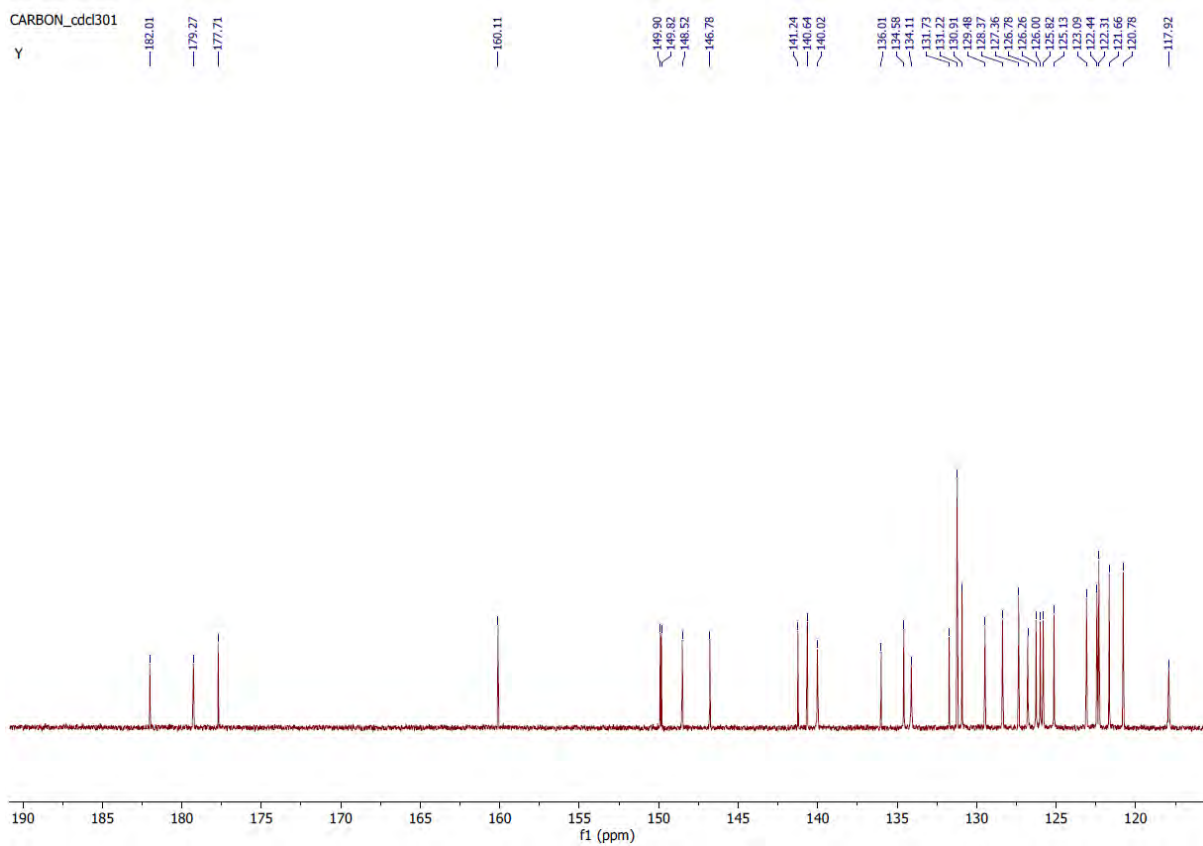
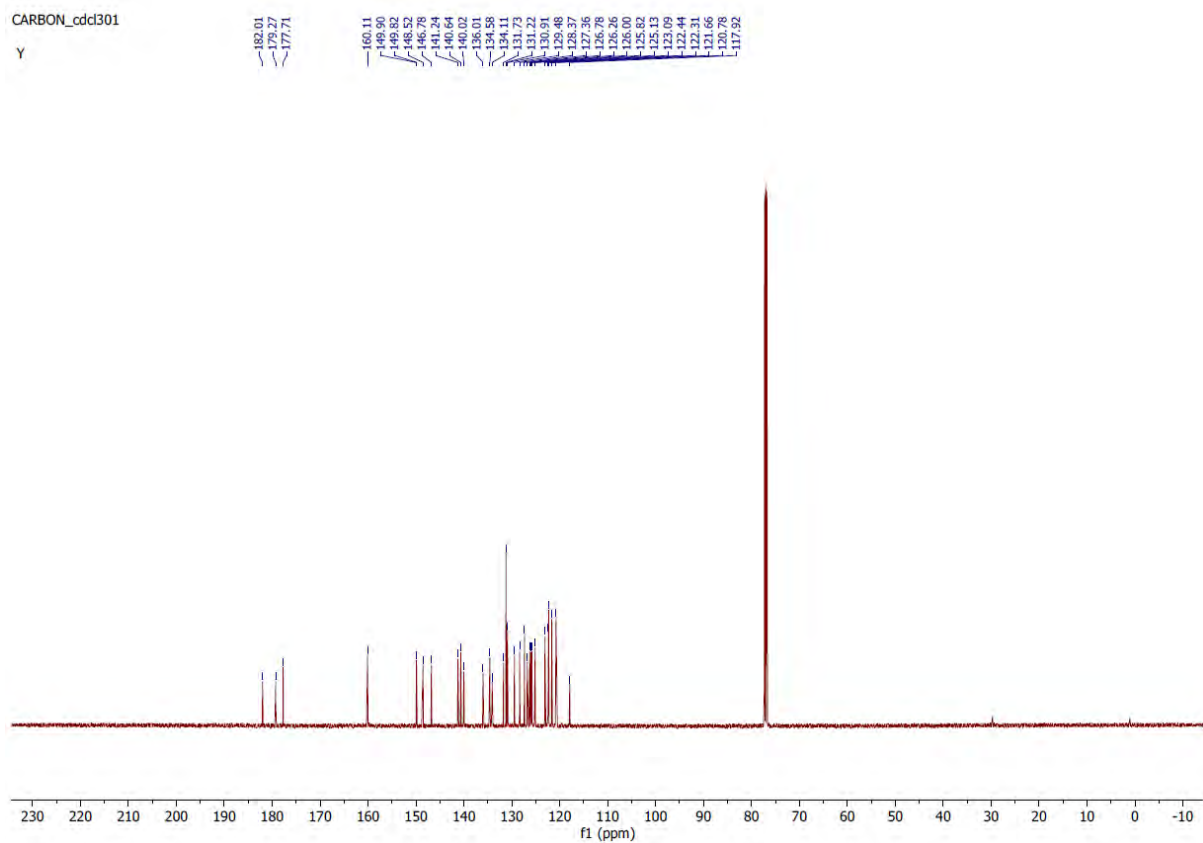


Figure S2b. ^{13}C NMR spectrum of complex Y.

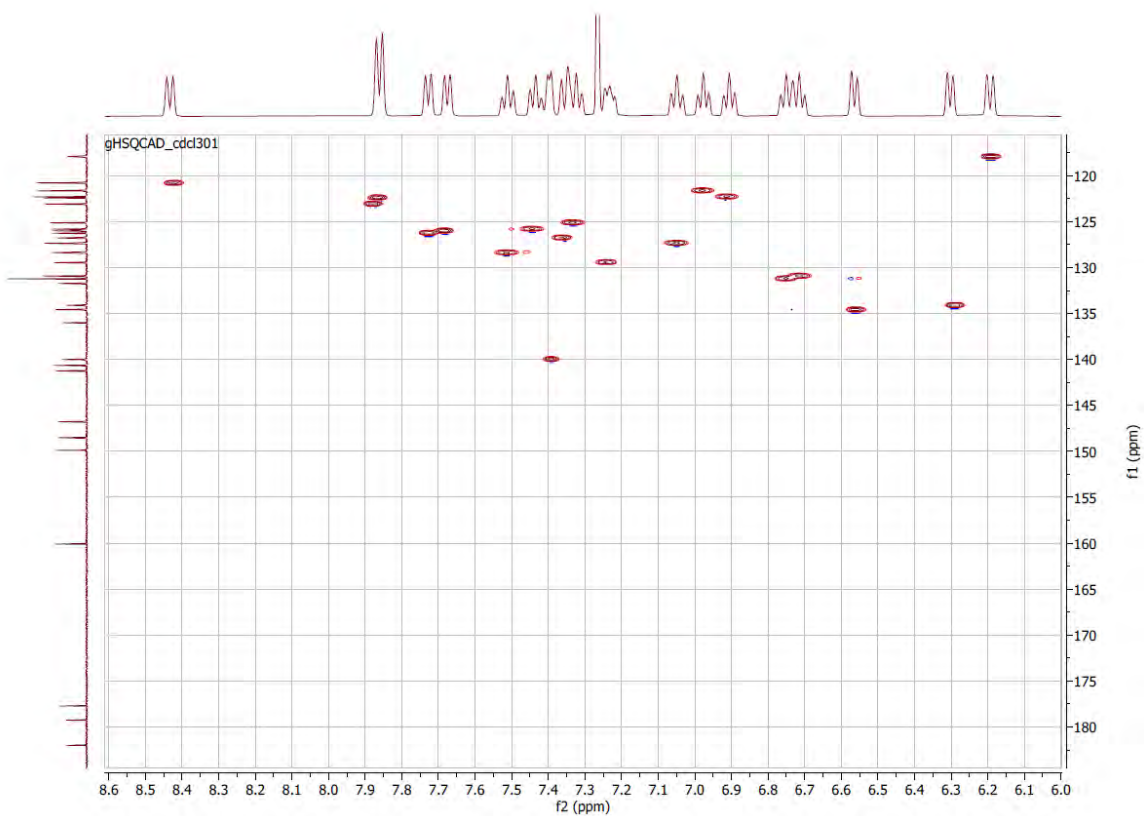


Figure S2c. HSQC spectrum of complex Y.

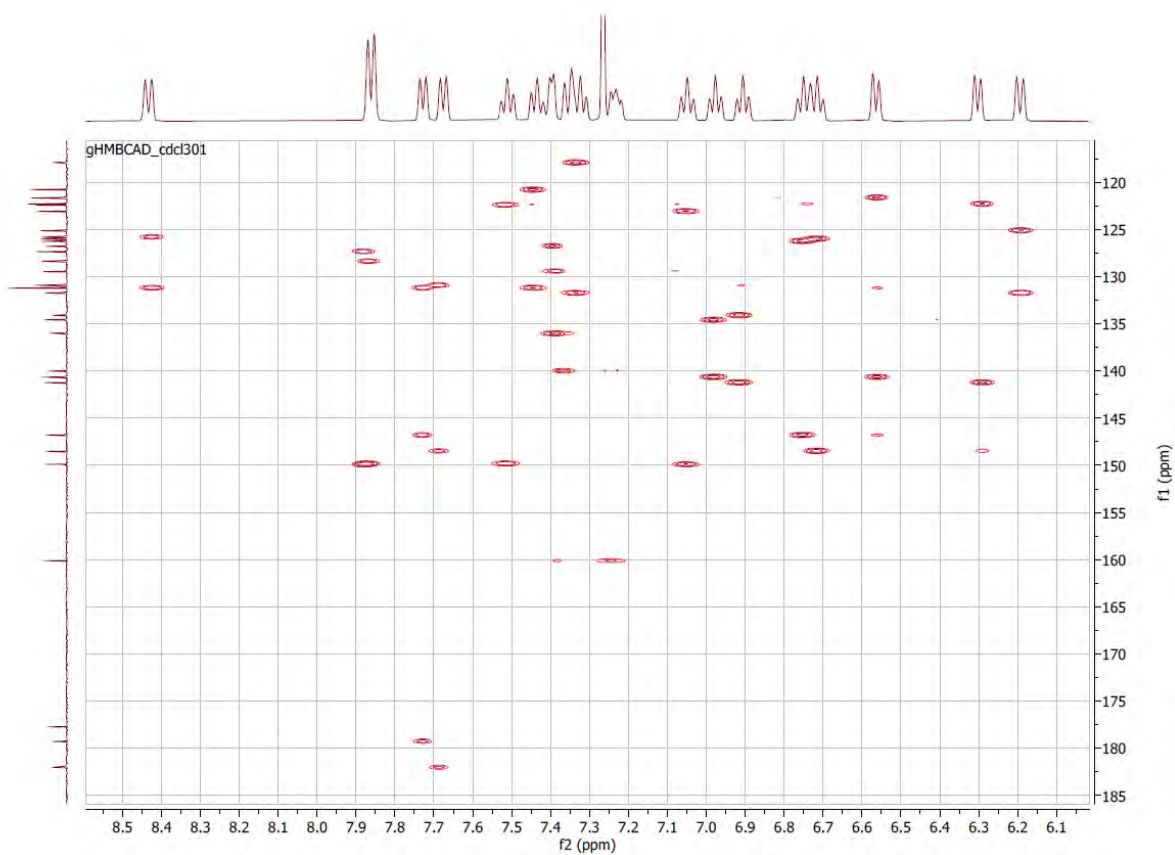


Figure S2d. HMBC spectrum of complex Y.

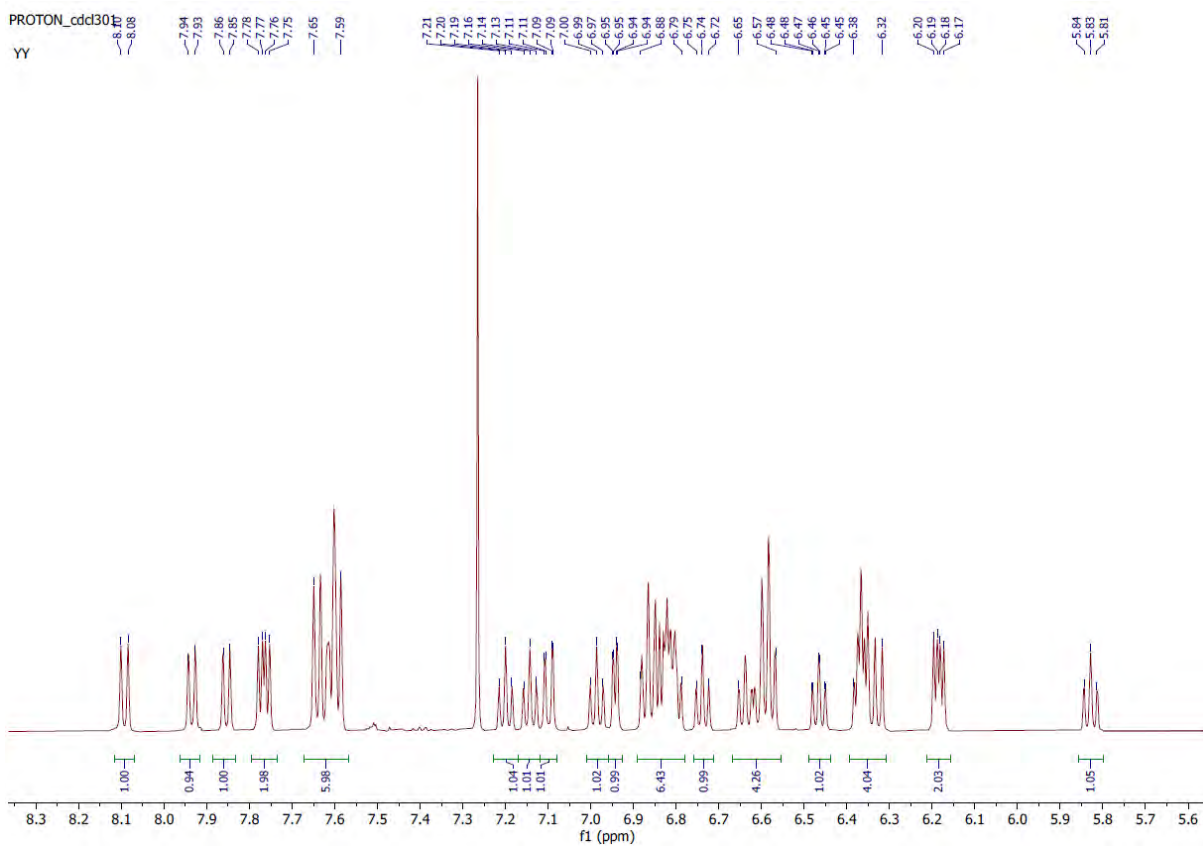
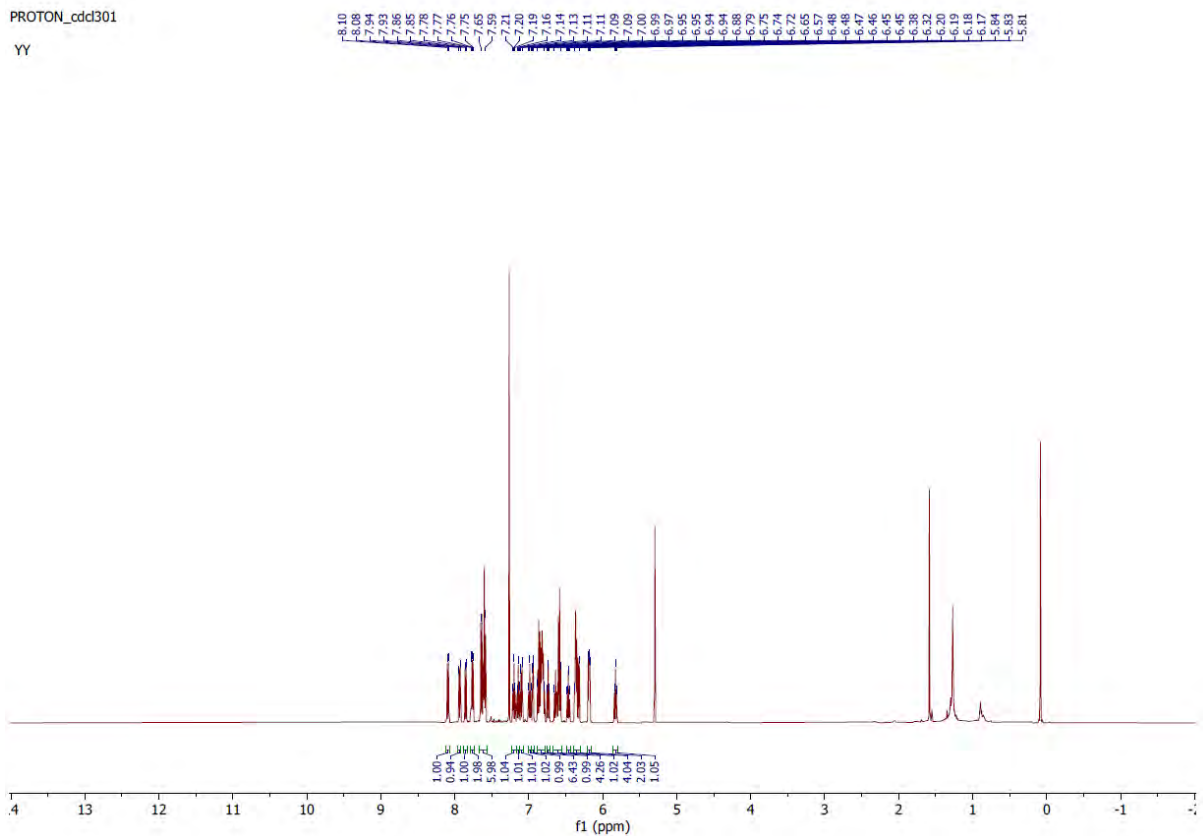


Figure S3a. ¹H NMR spectrum of complex YY.

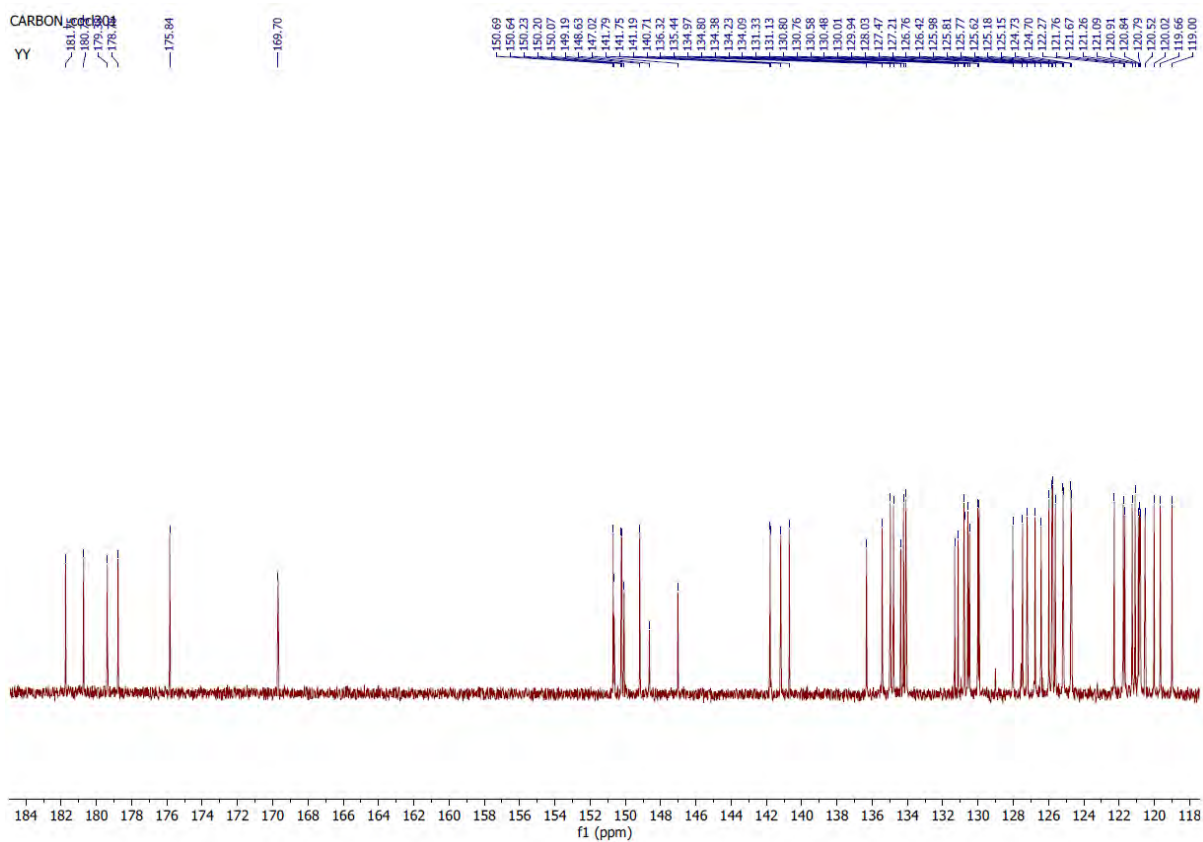
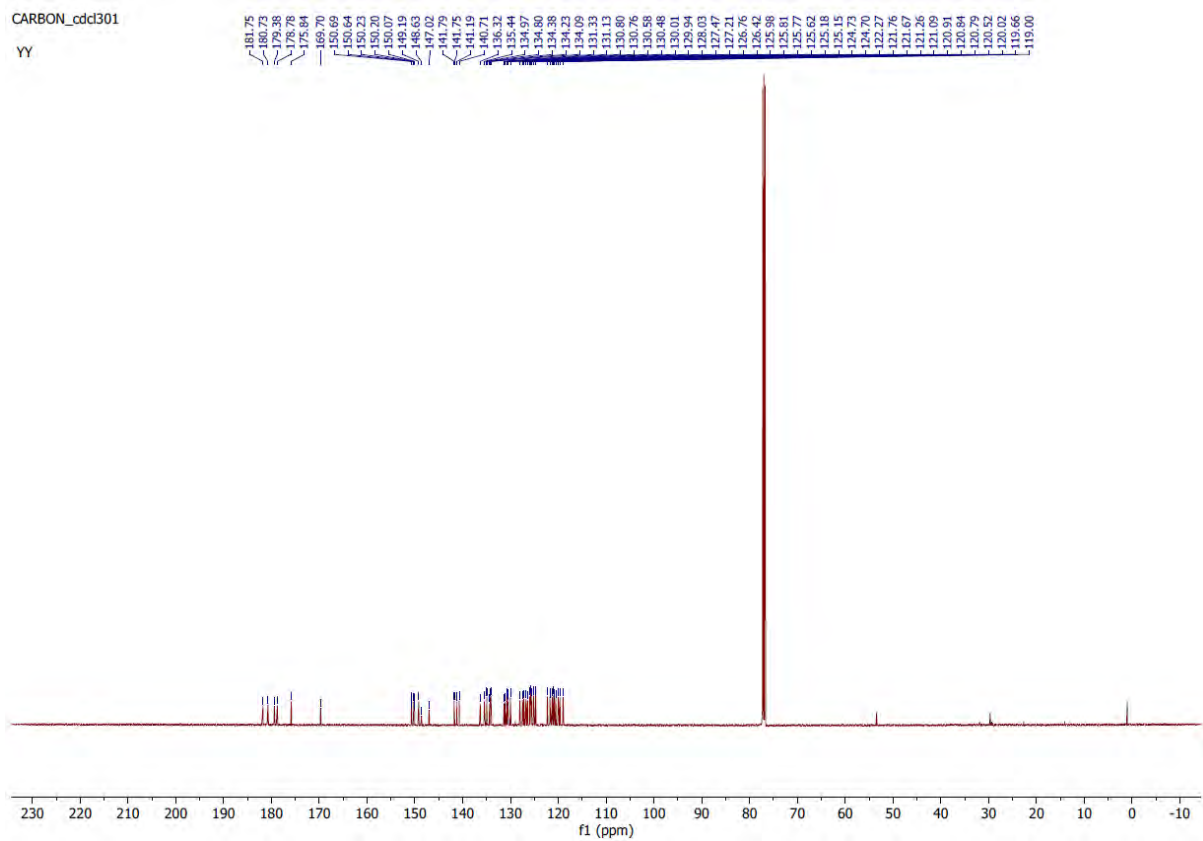


Figure S3b. ^{13}C NMR spectrum of complex YY.

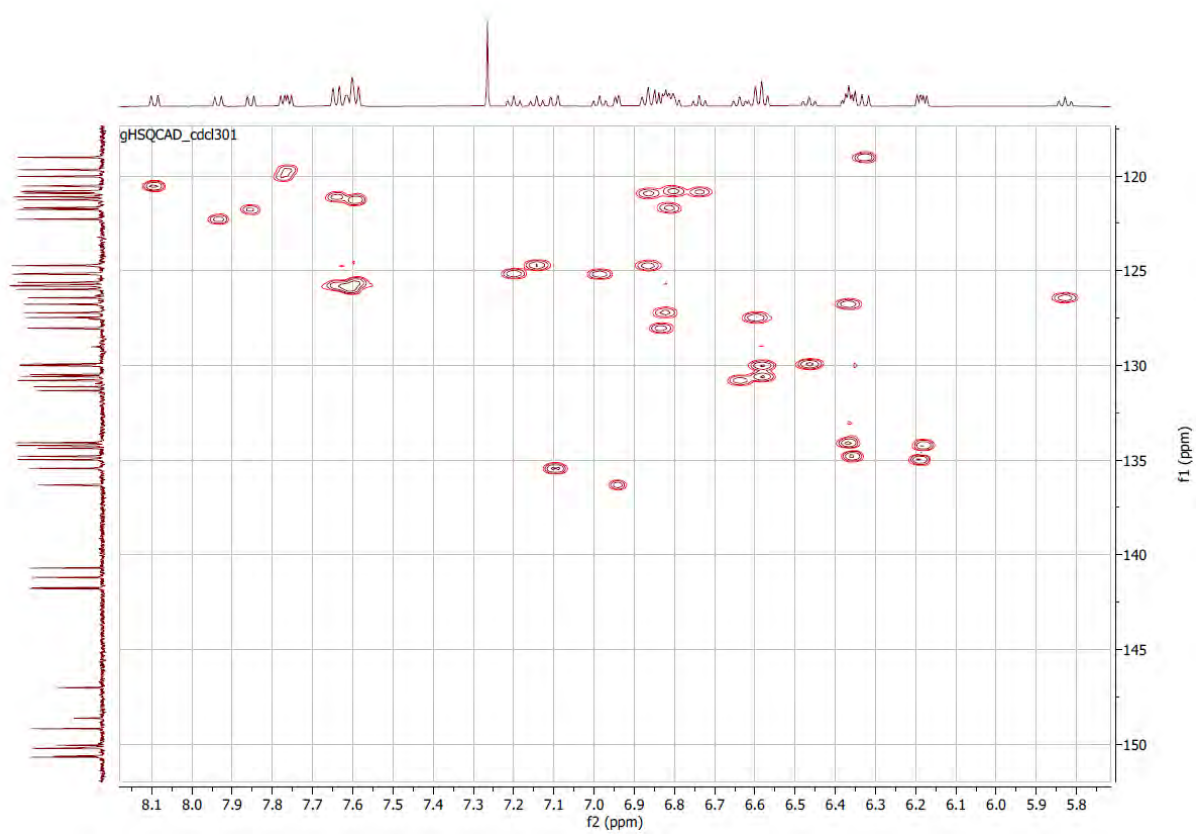


Figure S3c. HSQC spectrum of complex YY.

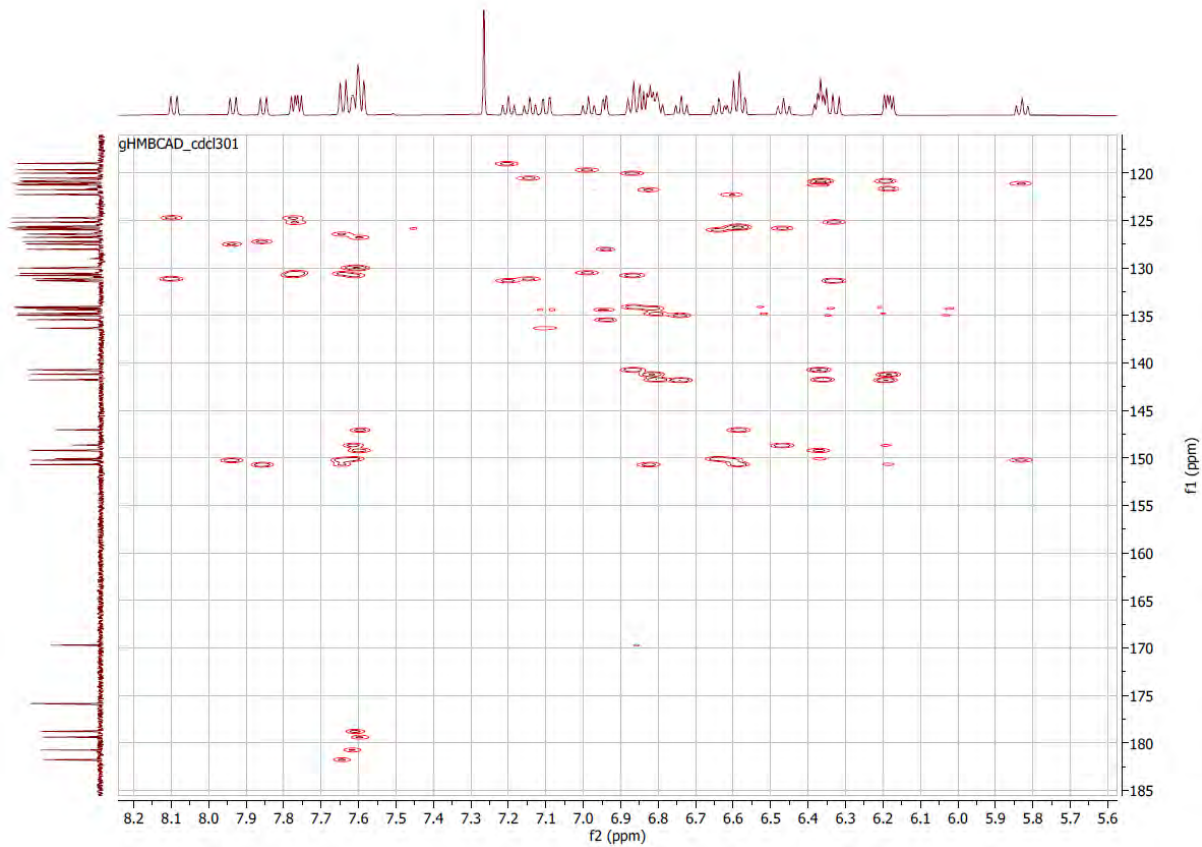


Figure S3d. HMBC spectrum of complex YY.

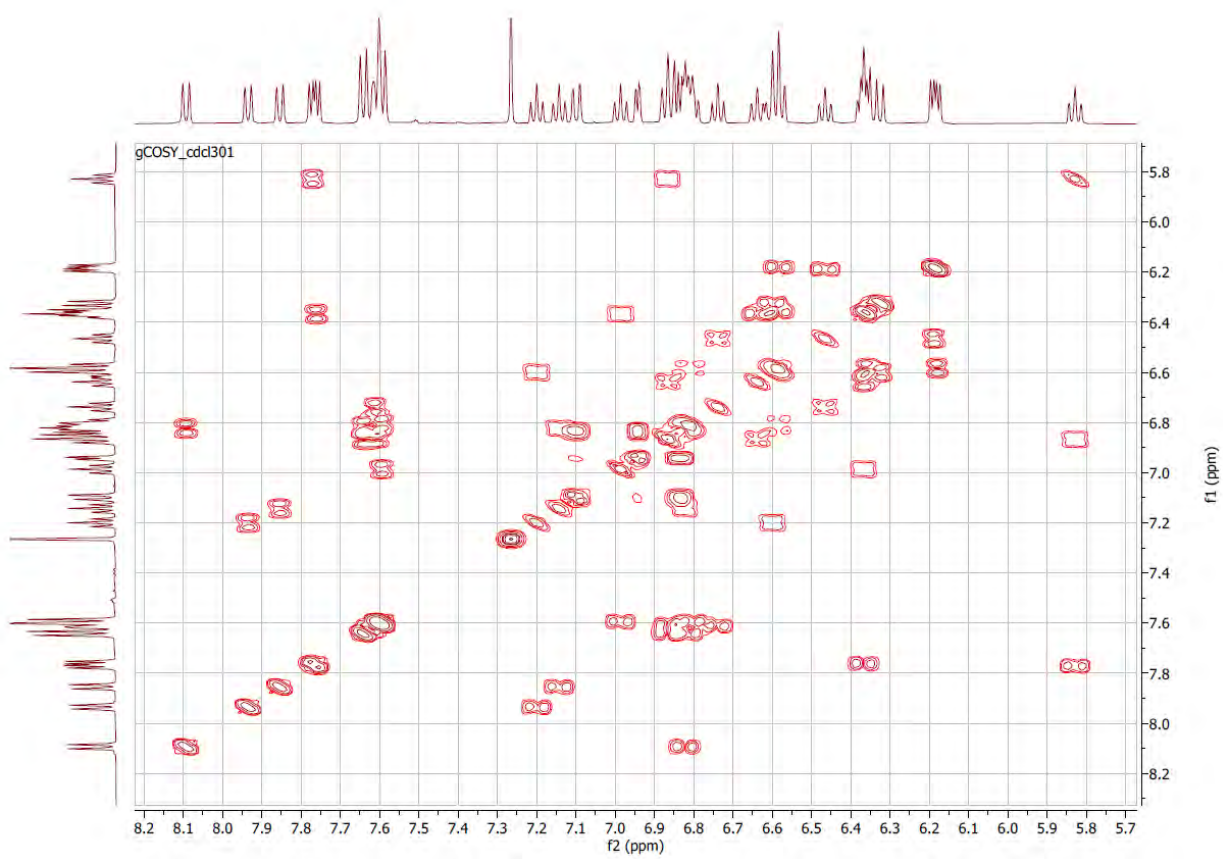


Figure S3e. COSY spectrum of complex YY.

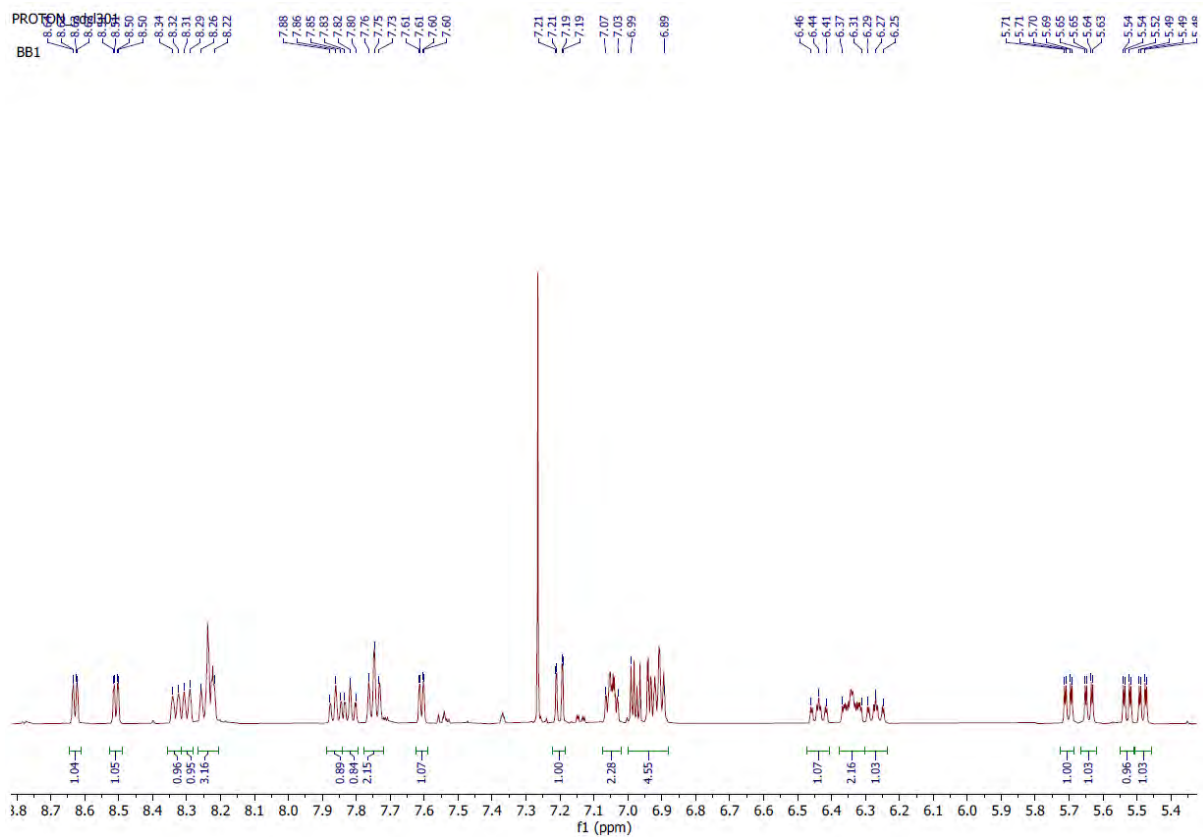
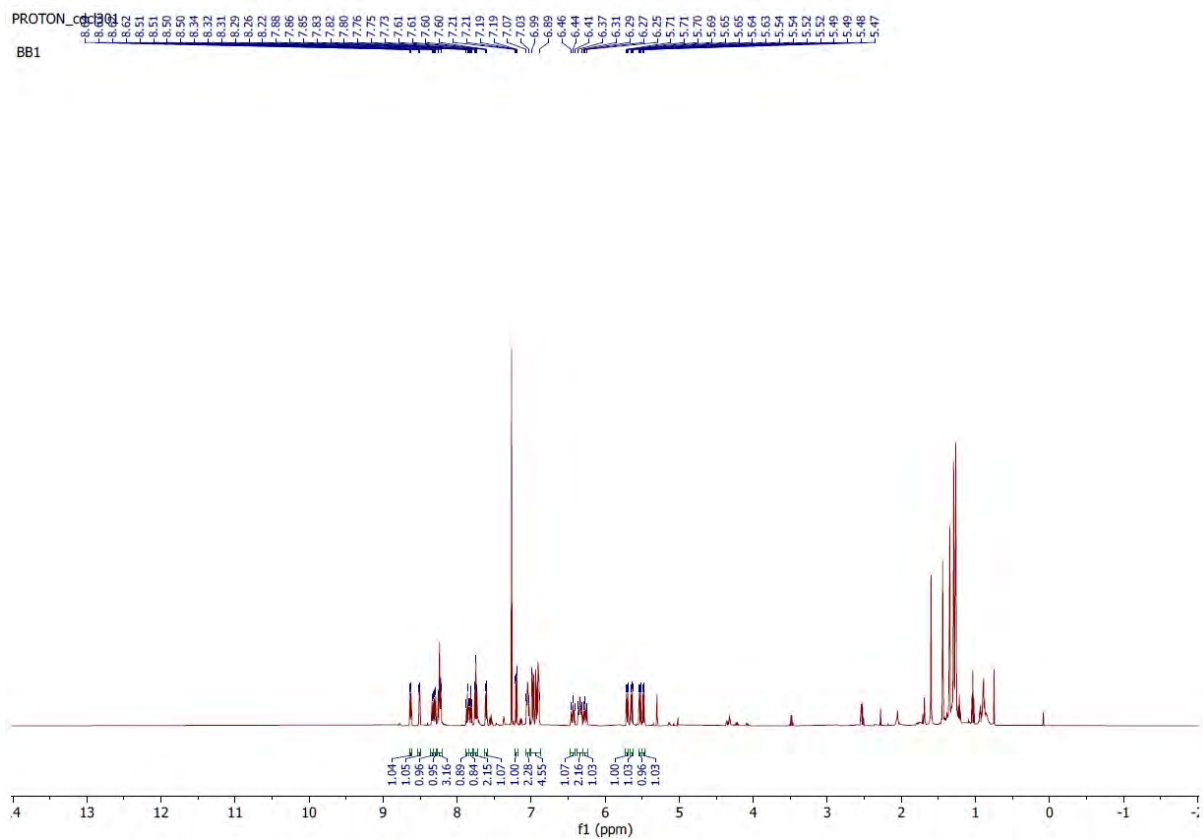


Figure S4a. ¹H NMR spectrum of complex BB1.

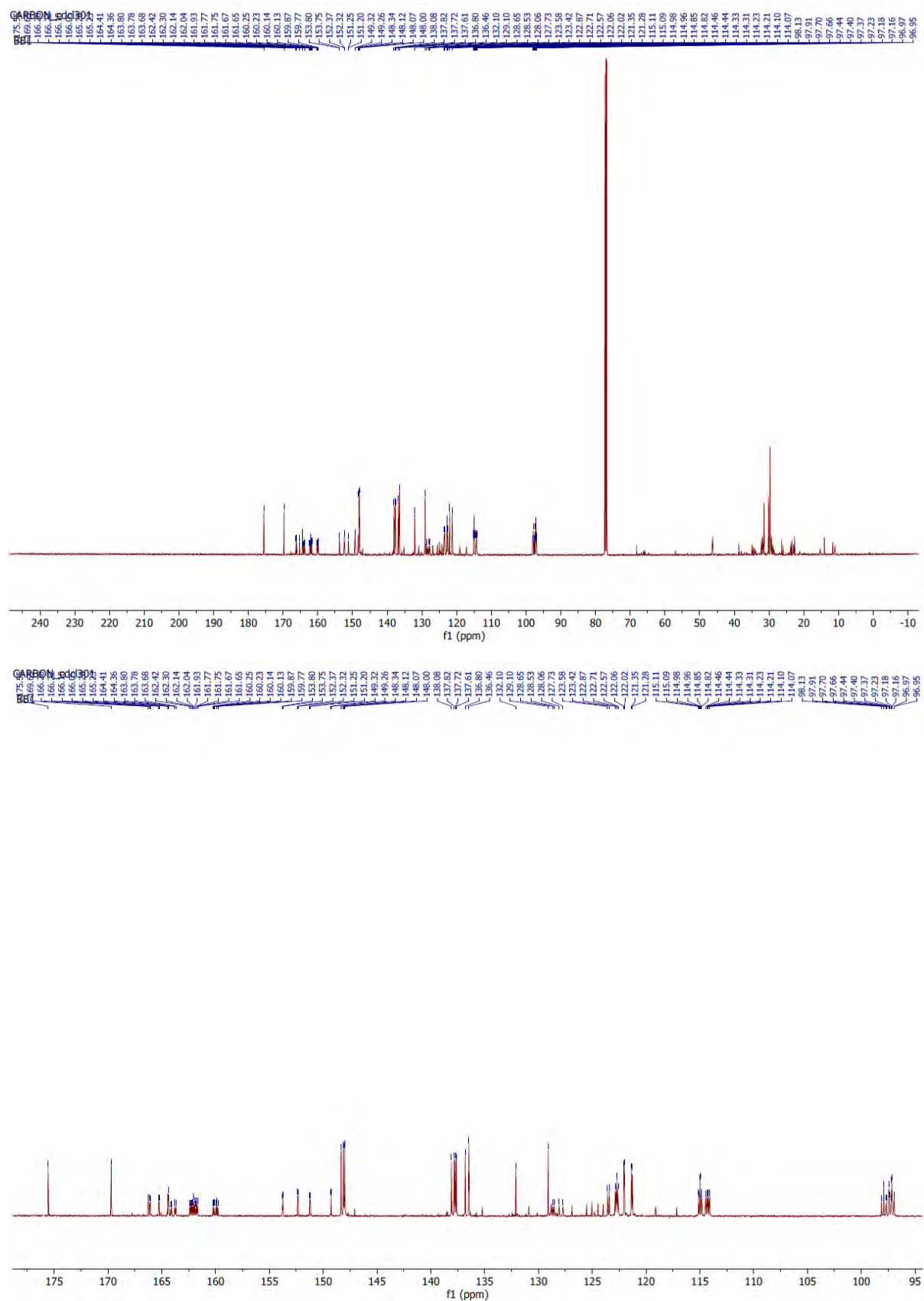


Figure S4b. ^{13}C NMR spectrum of complex **BB1**.

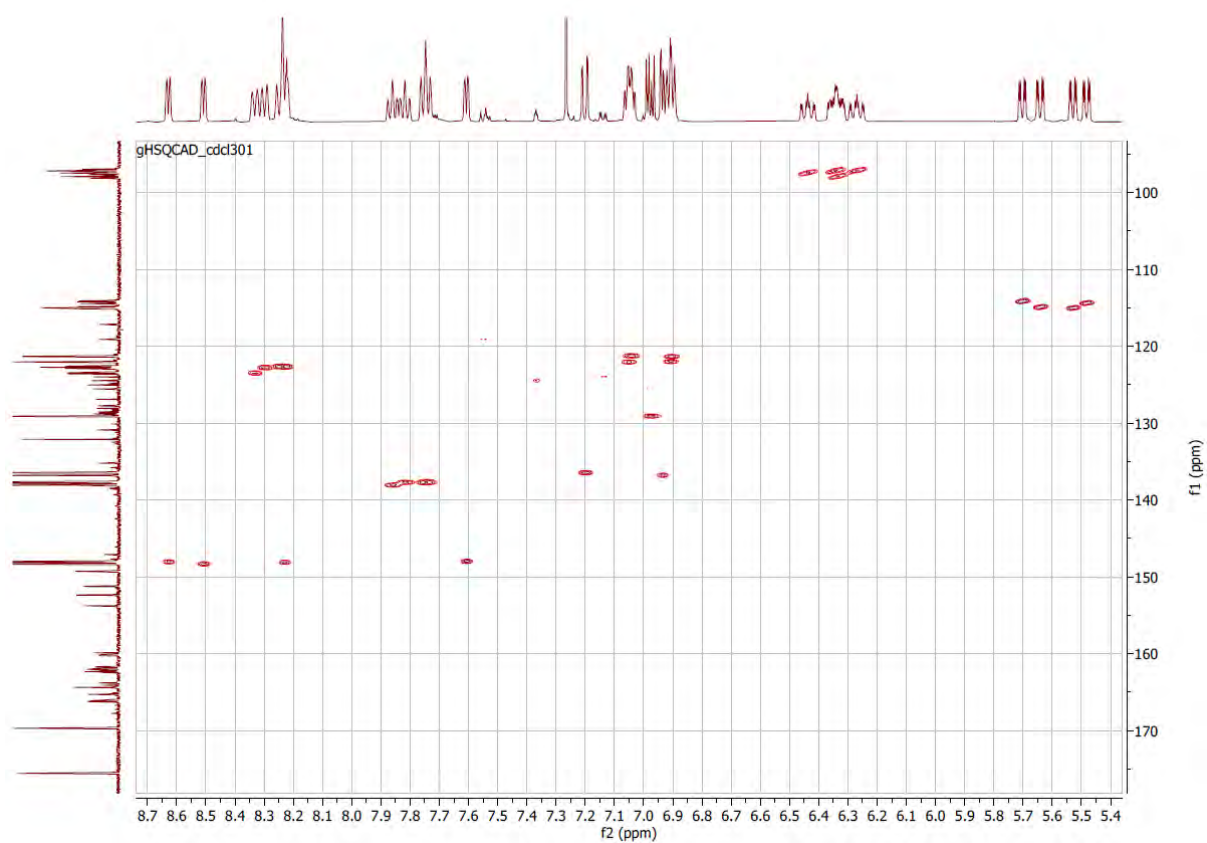


Figure S4c. HSQC spectrum of complex **BB1**.

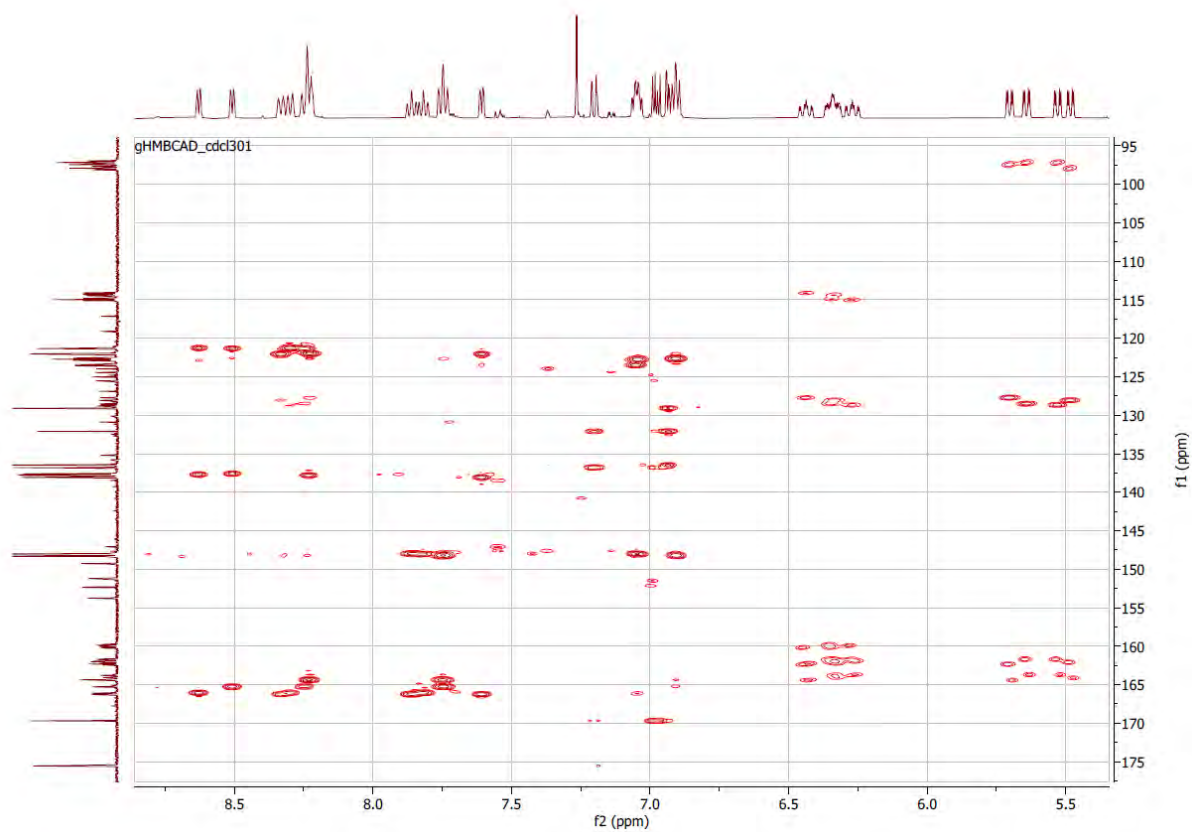


Figure S4d. HMBC spectrum of complex **BB1**.

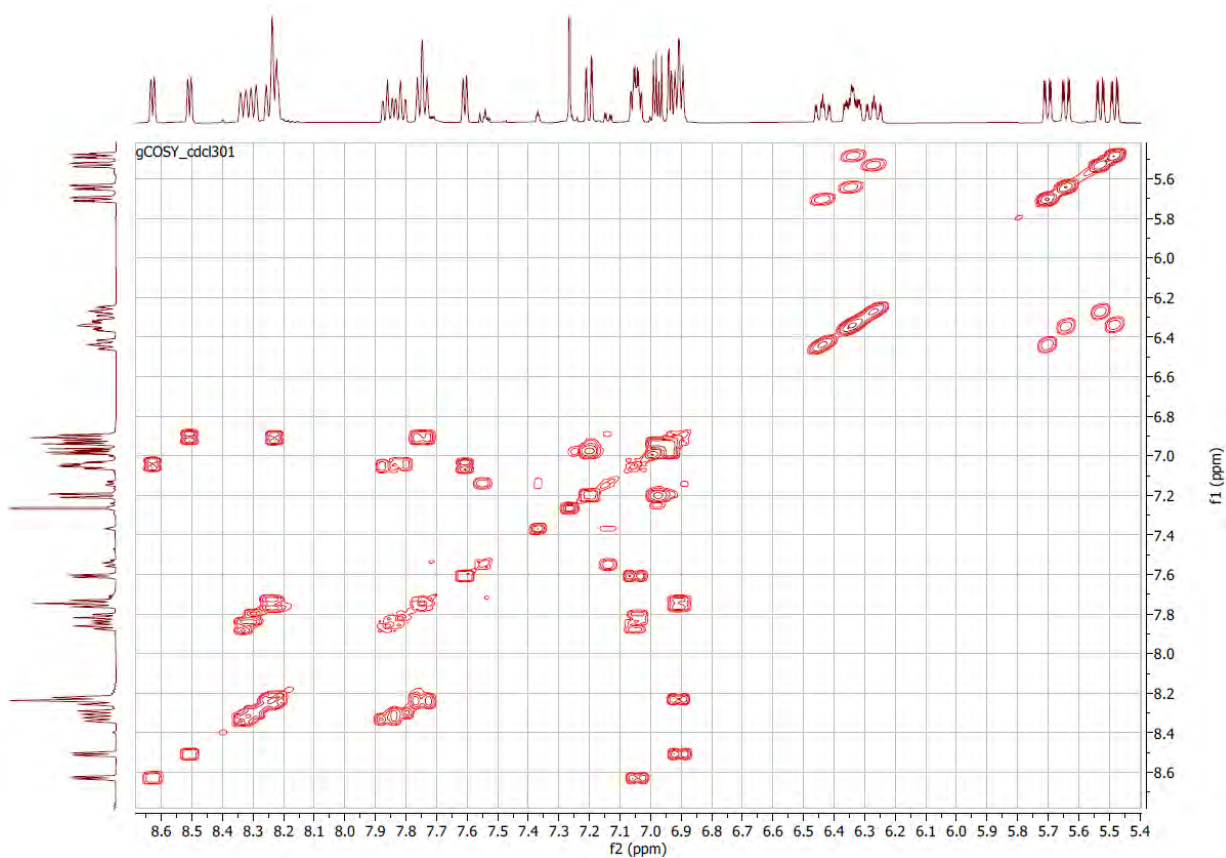


Figure S4e. COSY spectrum of complex **BB1**.

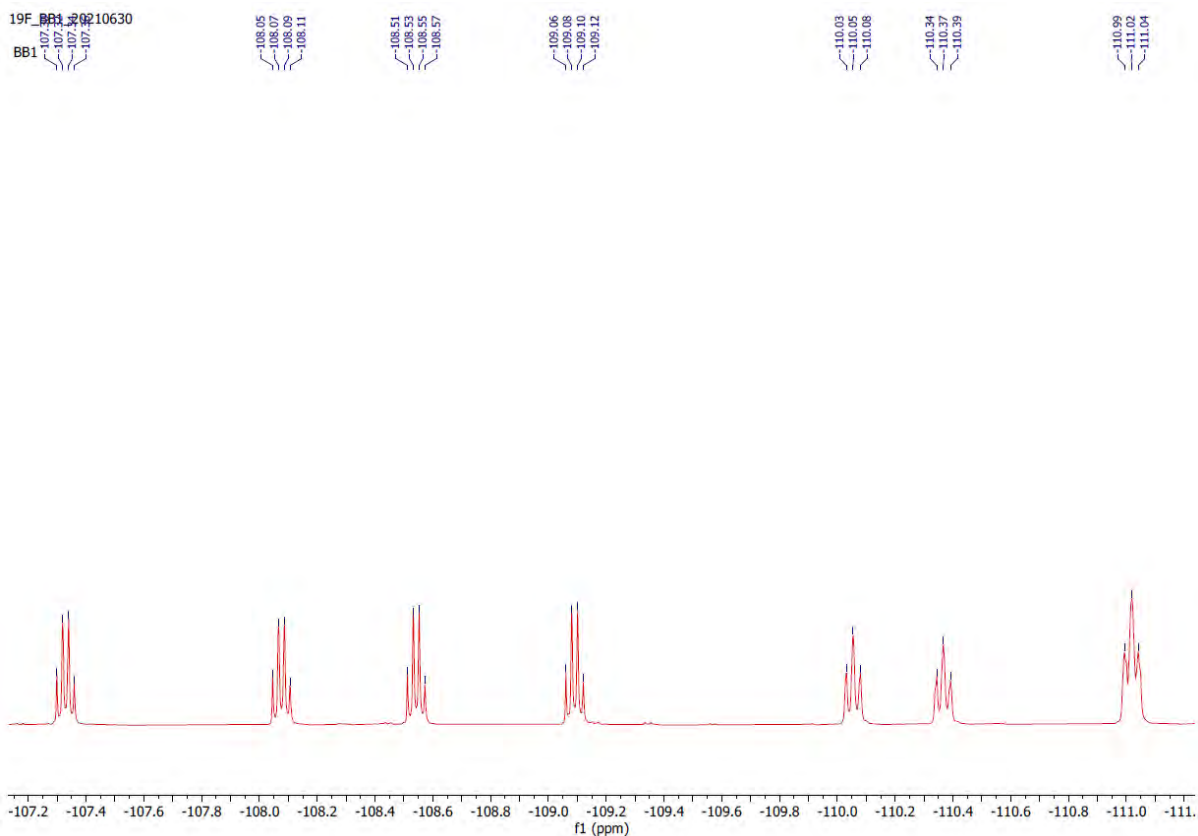


Figure S4f. ^{19}F NMR spectrum of complex **BB1**.

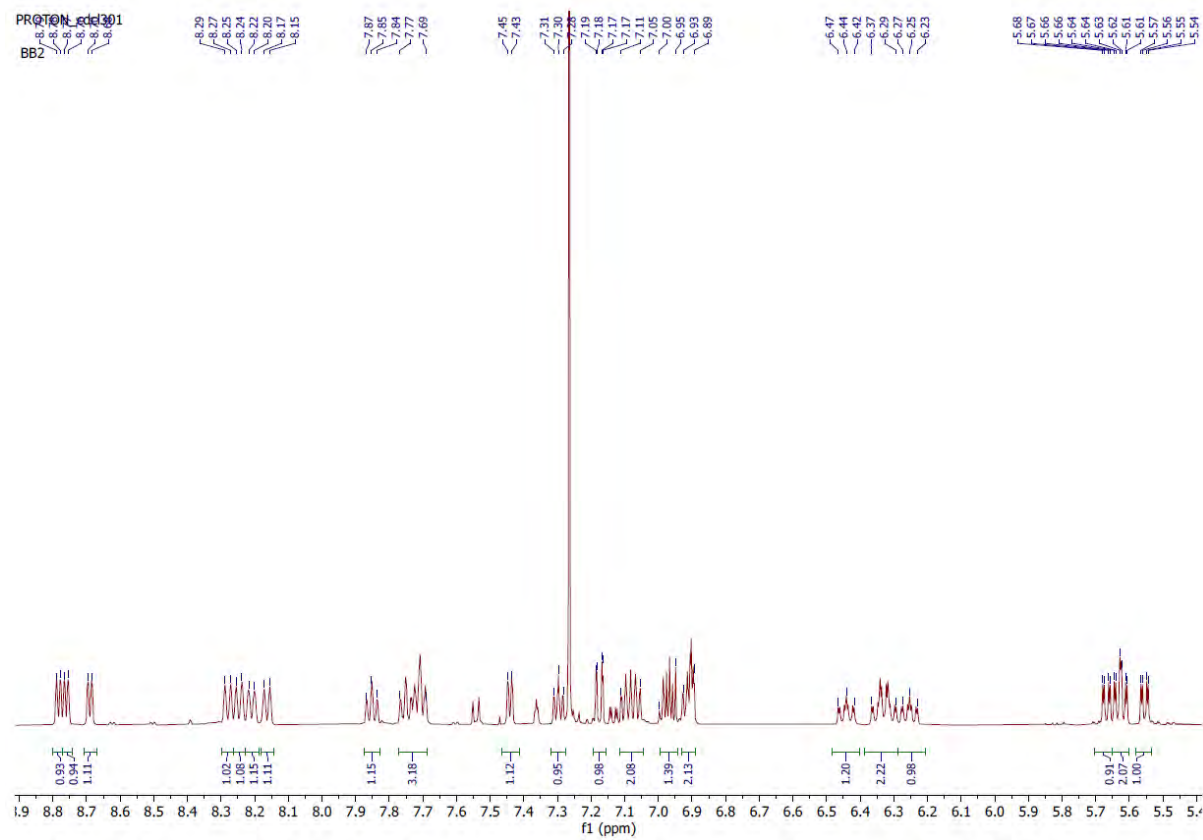
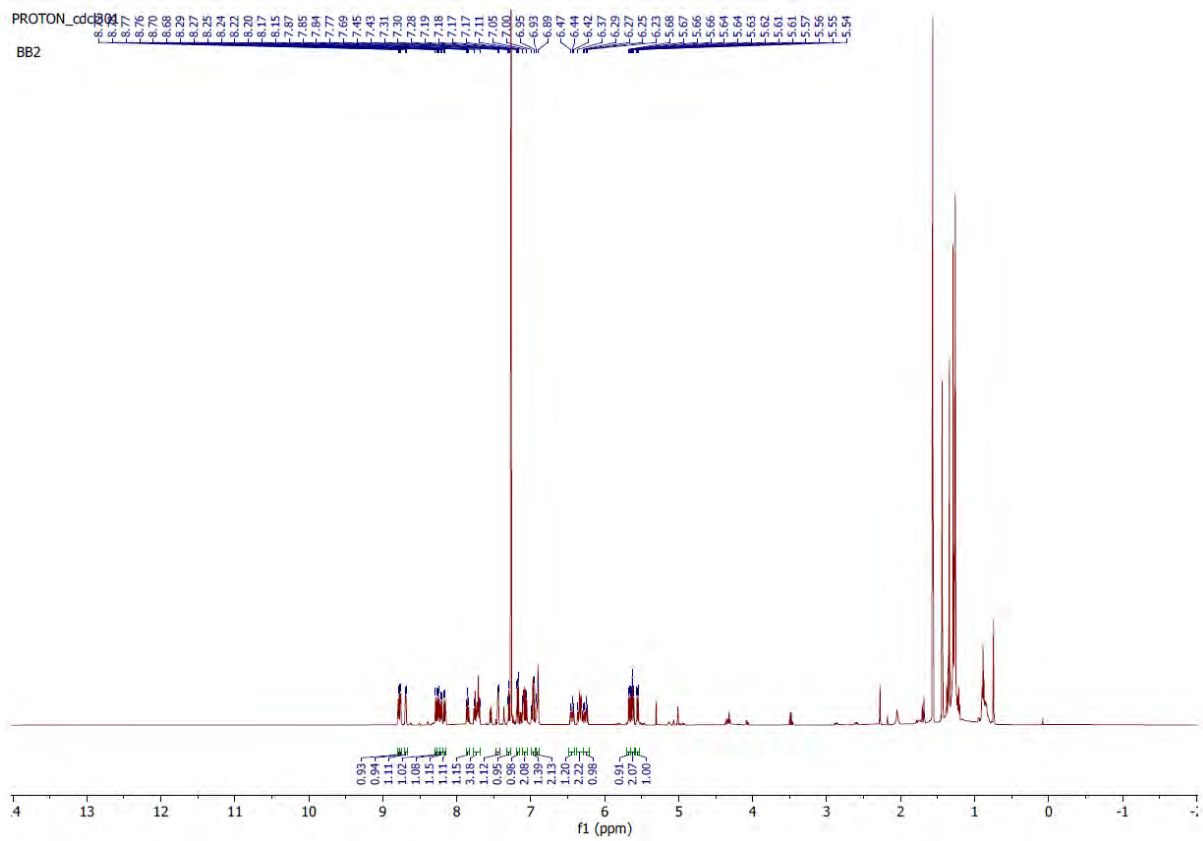


Figure S5a. ¹H NMR spectrum of complex **BB2**.

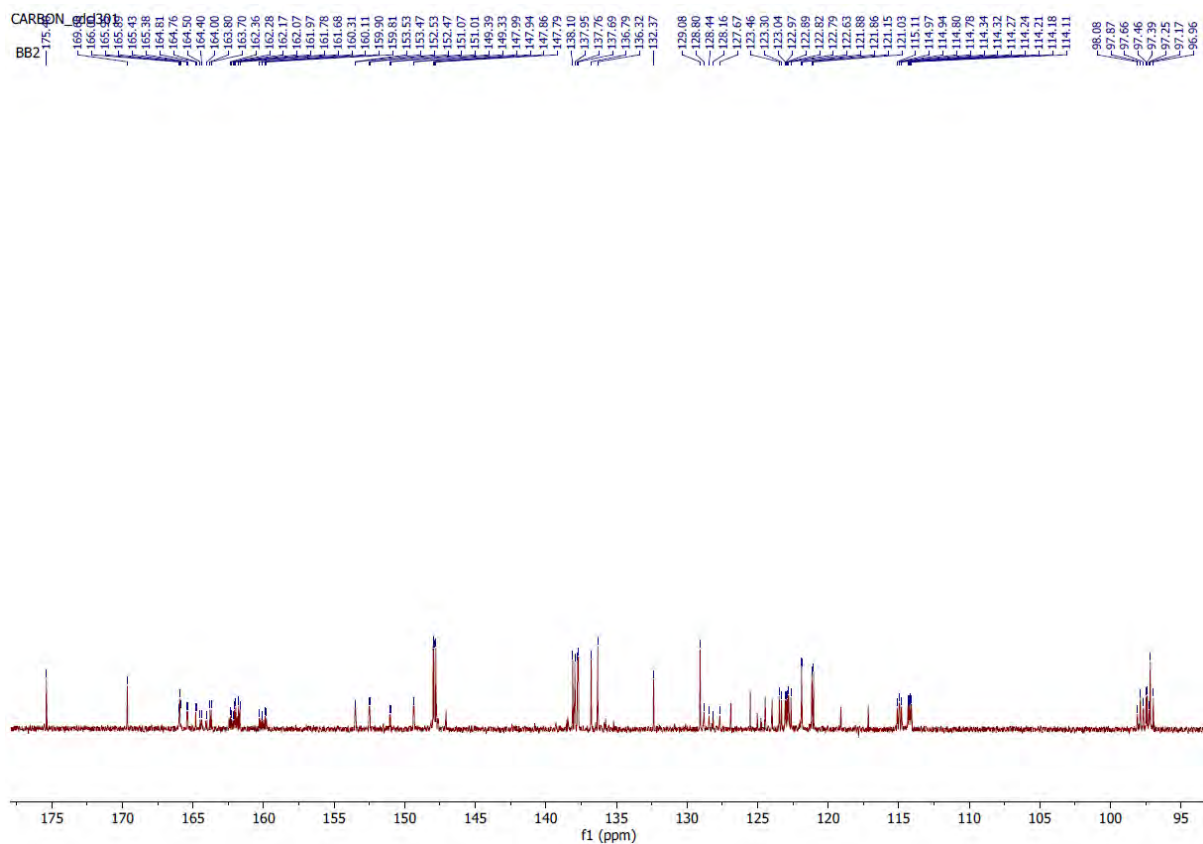
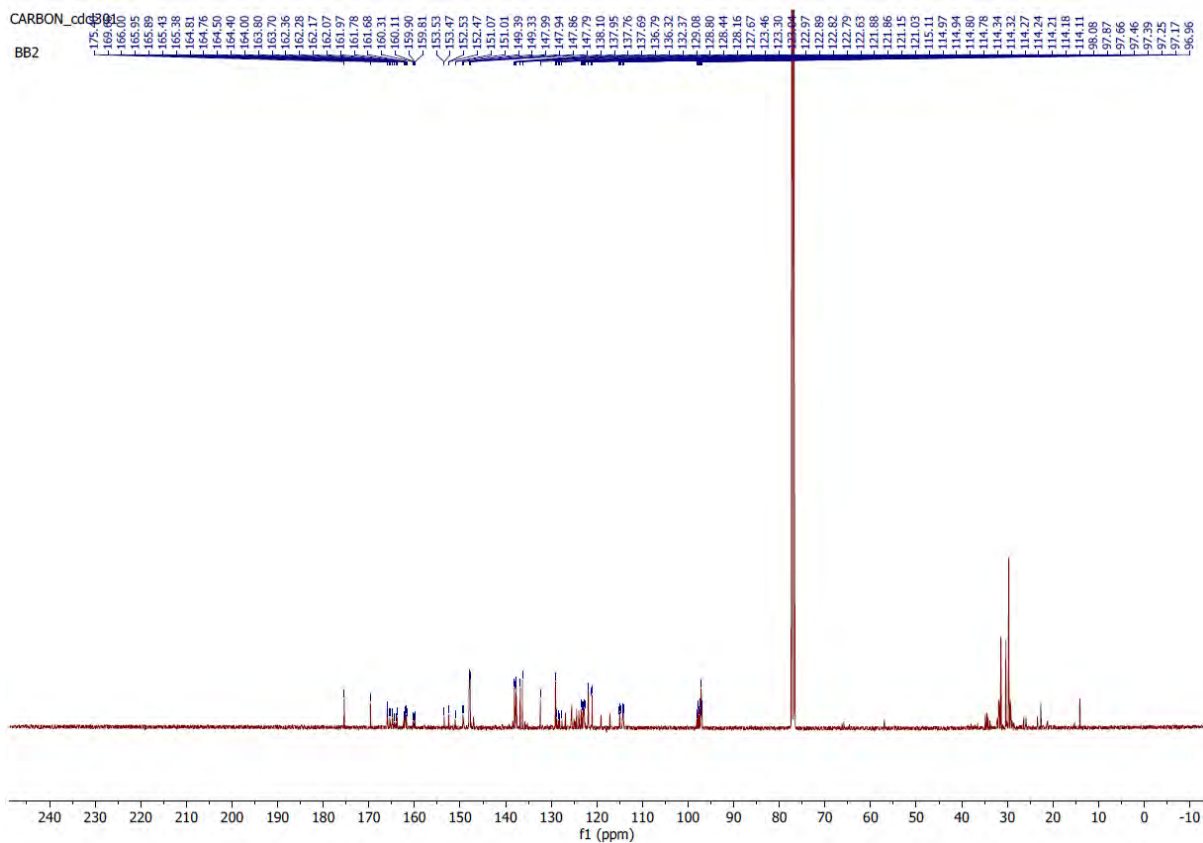


Figure S5b. ^{13}C NMR spectrum of complex BB2.

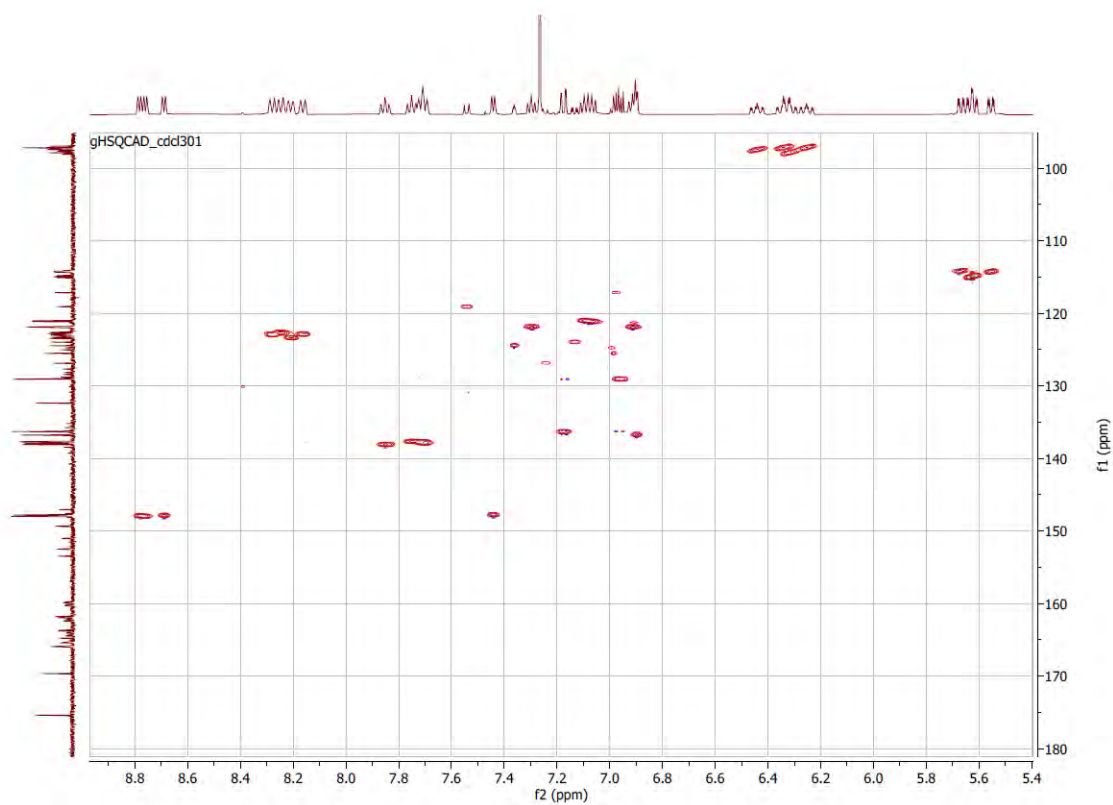


Figure S5c. HSQC spectrum of complex **BB2**.

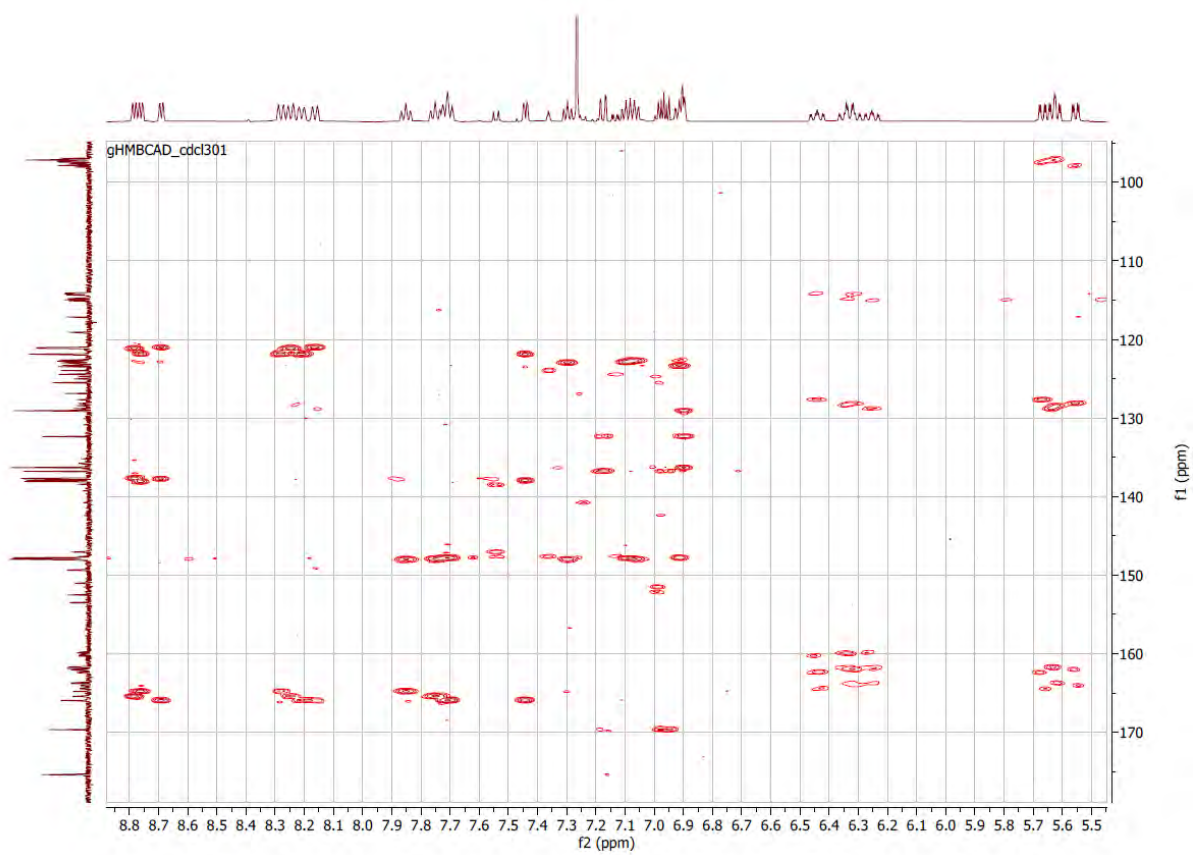


Figure S5d. HMBC spectrum of complex **BB2**.

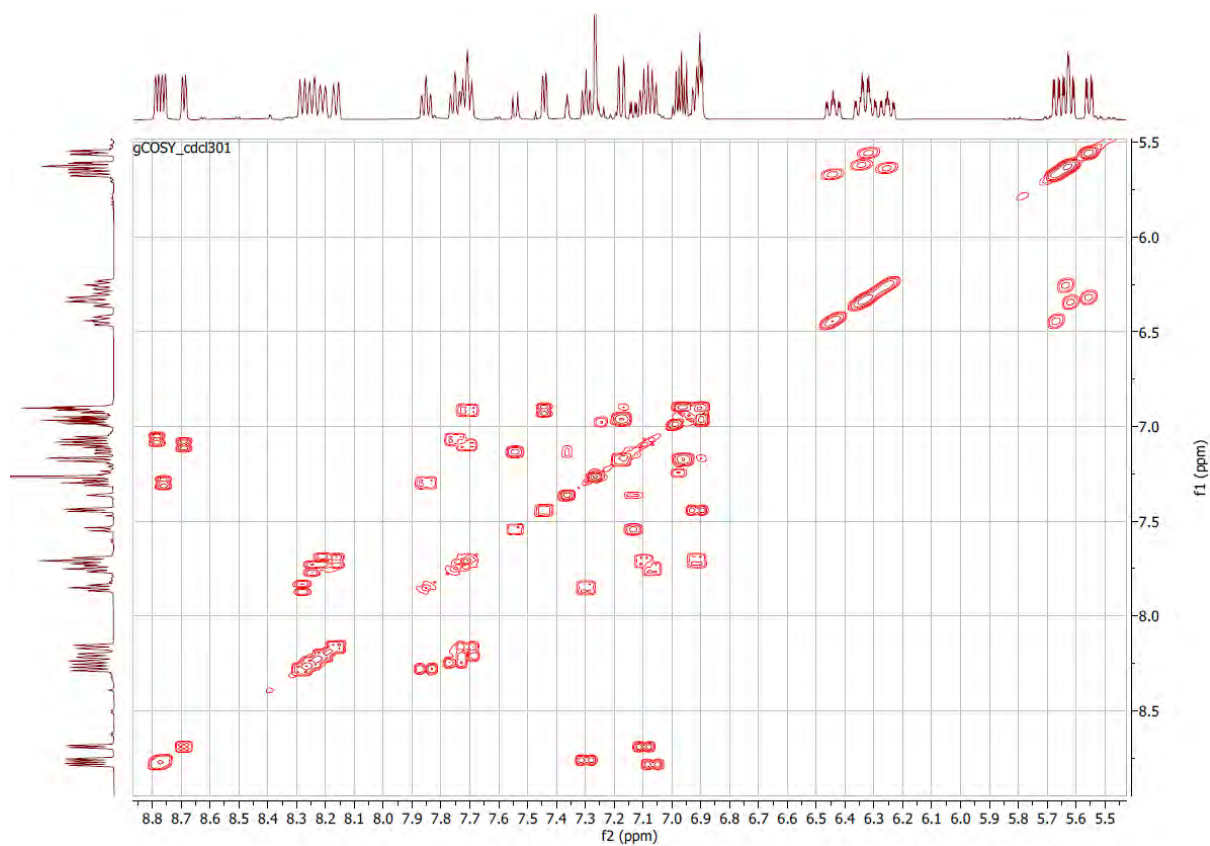


Figure S5e. COSY spectrum of complex **BB2**.

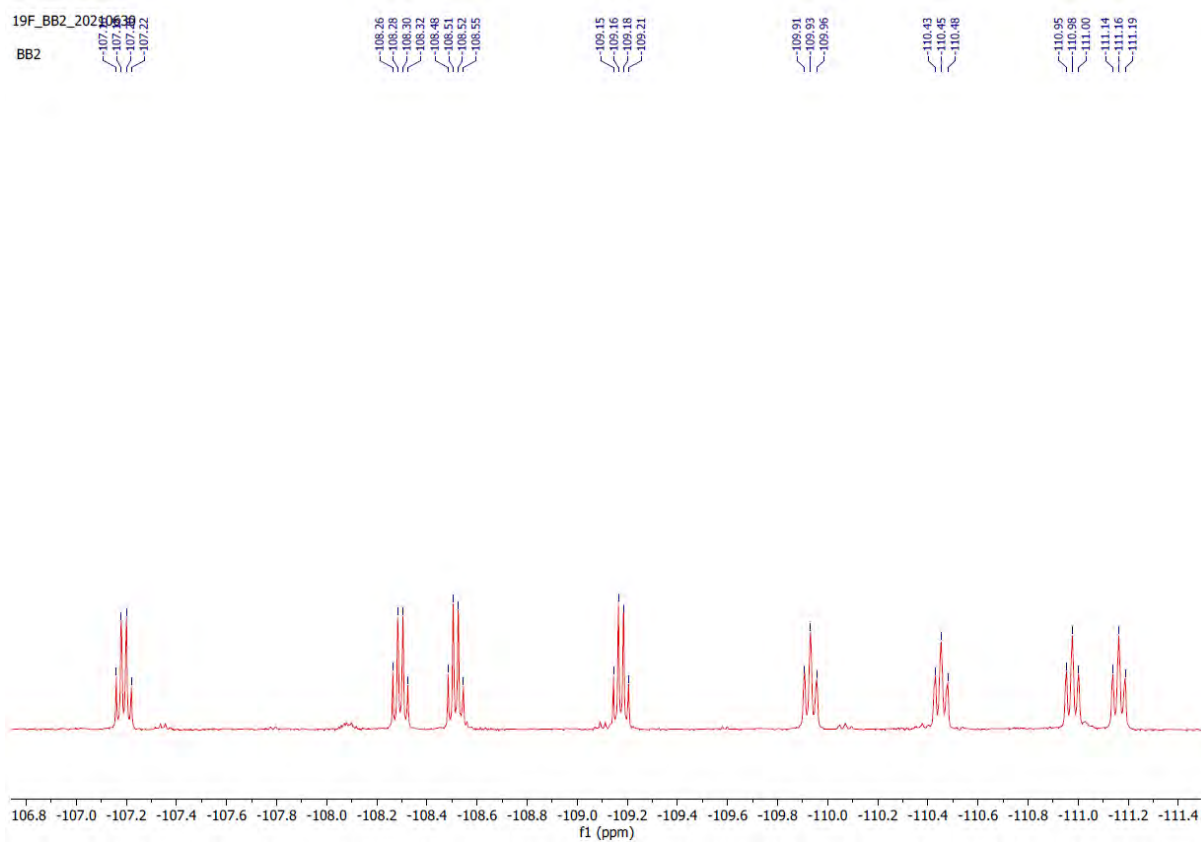


Figure S5f. ^{19}F NMR spectrum of complex **BB2**.

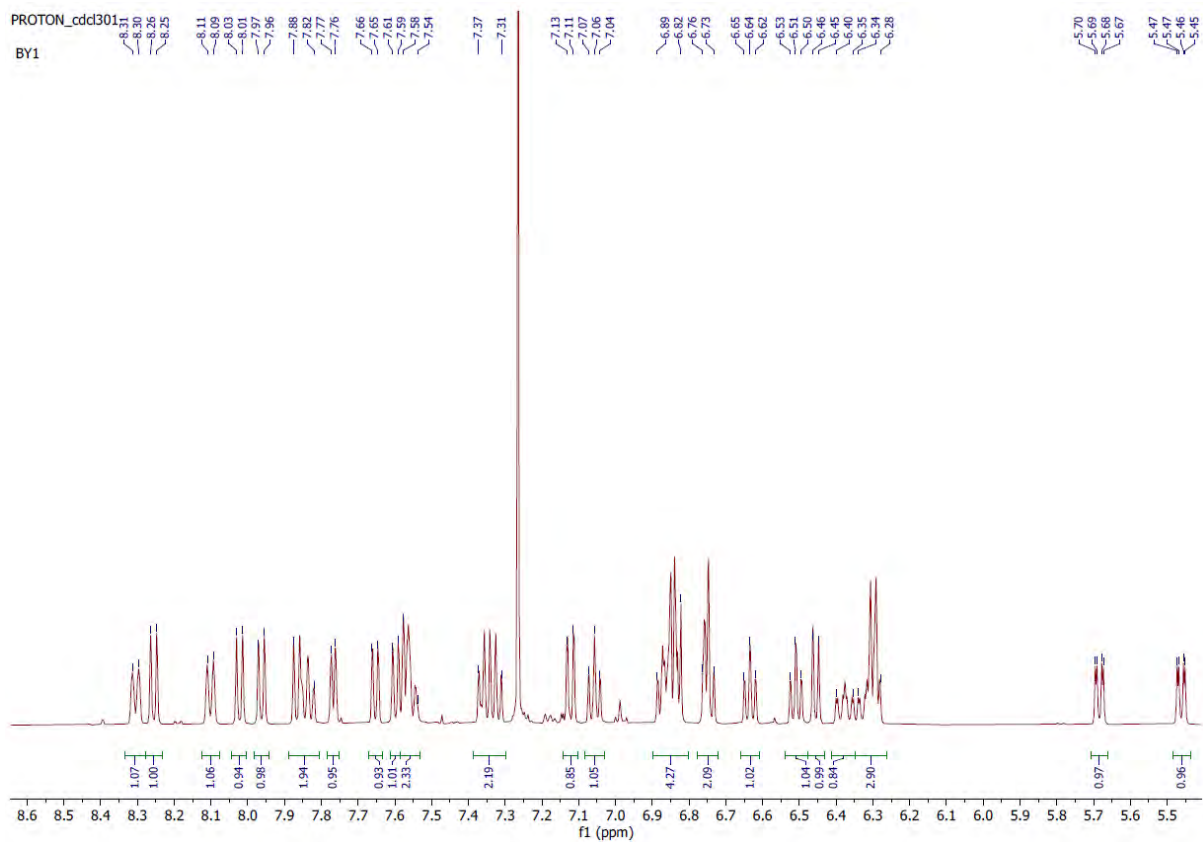
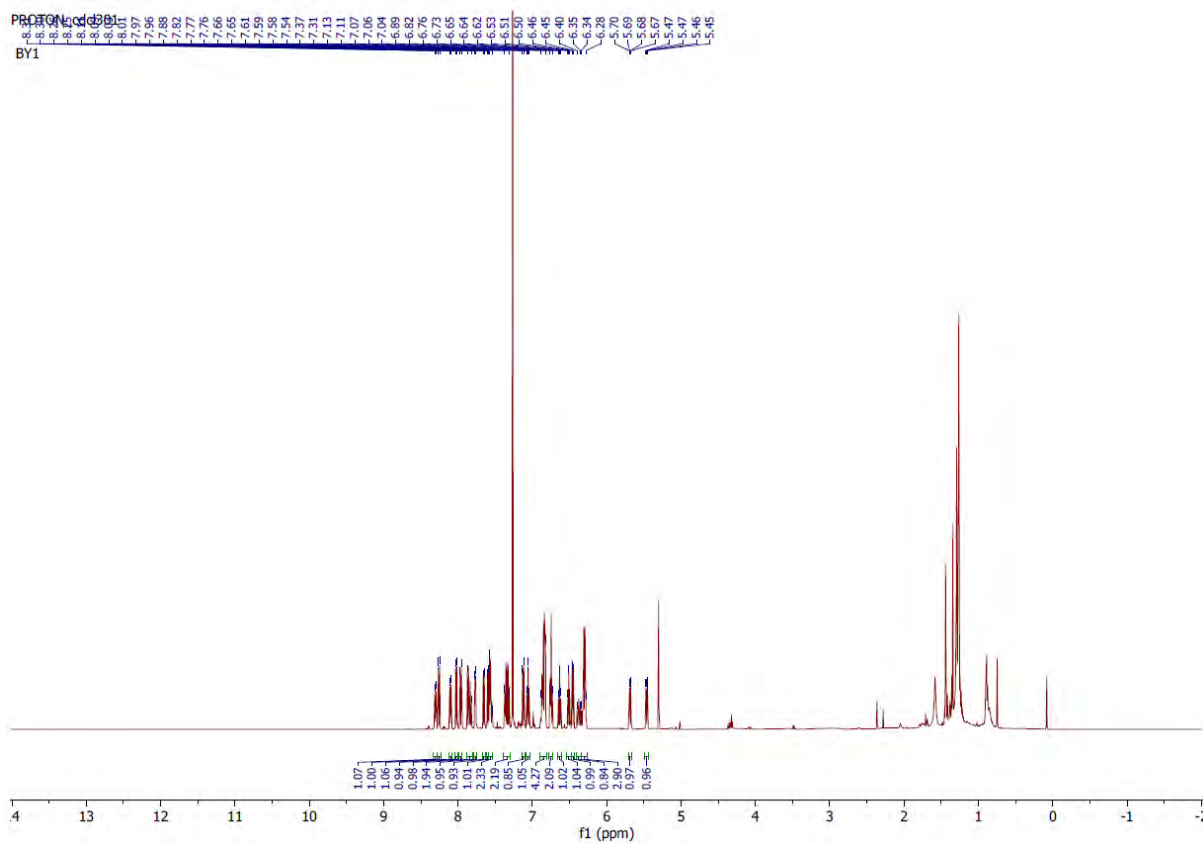


Figure S6a. ¹H NMR spectrum of complex **BY1**.

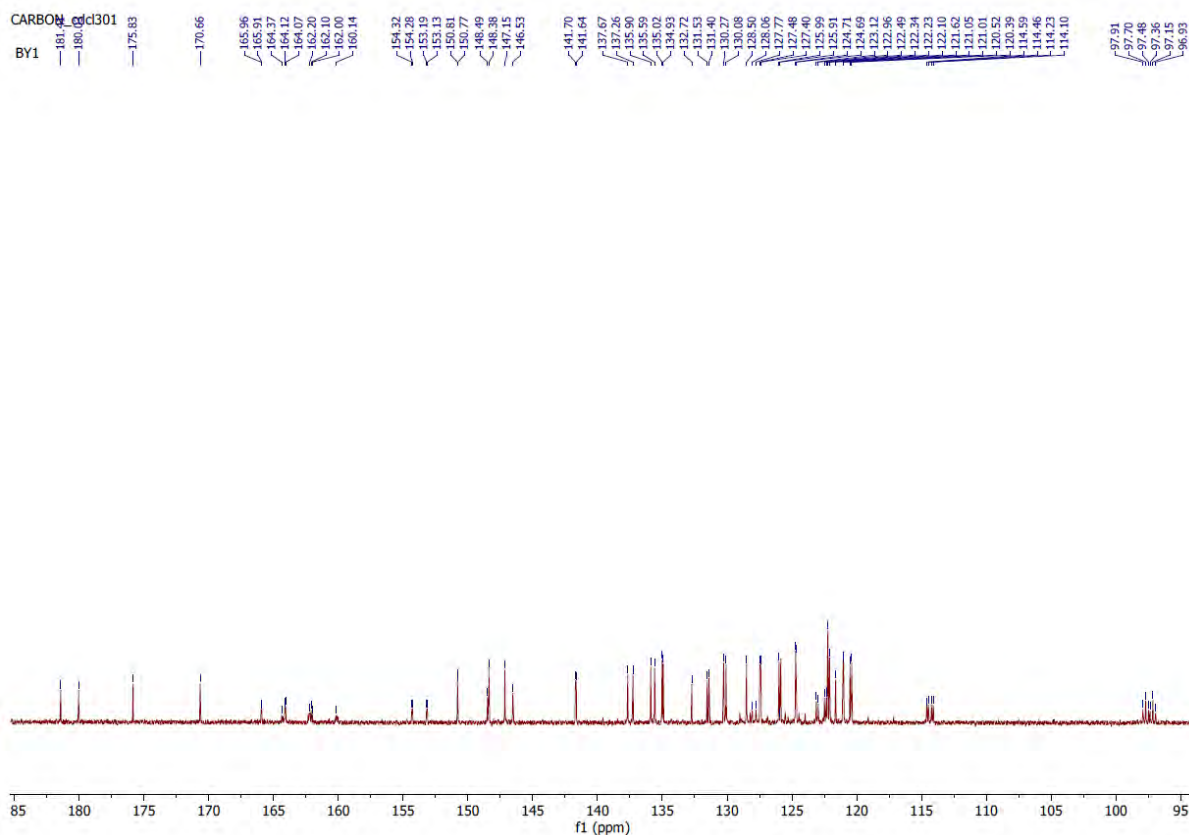
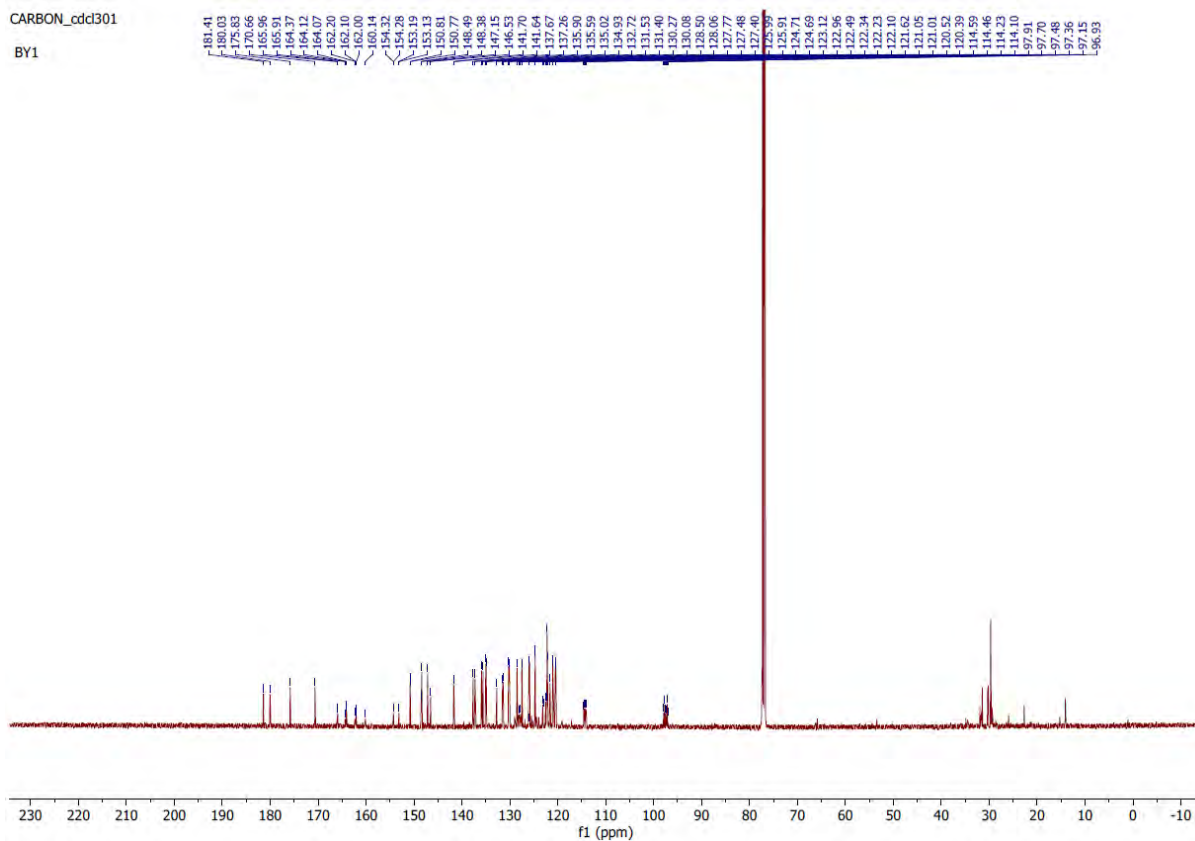


Figure S6b. ^{13}C NMR spectrum of complex BY1.

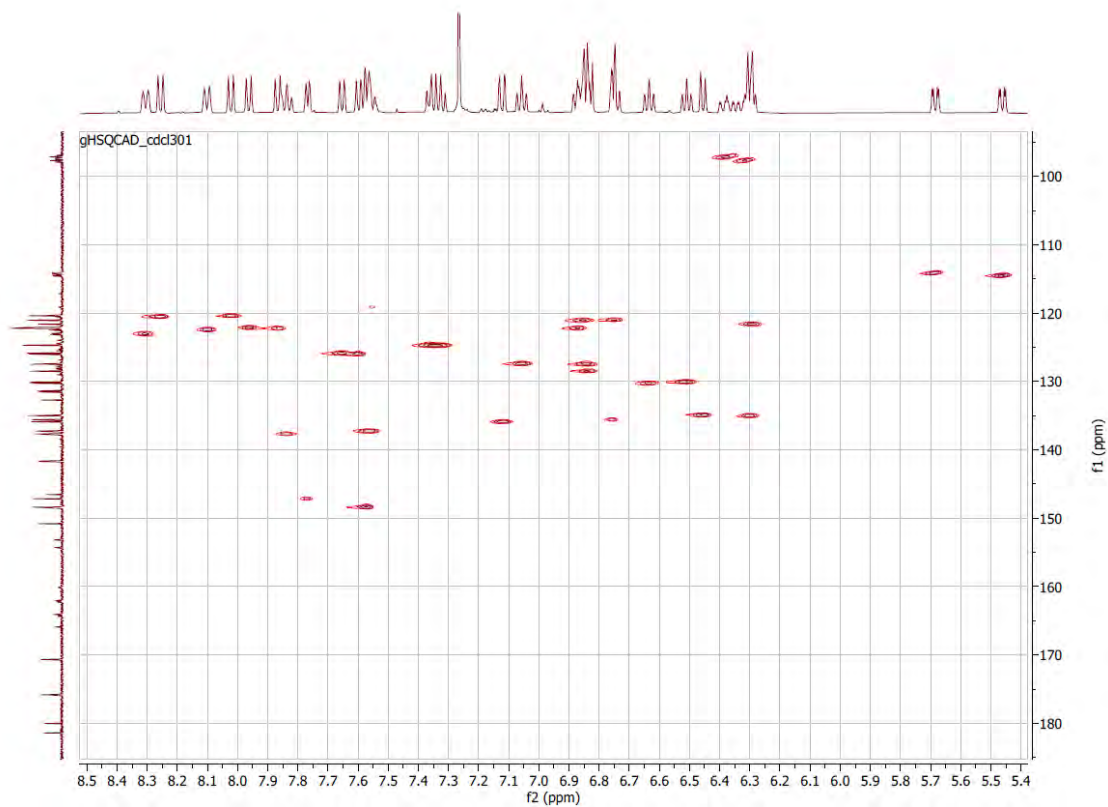


Figure S6c. HSQC spectrum of complex **BY1**.

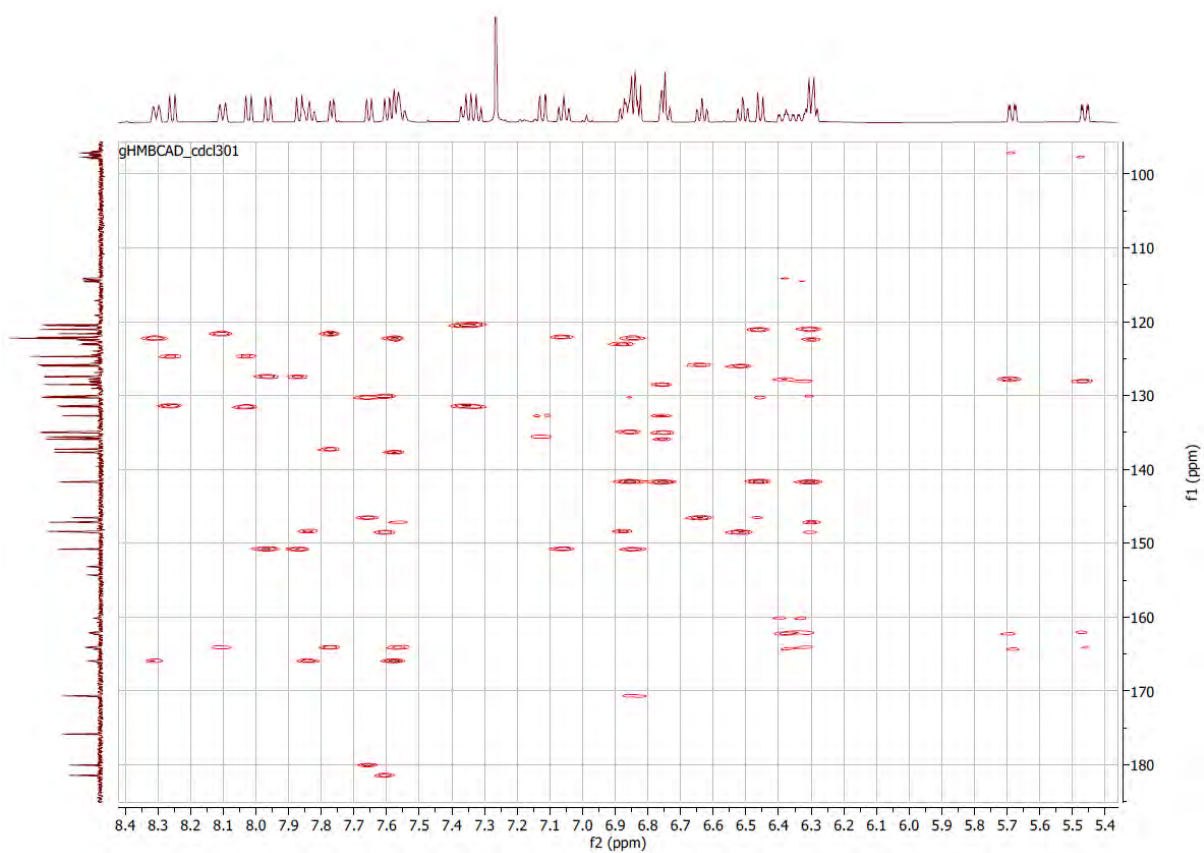


Figure S6d. HMBC spectrum of complex **BY1**.

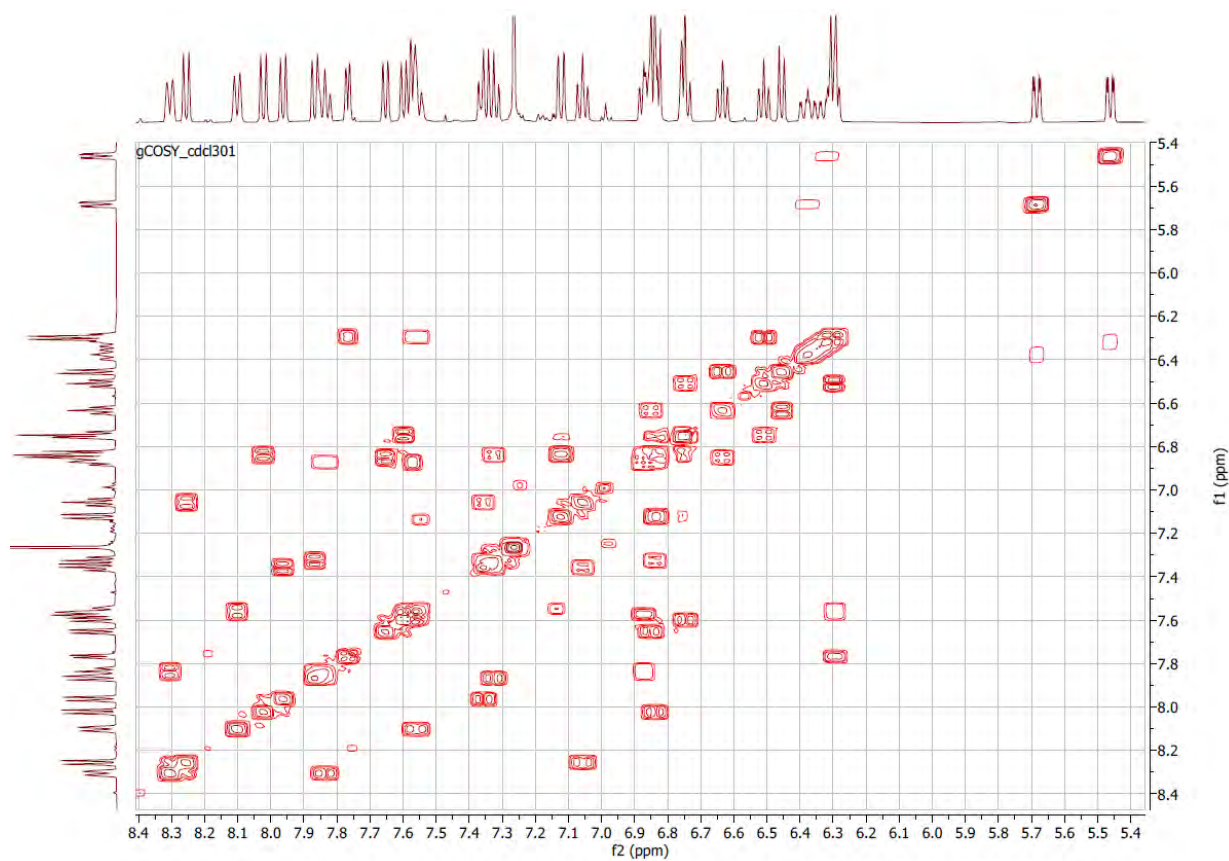


Figure S6e. COSY spectrum of complex **BY1**.

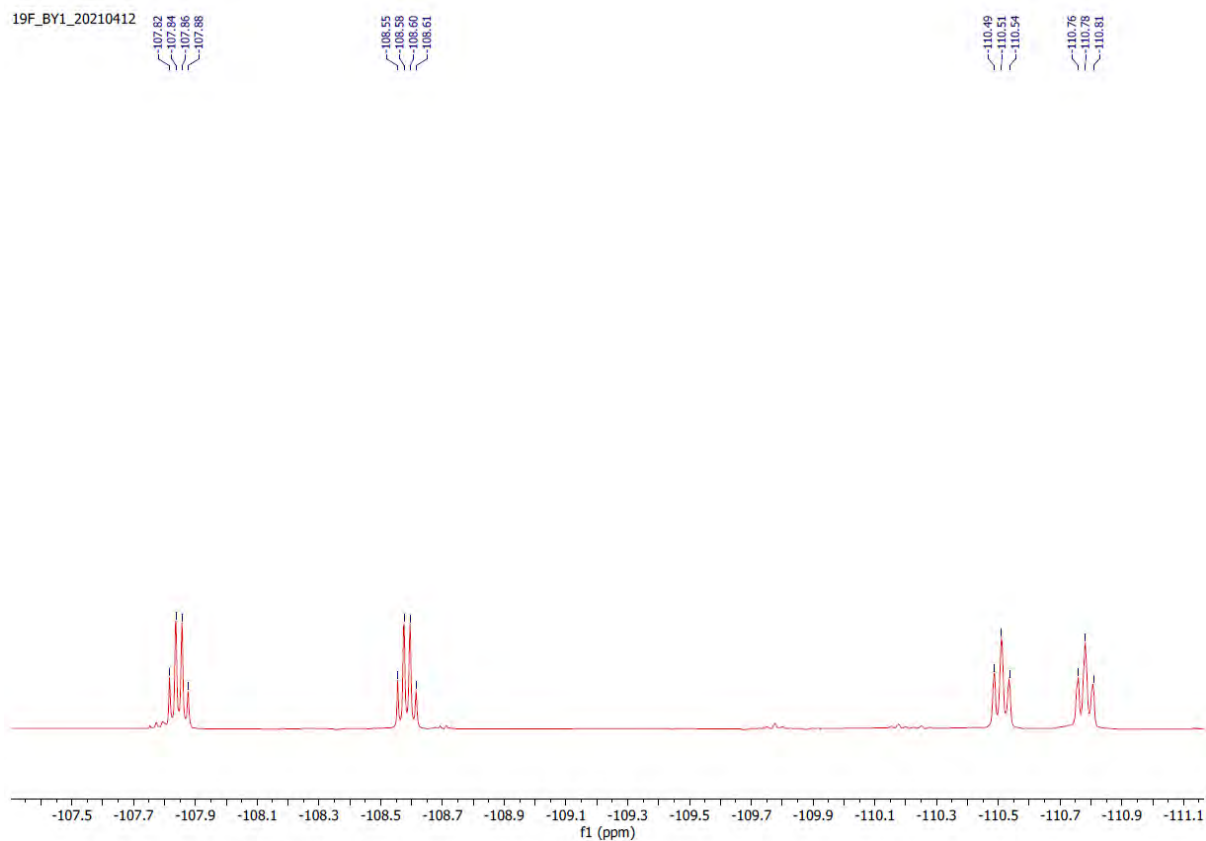


Figure S6f. ^{19}F NMR spectrum of complex **BY1**.

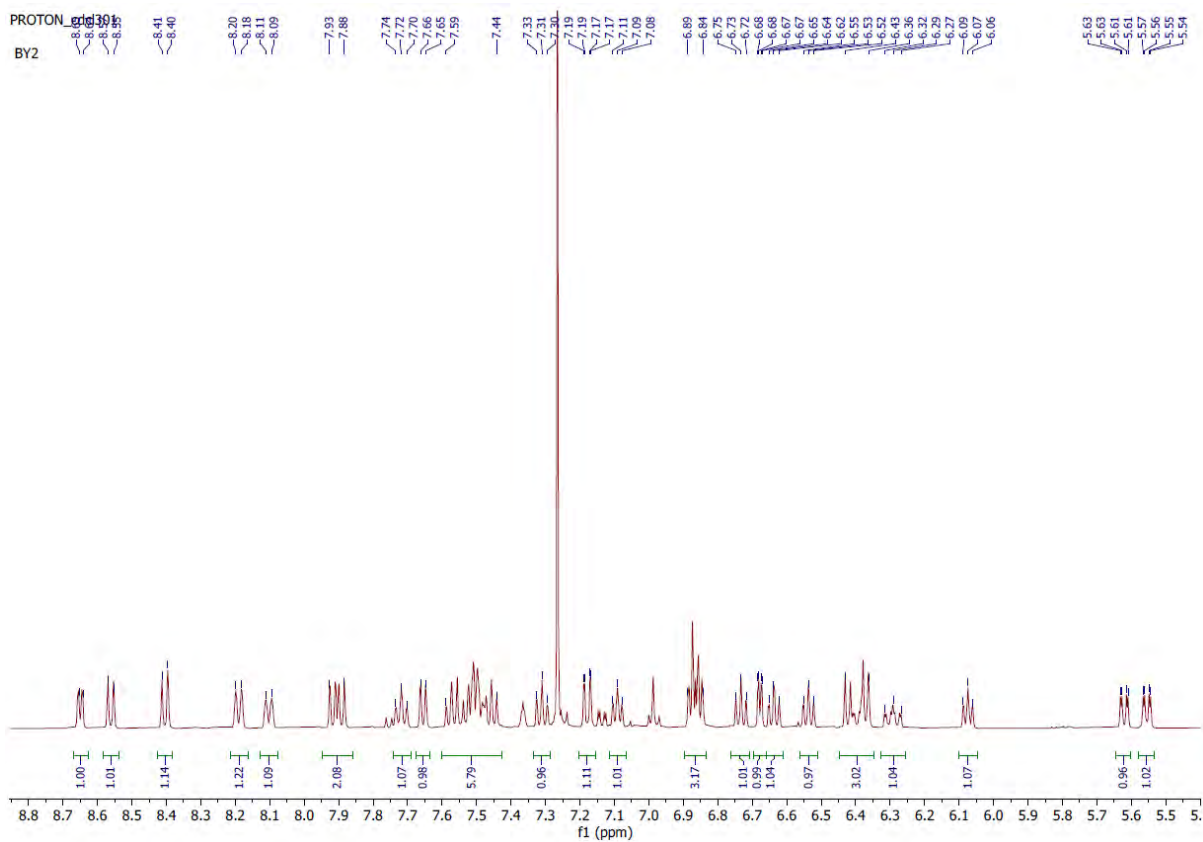
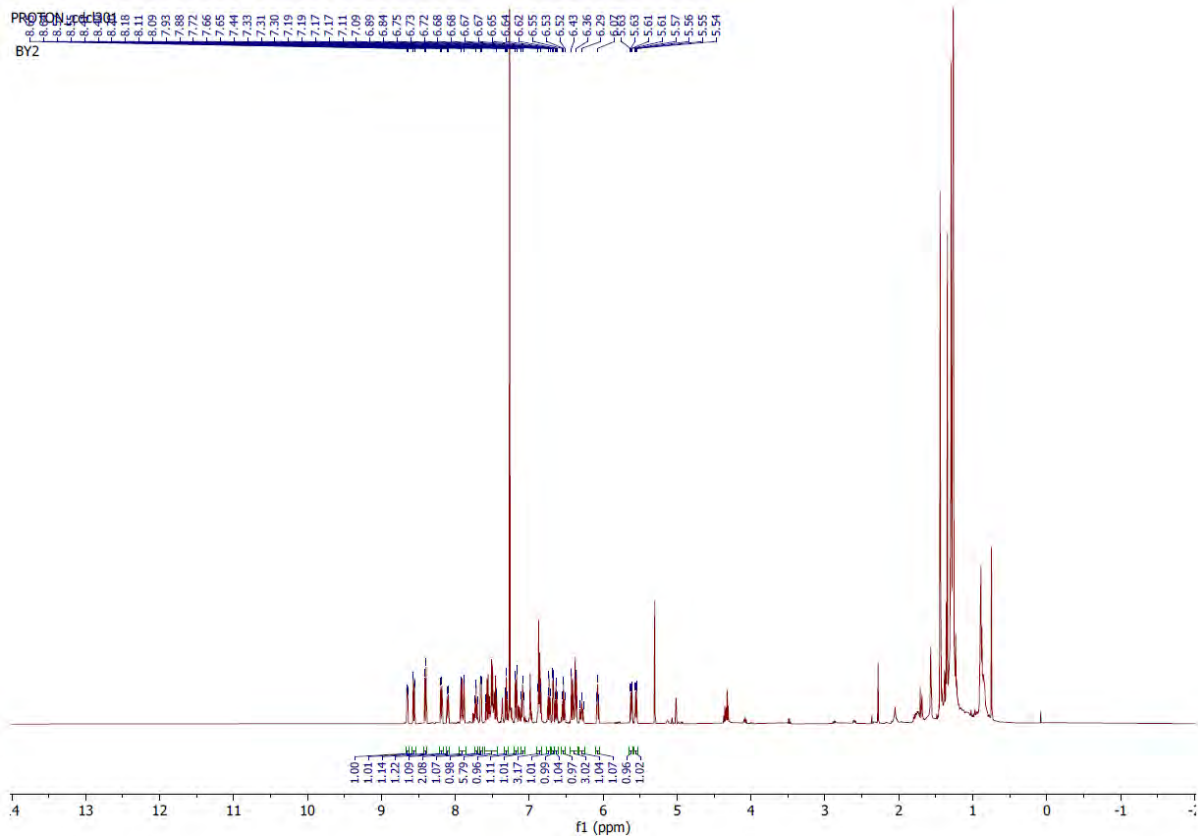


Figure S7a. ¹H NMR spectrum of complex BY2.

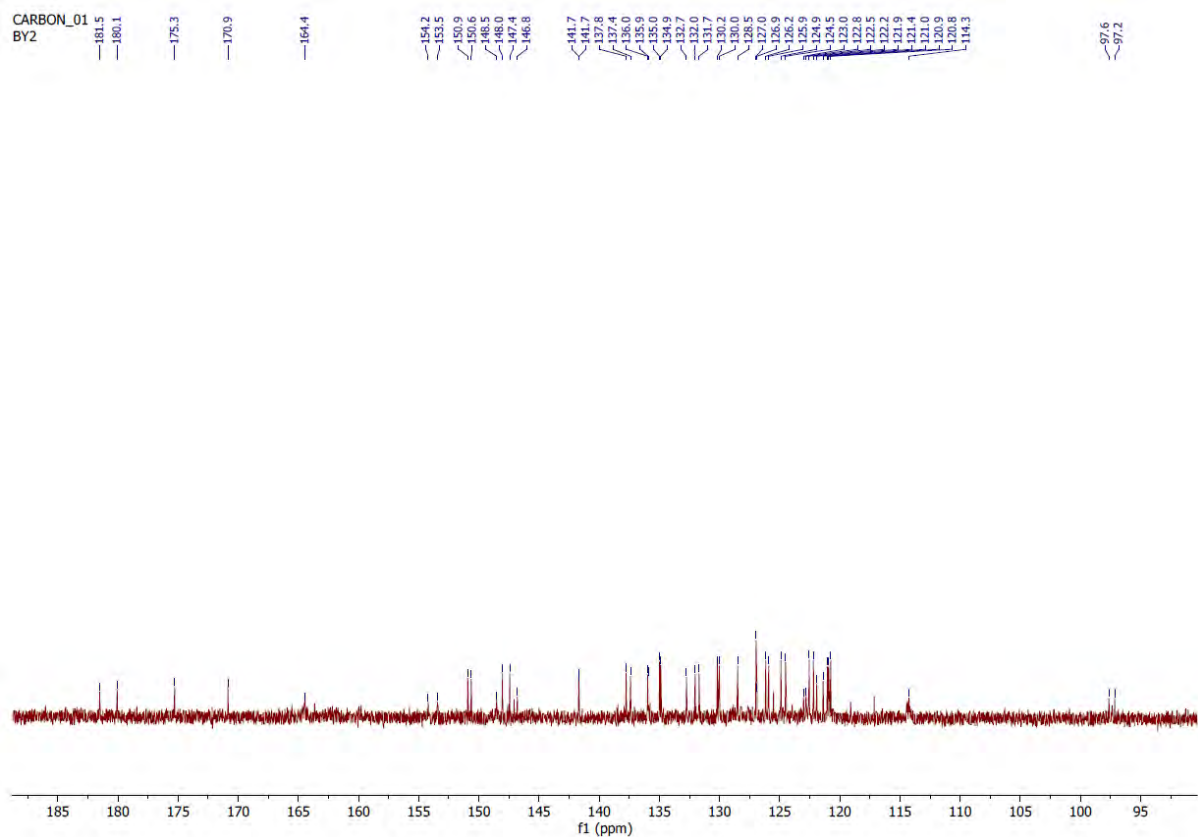
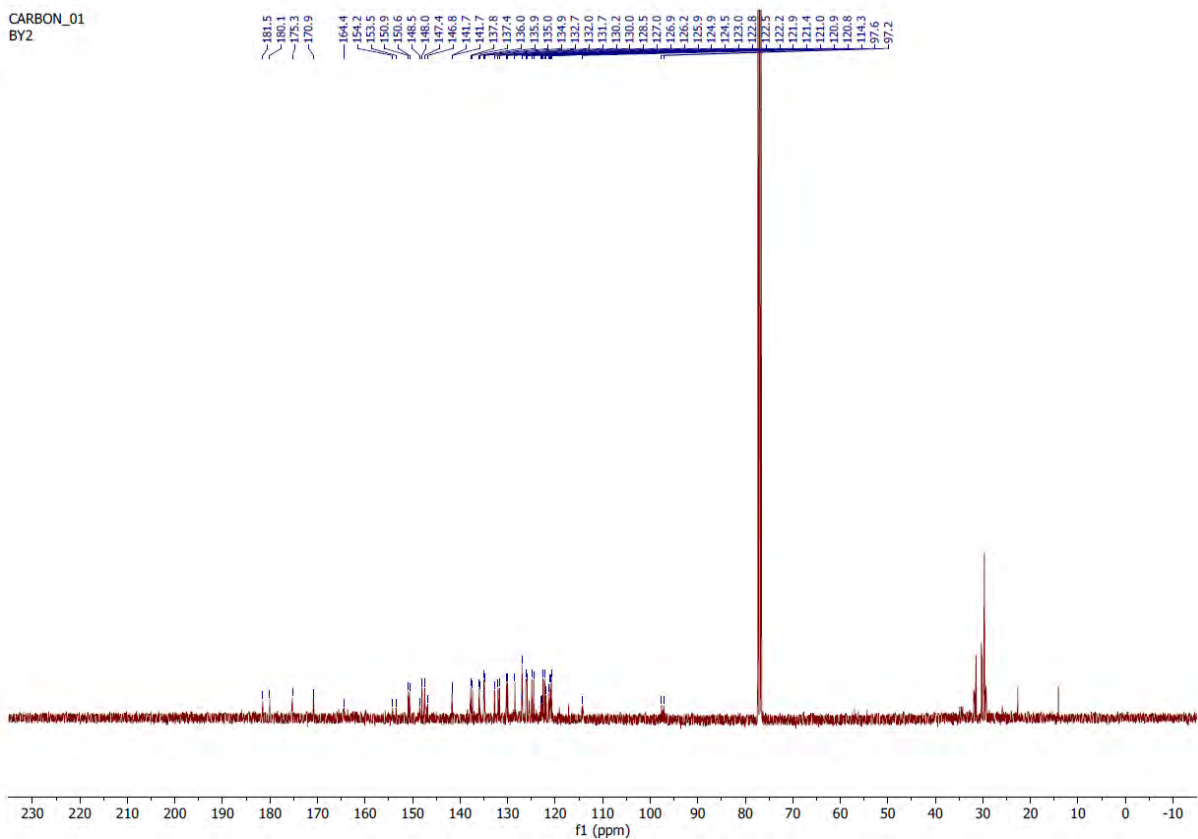


Figure S7b. ^{13}C NMR spectrum of complex BY2.

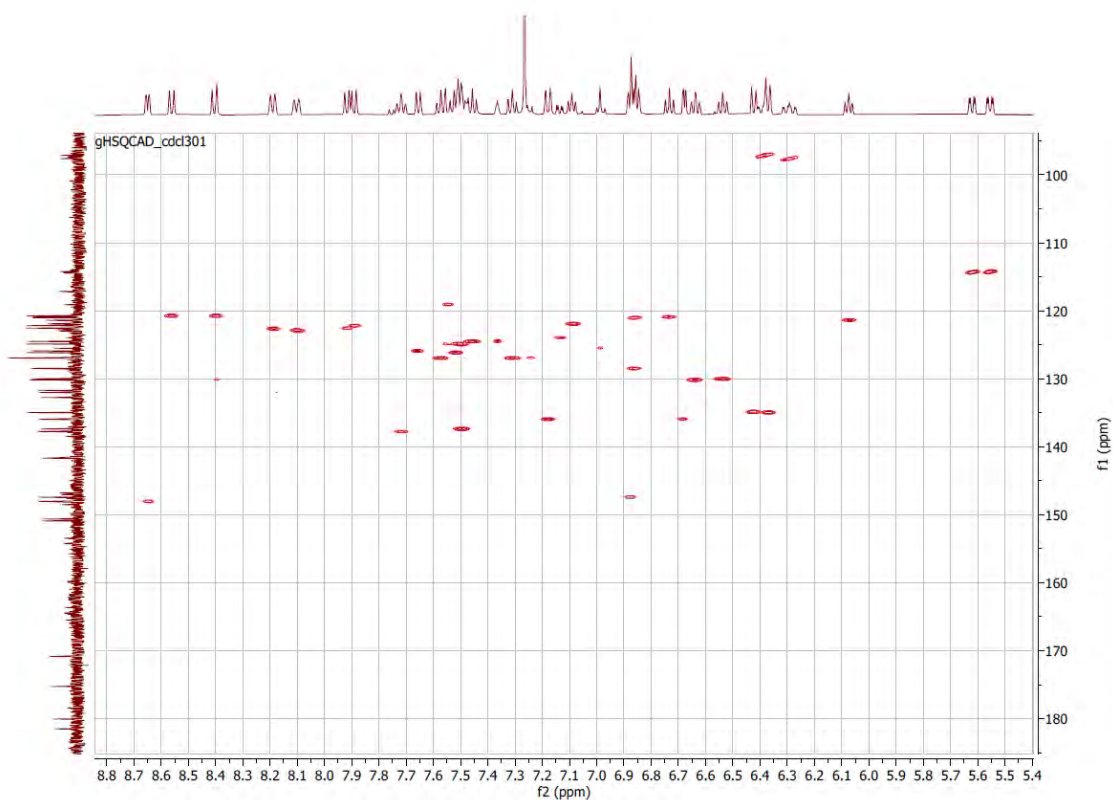


Figure S7c. HSQC spectrum of complex **BY2**.

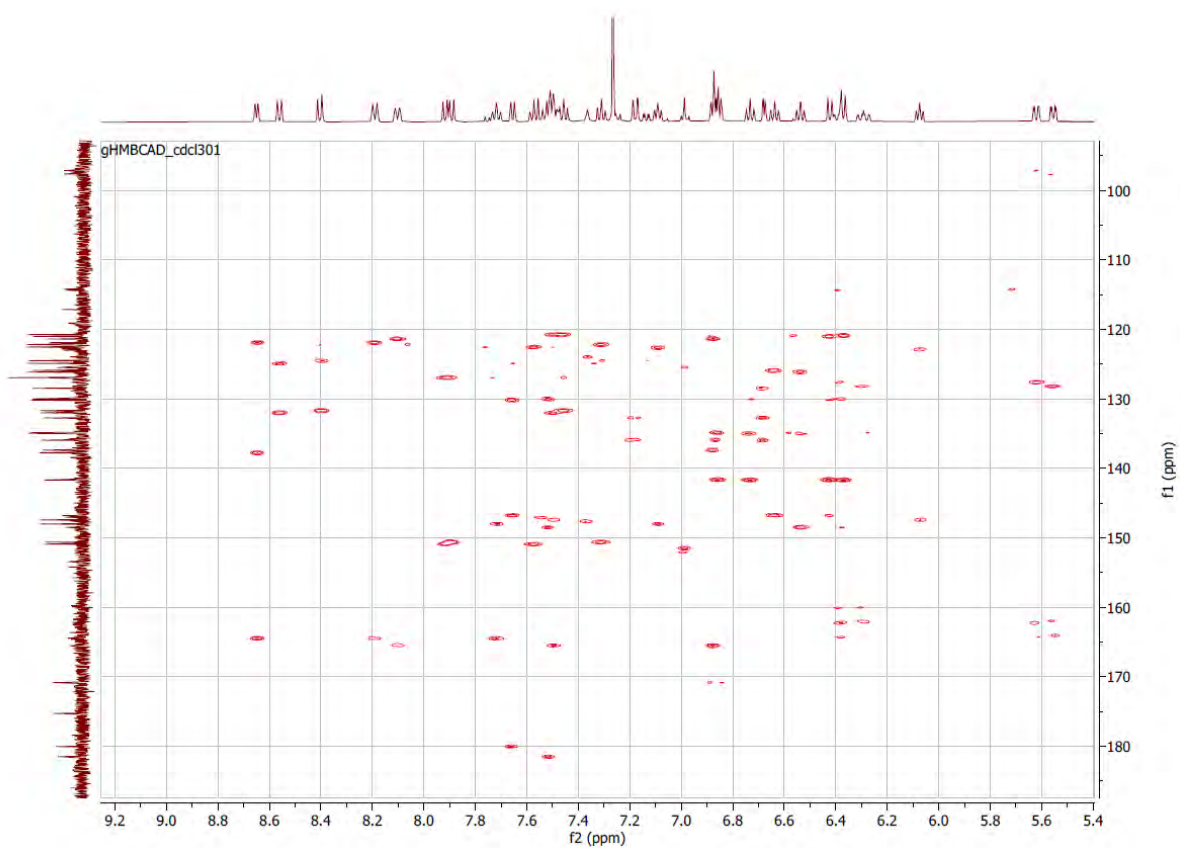


Figure S7d. HMBC spectrum of complex **BY2**.

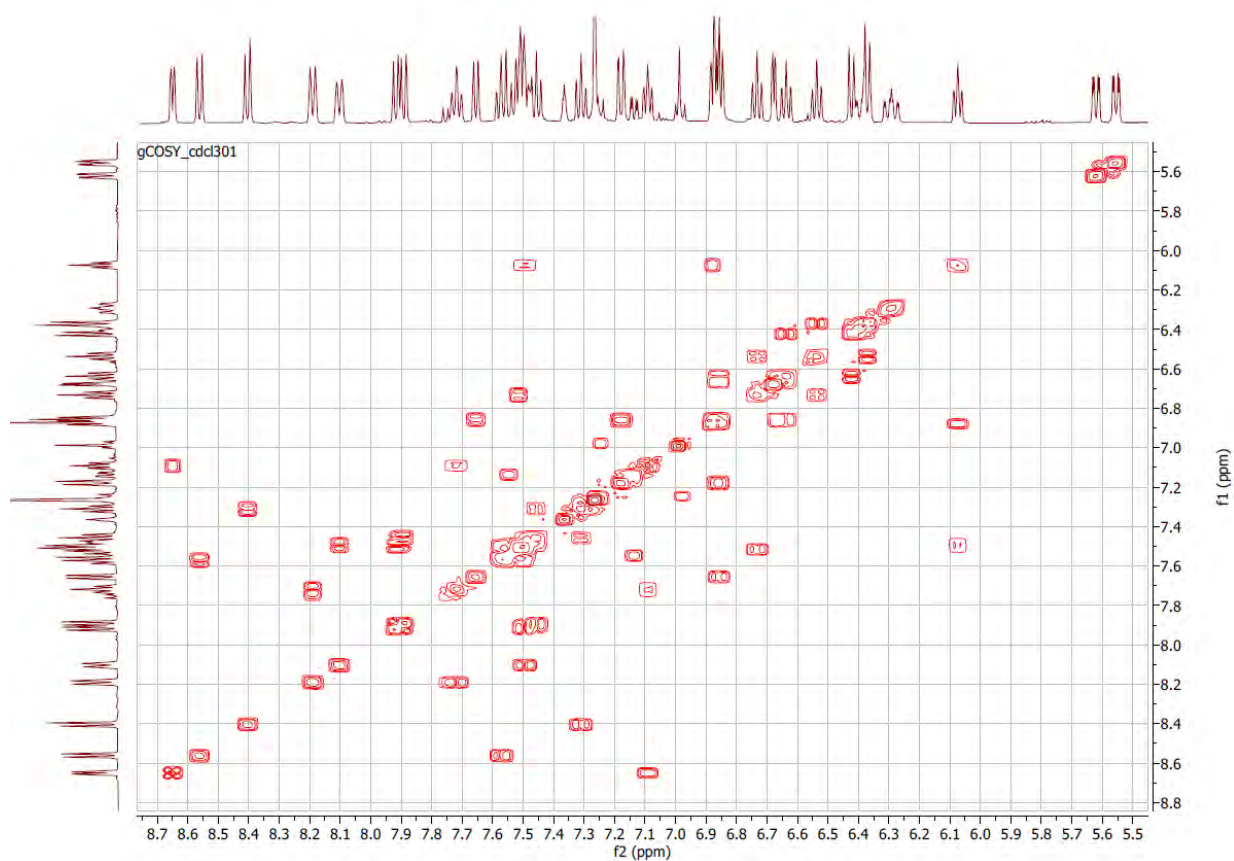


Figure S7e. COSY spectrum of complex **BY2**.

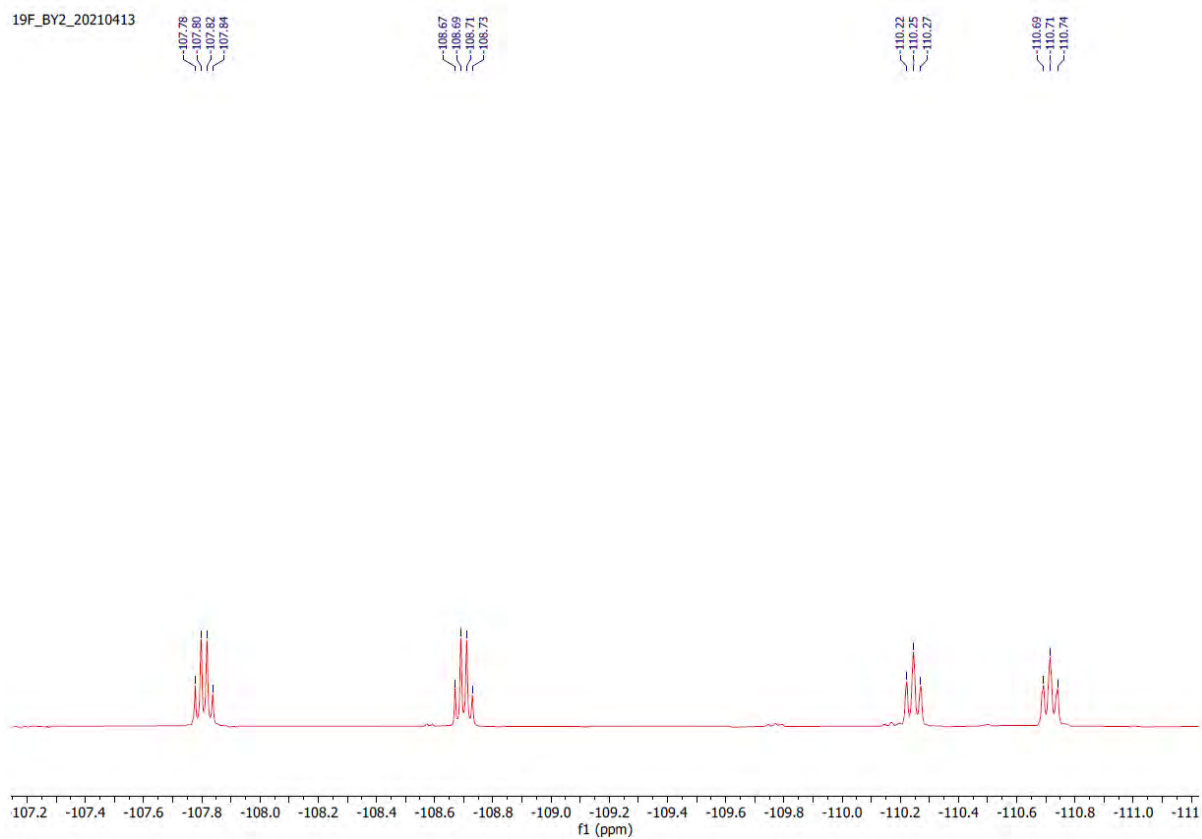


Figure S7f. ^{19}F NMR spectrum of complex **BY2**.

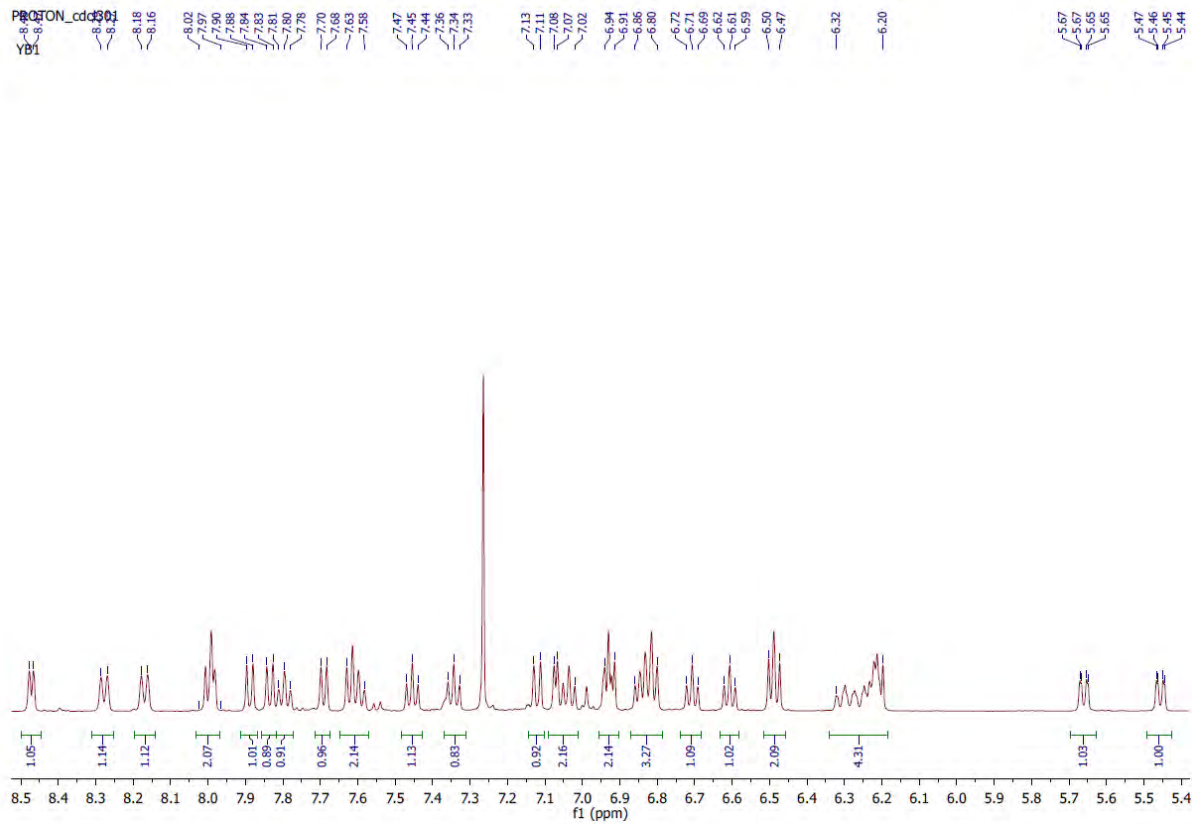
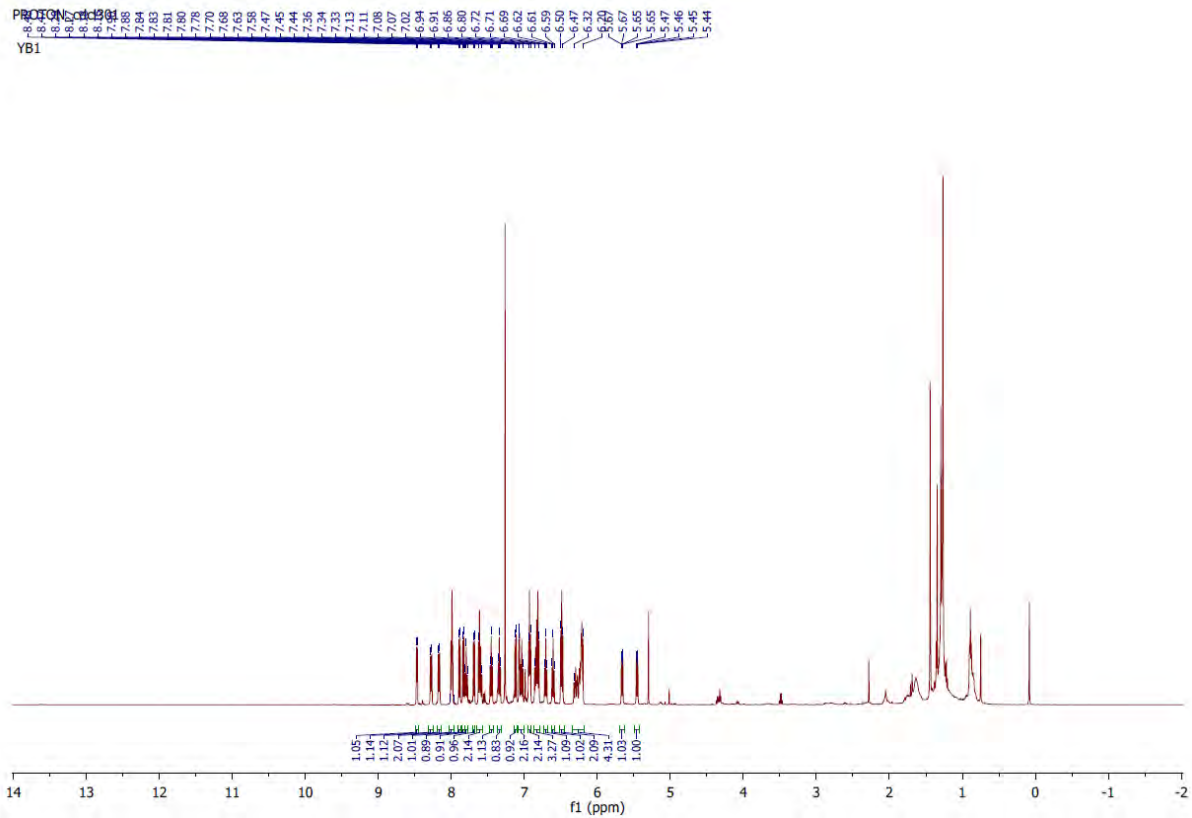
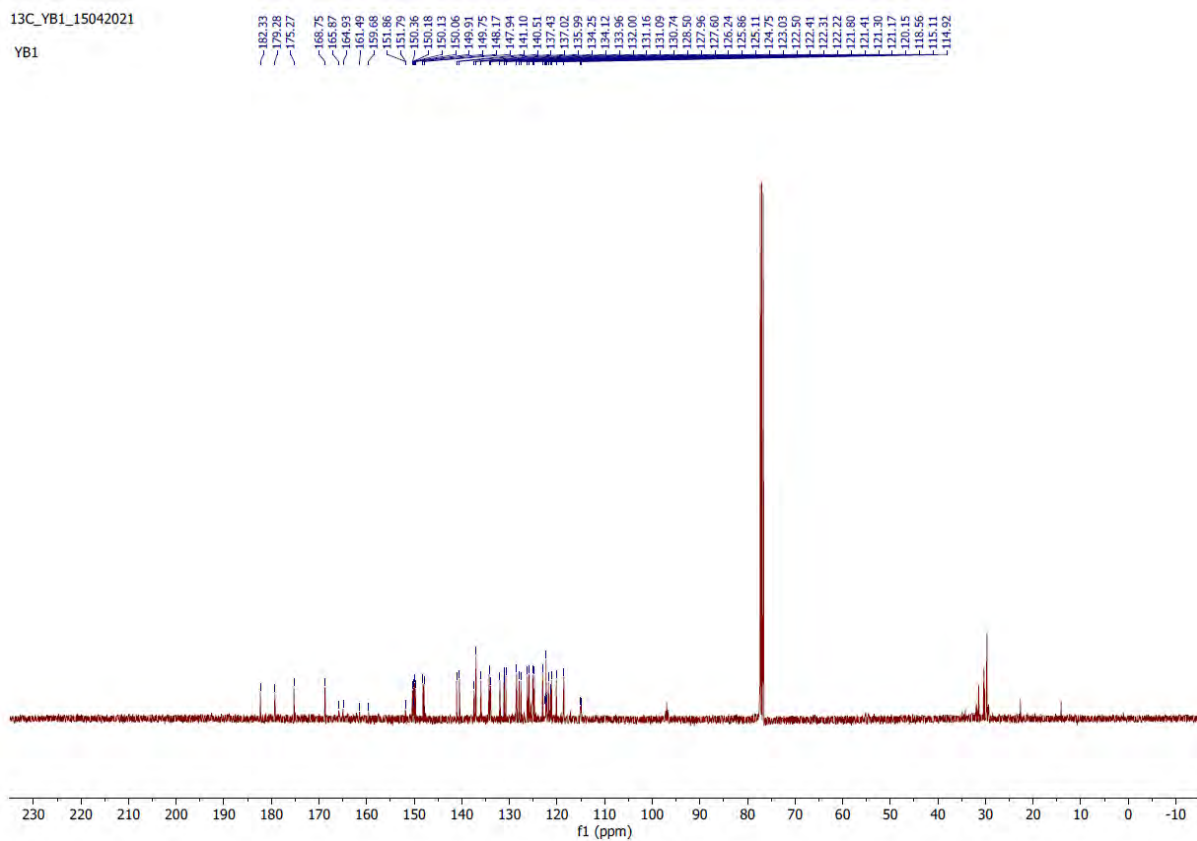


Figure S8a. ¹H NMR spectrum of complex YB1.

¹³C_YB1_15042021
YB1



¹³C_YB1_15042021
YB1

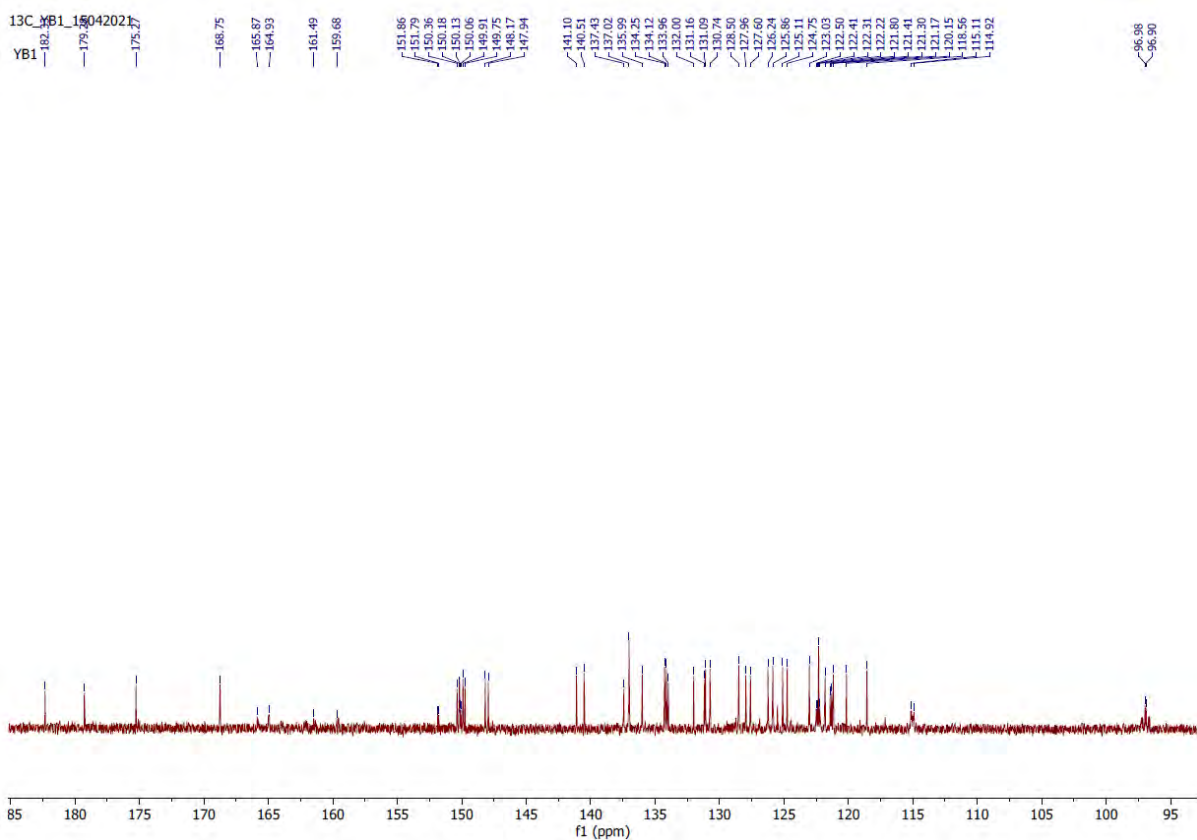


Figure S8b. ¹³C NMR spectrum of complex YB1.

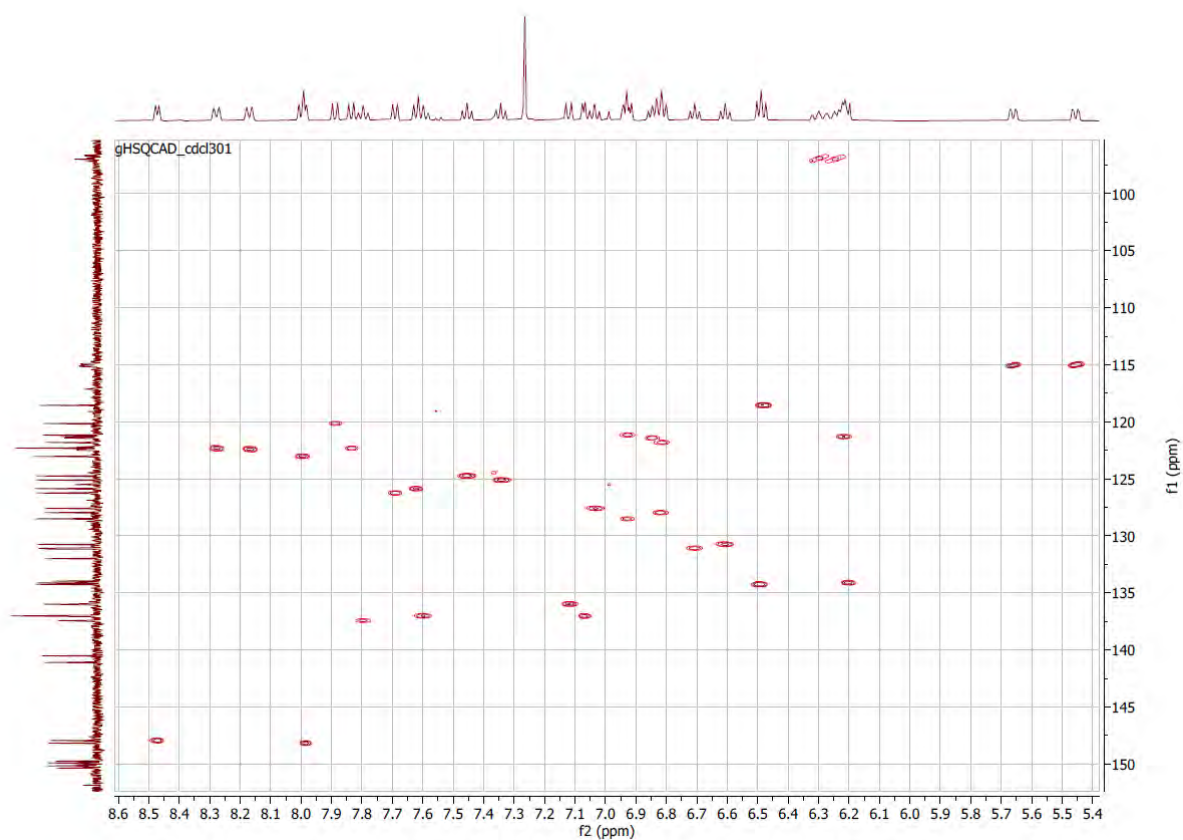


Figure S8c. HSQC spectrum of complex YB1.

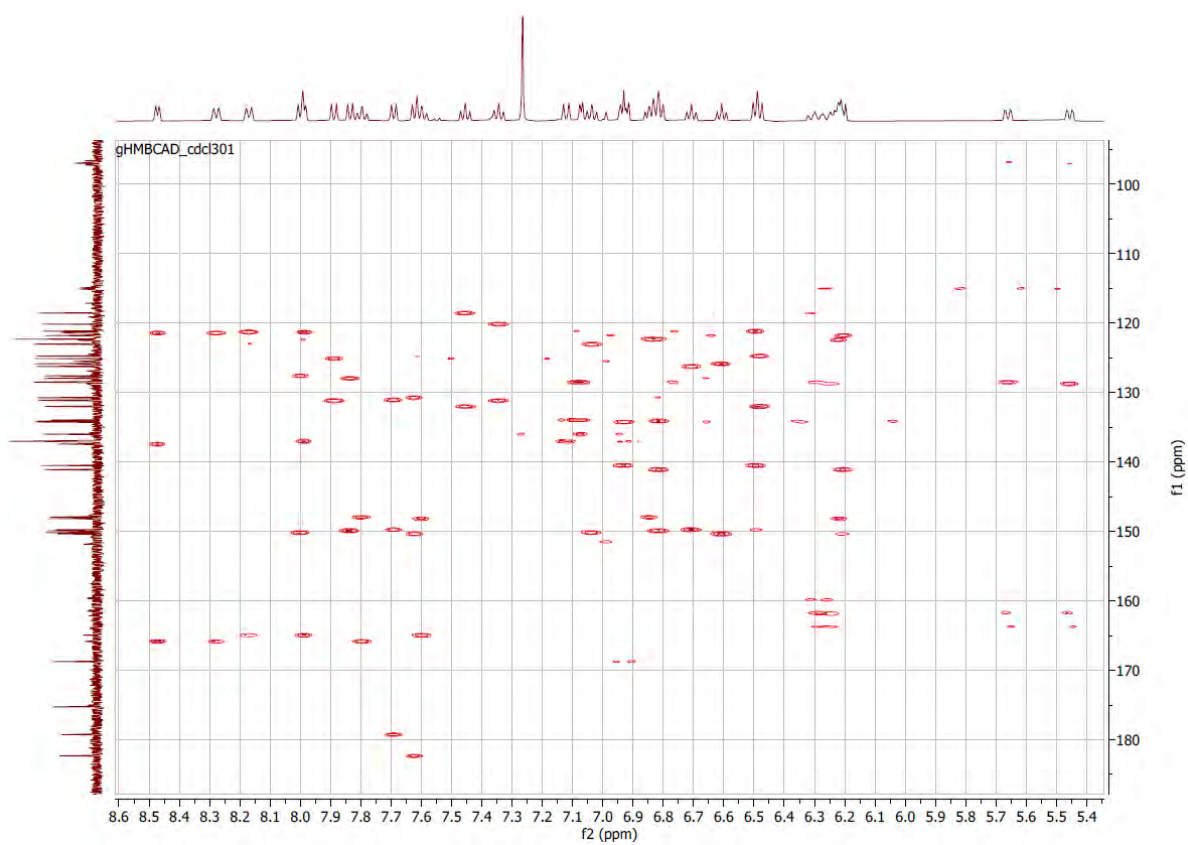


Figure S8d. HMBC spectrum of complex YB1.

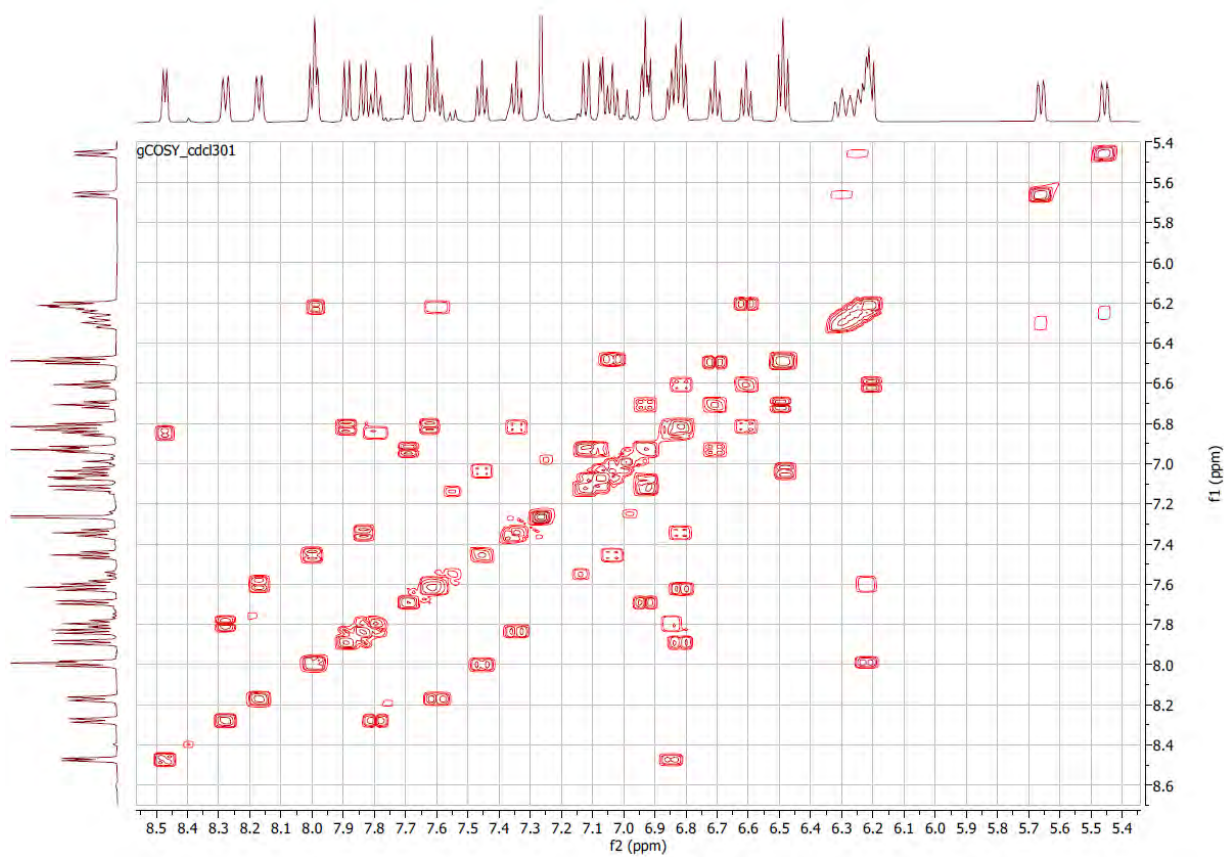


Figure S8e. COSY spectrum of complex YB1.

19F_YB1_20210413
YB1

-108.93
-108.95
-108.97
-108.99

-109.54
-109.56
-109.58
-109.60

-111.41
-111.44
-111.46
-111.57
-111.60
-111.62

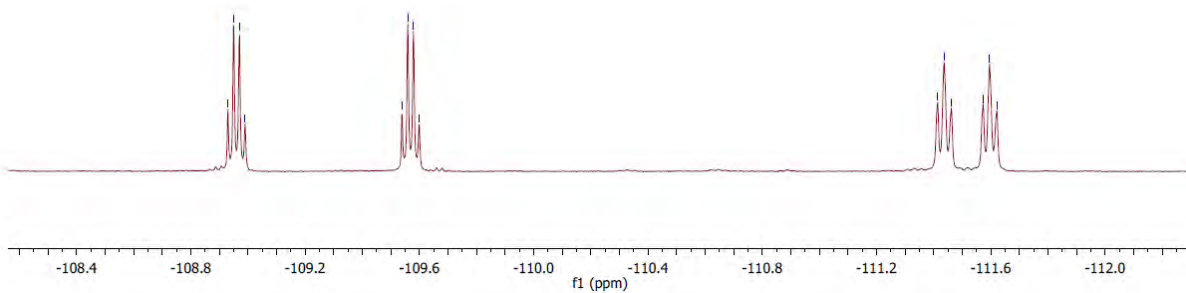


Figure S8f. ^{19}F NMR spectrum of complex YB1.

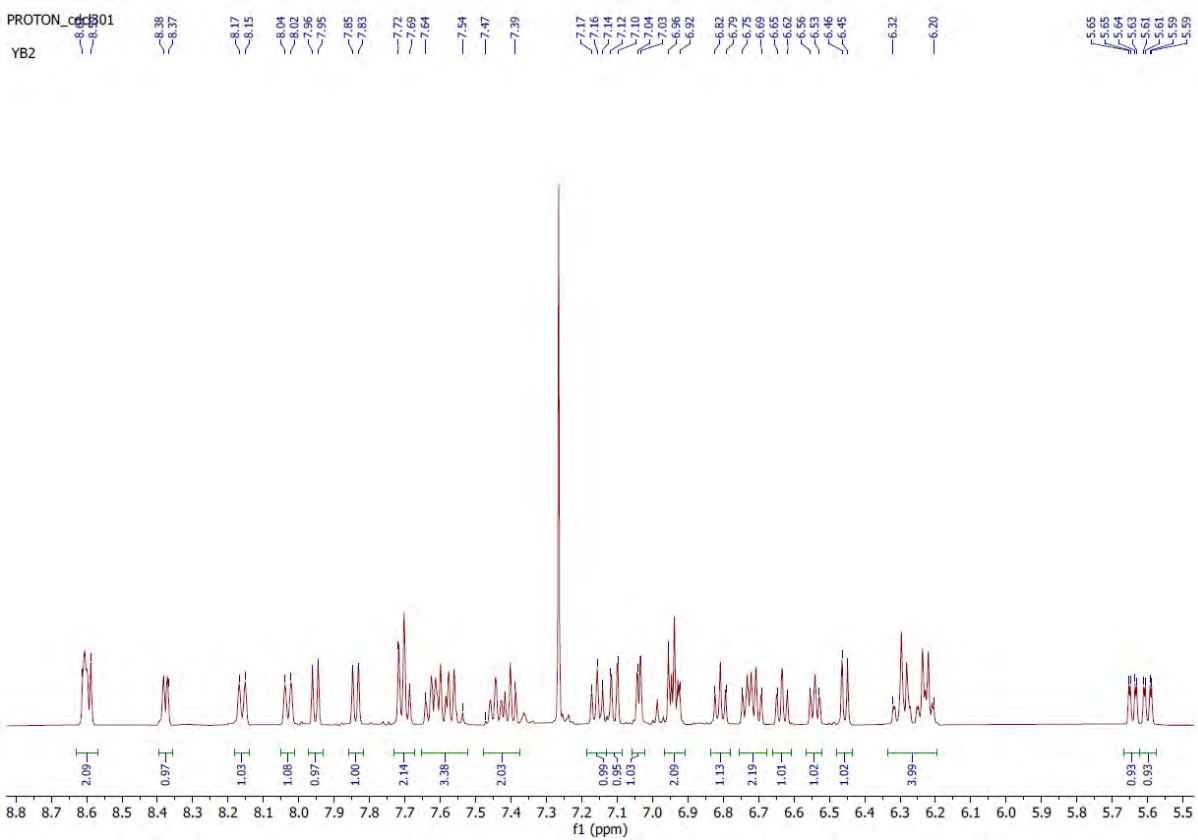
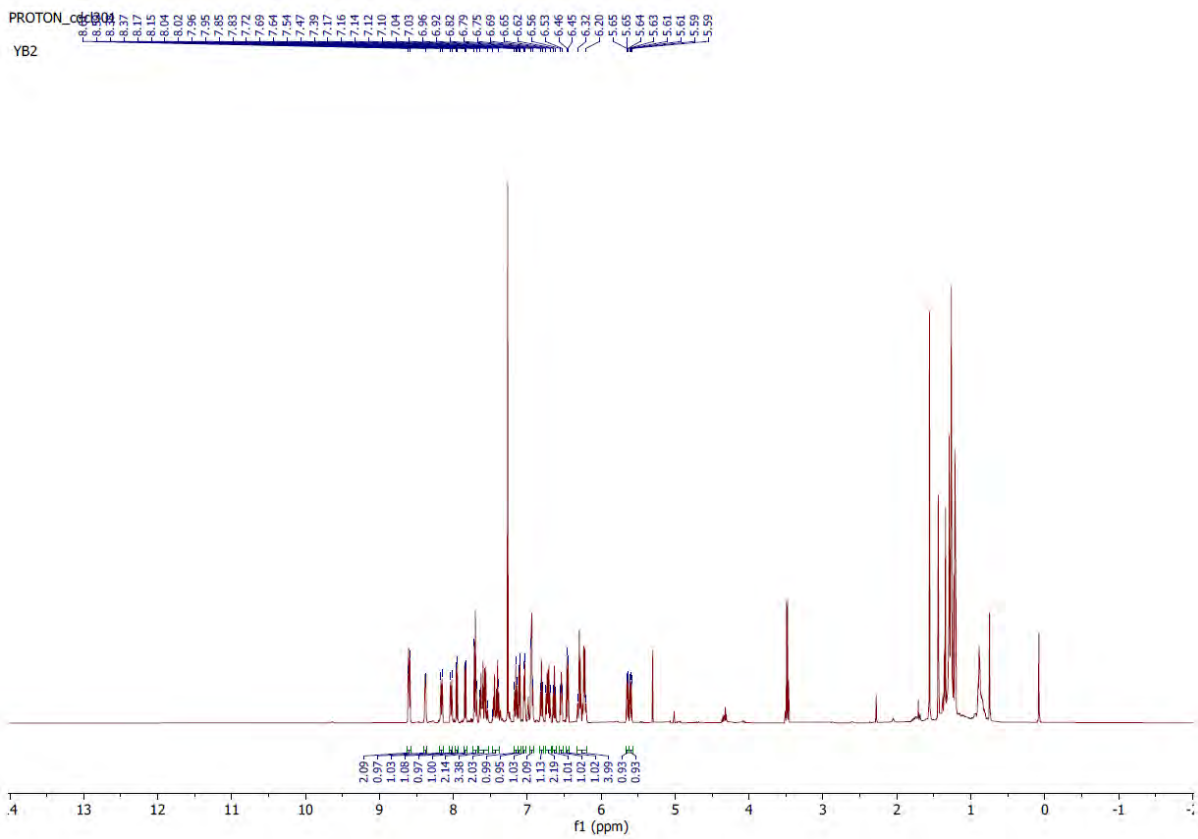


Figure S9a. ¹H NMR spectrum of complex YB2.

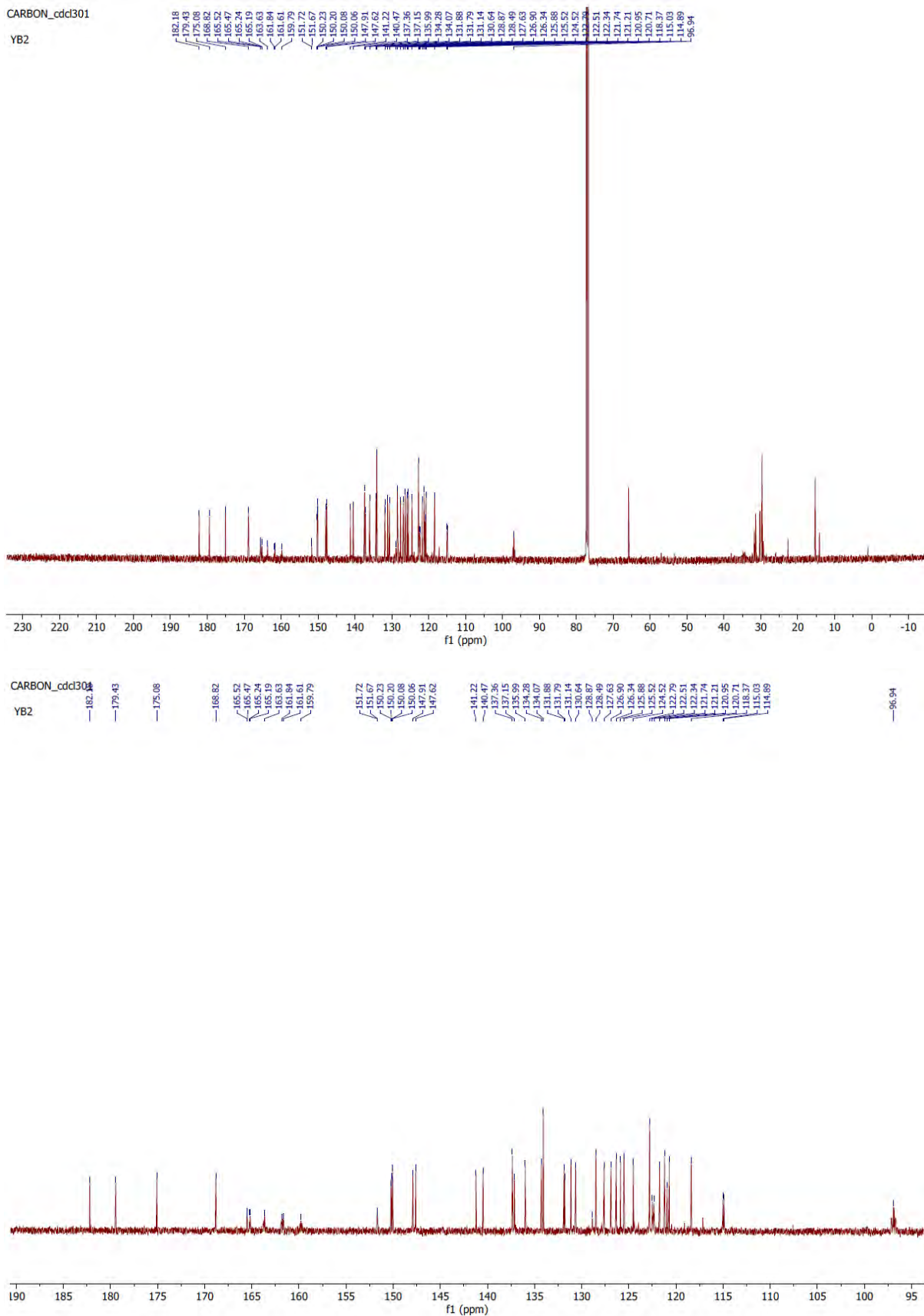


Figure S9b. ^{13}C NMR spectrum of complex YB2.

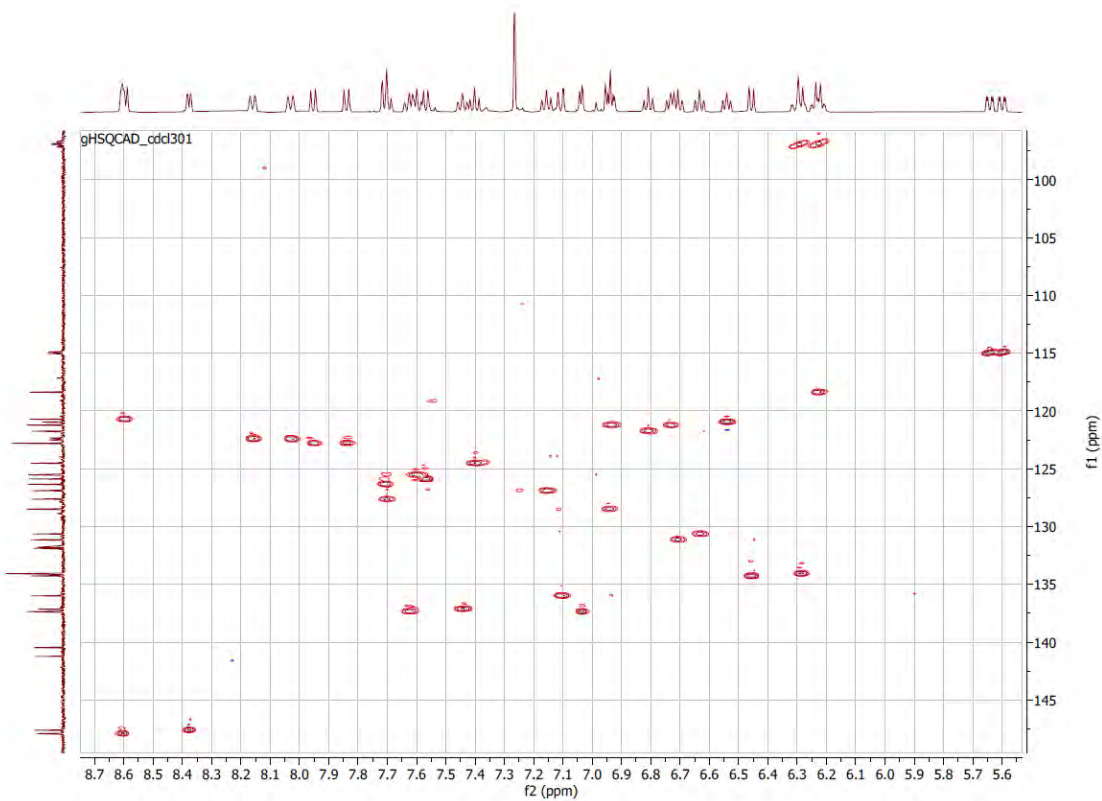


Figure S9c. HSQC spectrum of complex YB2.

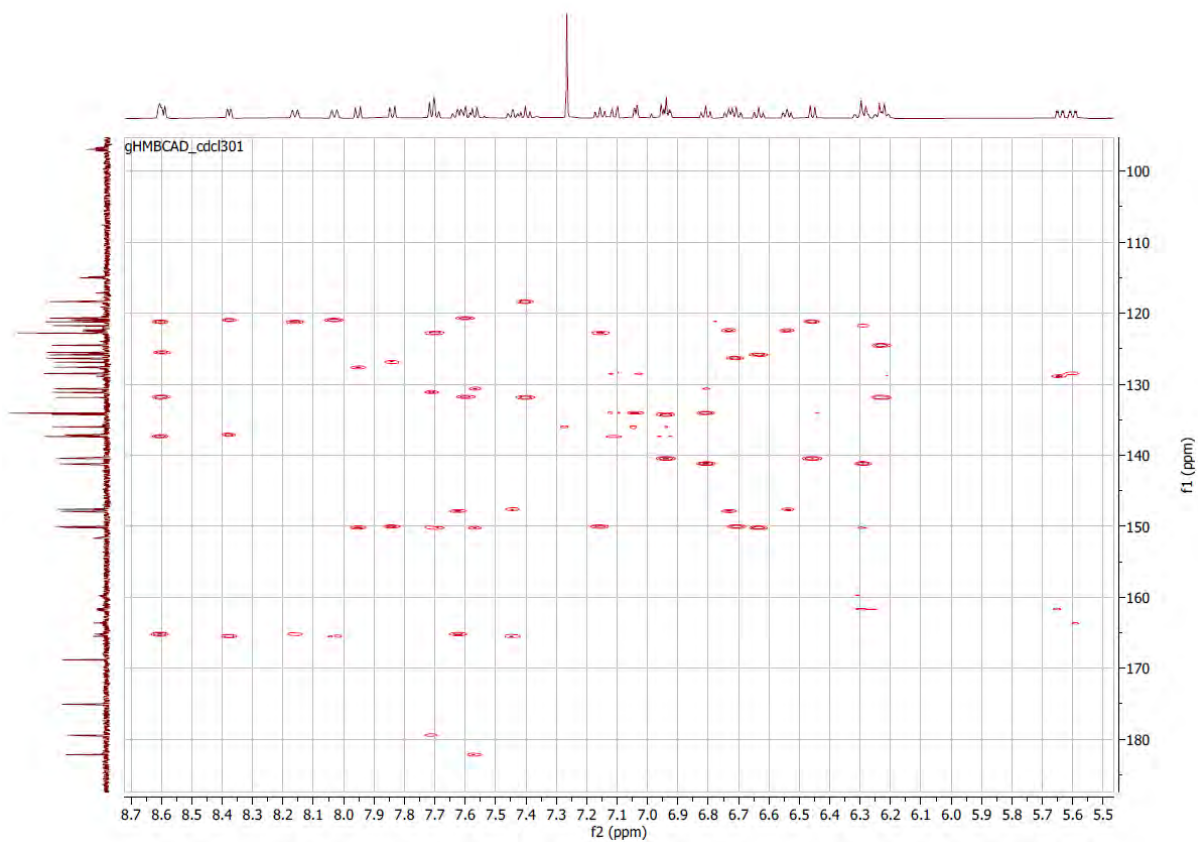


Figure S9d. HMBC spectrum of complex YB2.

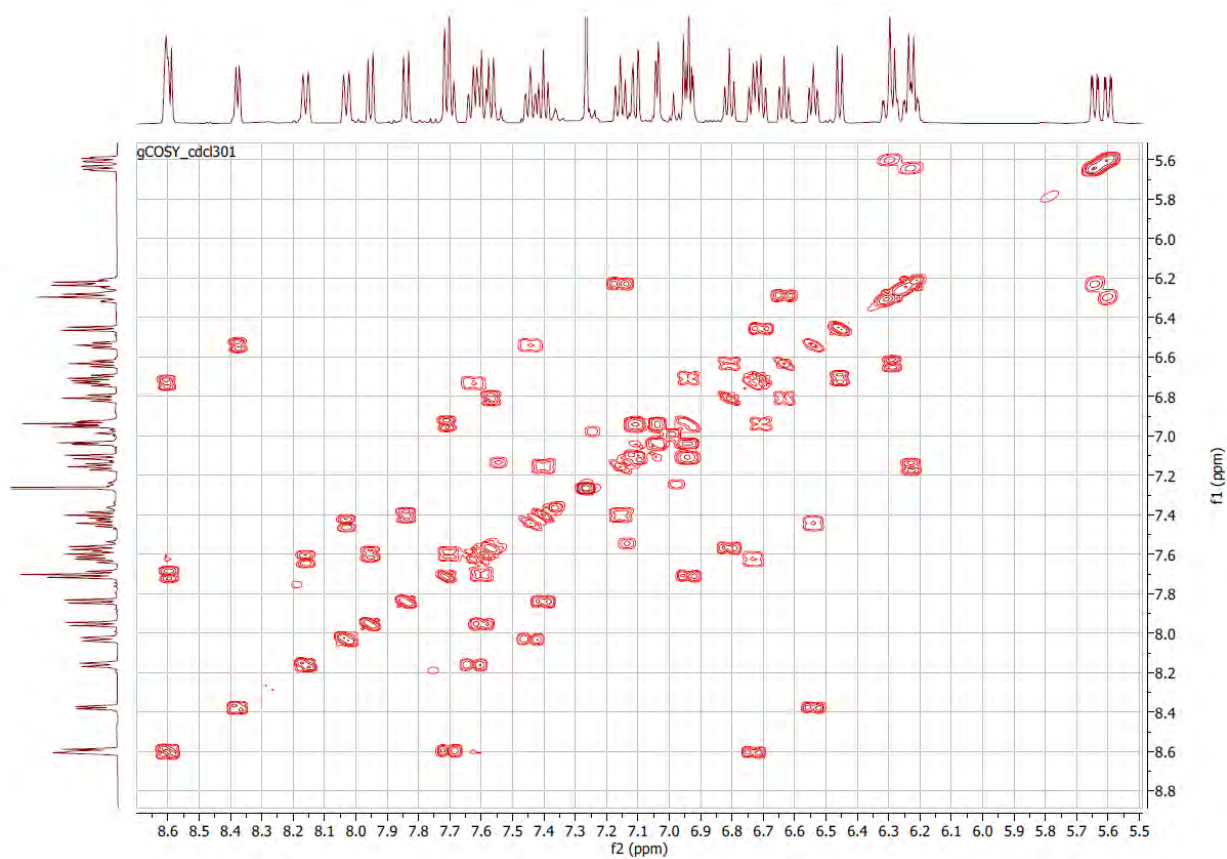


Figure S9e. COSY spectrum of complex YB2.

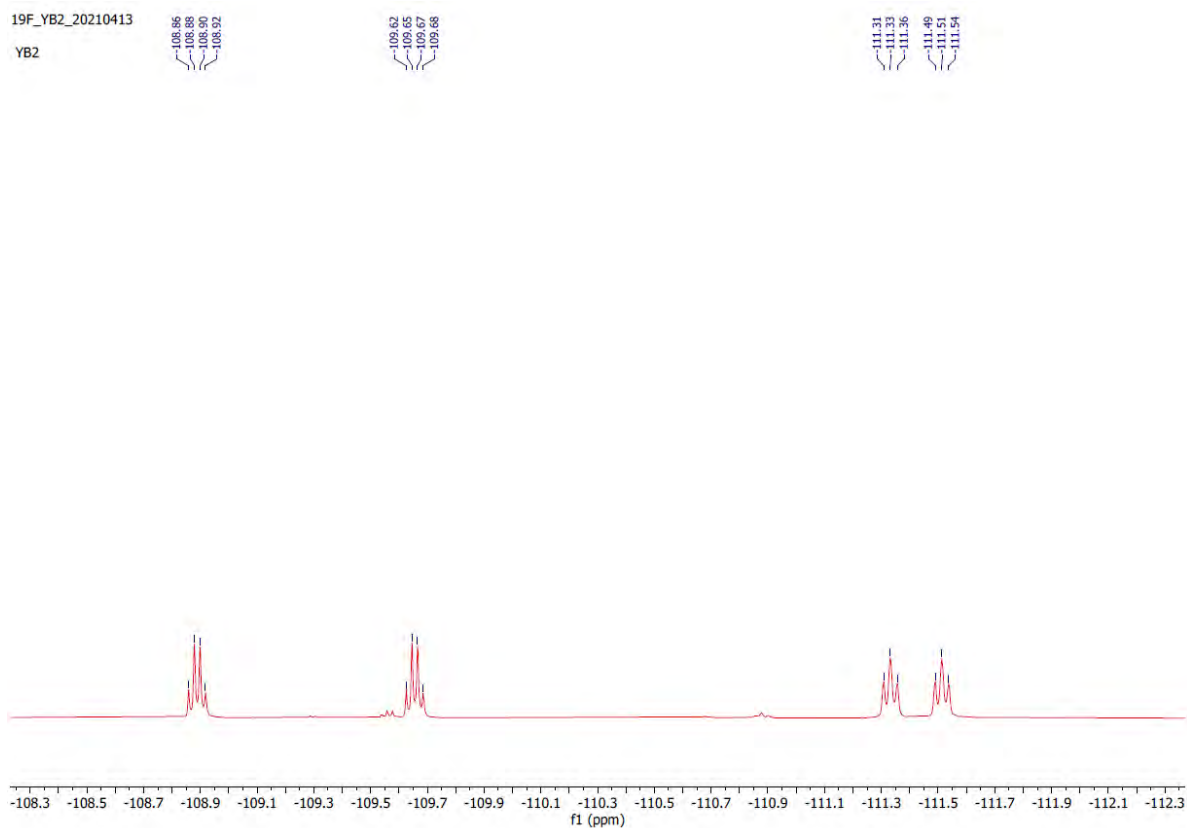


Figure S9f. ^{19}F NMR spectrum of complex YB2.

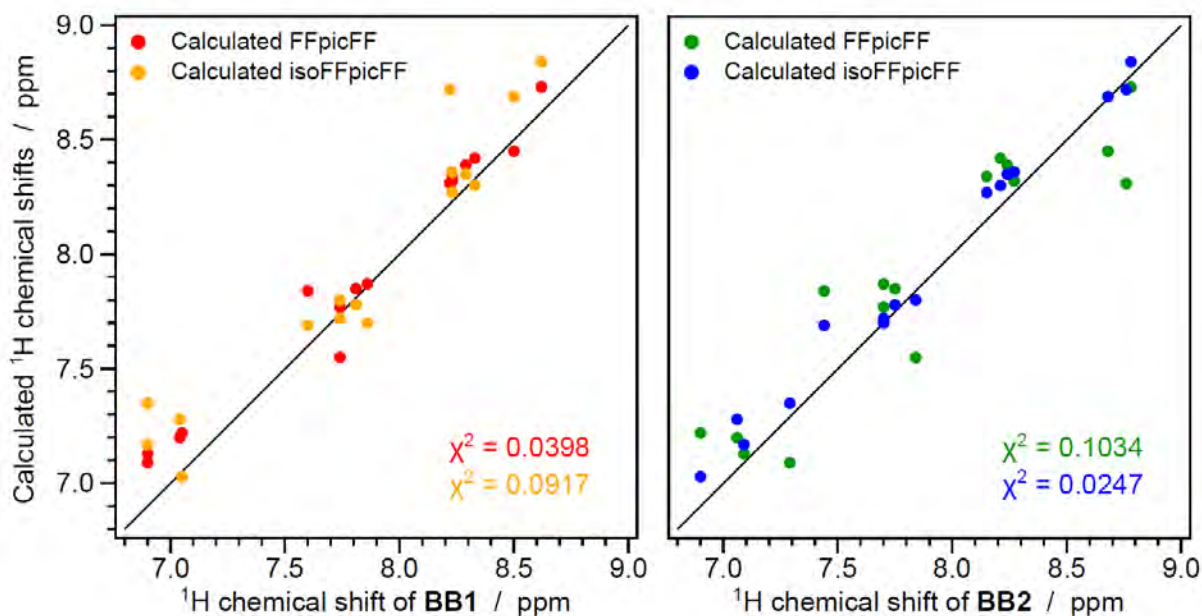


Figure S10. Correlation between experimental data and theoretical results for the 16 protons on the pyridine rings (in ppm) for complexes **BB1** and **BB2**.

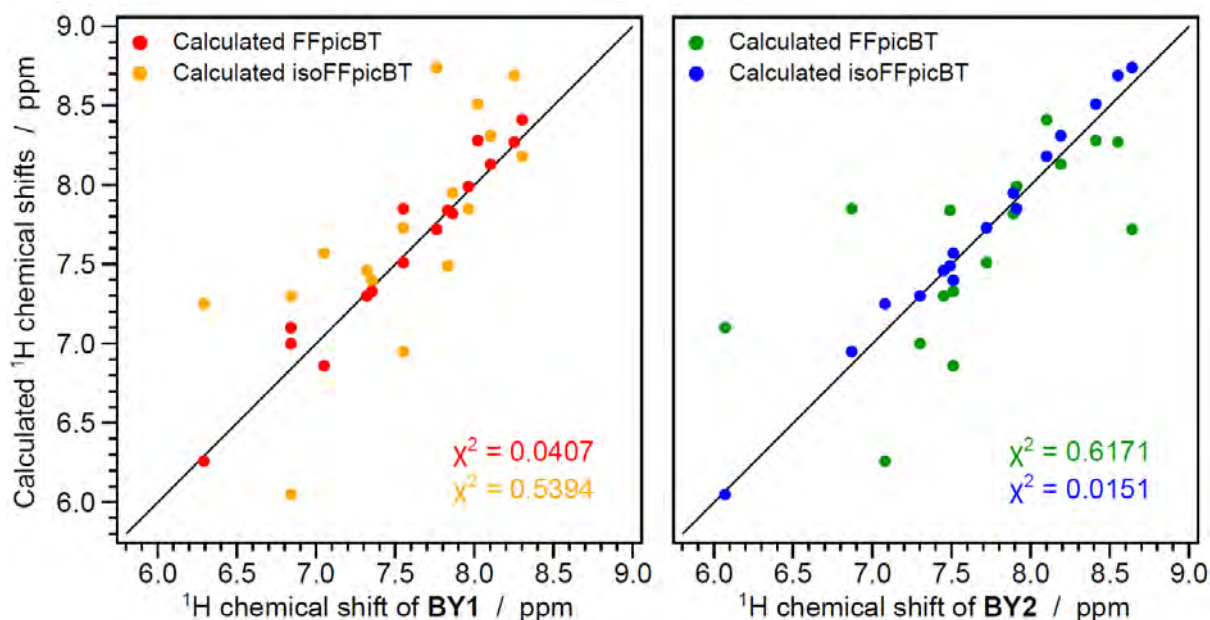


Figure S11. Correlation between experimental data and theoretical results for the 16 protons on the pyridine rings (in ppm) for complexes **BY1** and **BY2**.

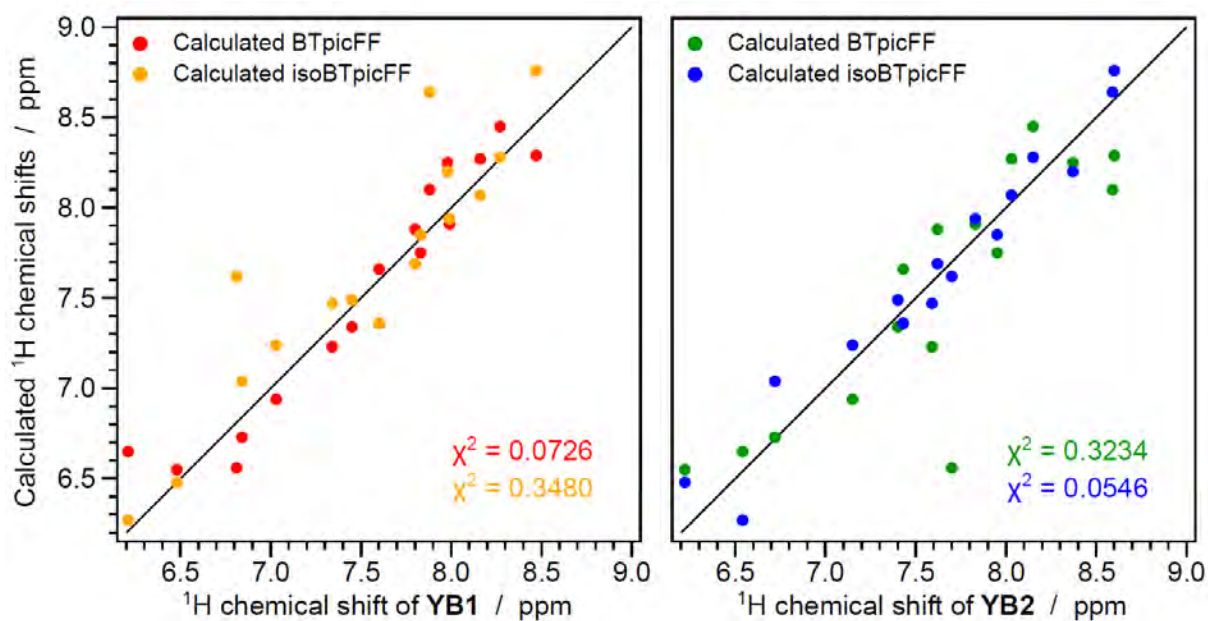


Figure S12. Correlation between experimental data and theoretical results for the 16 protons on the pyridine rings (in ppm) for complexes YB1 and YB2.

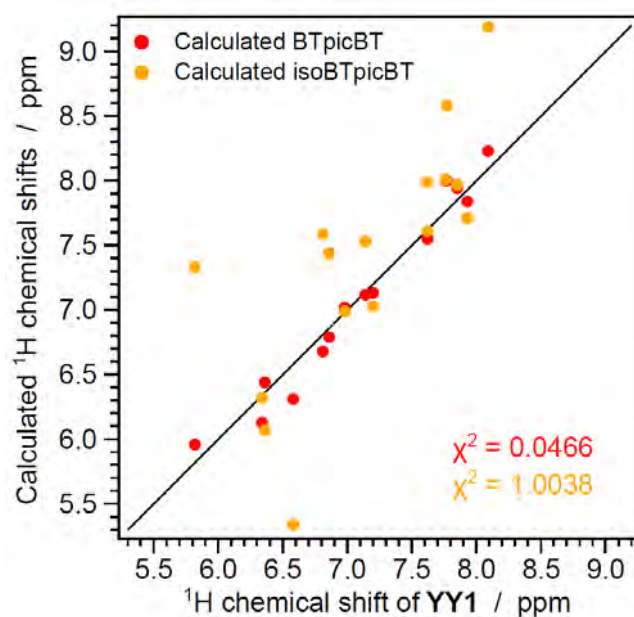


Figure S13. Correlation between experimental data and theoretical results for the 16 protons on the pyridine rings (in ppm) for complexes YY.

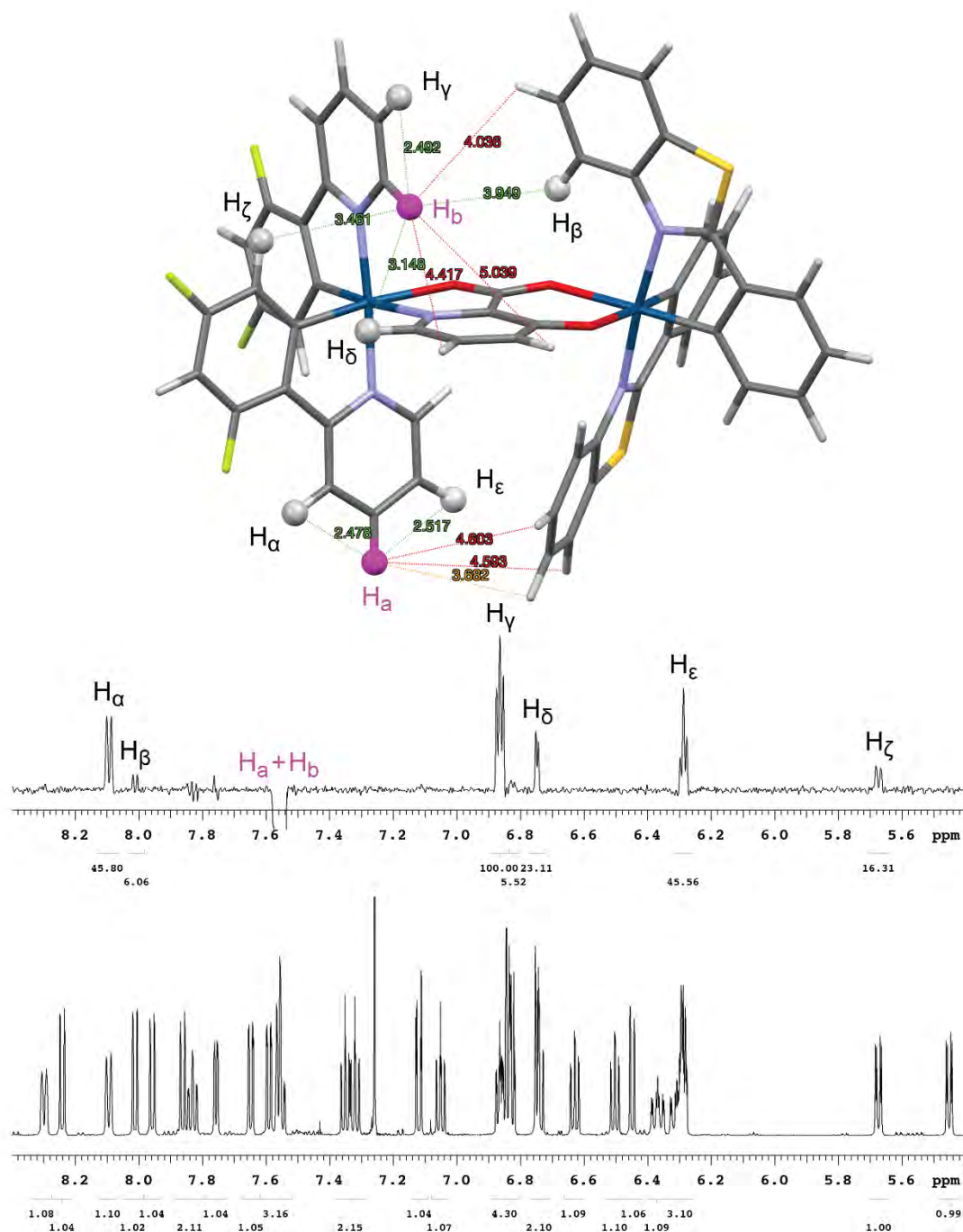


Figure S14. NOE (7.55 ppm) spectrum of complex **BY1**. Pink protons: protons irradiated during the experiment; white protons: nucleus affected by the NOE effect. Visible protons are $< 4 \text{ \AA}$ (green lines), non-visible protons are at $> 4 \text{ \AA}$ (red lines).

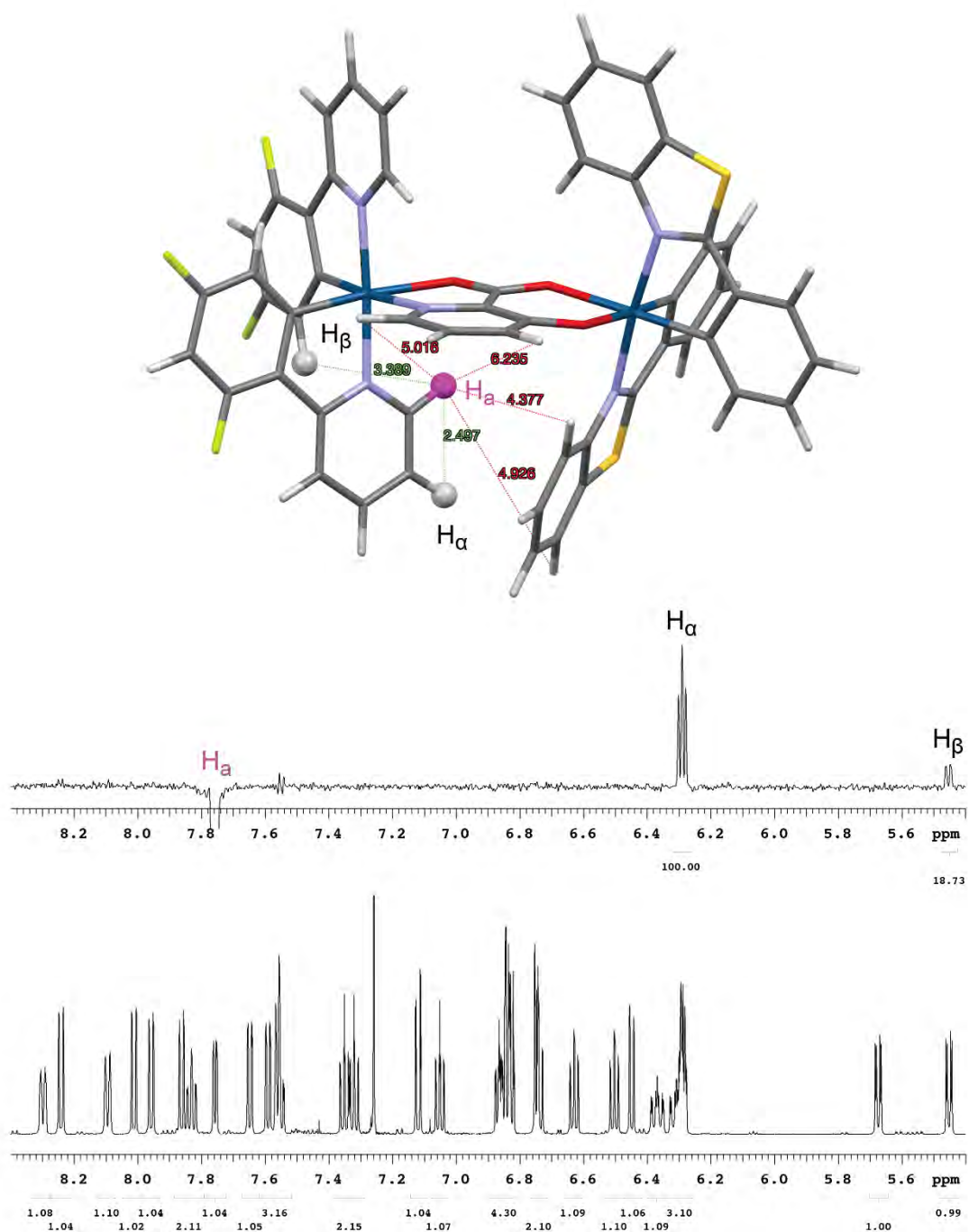


Figure S15. NOE (7.76 ppm) spectrum of complex **BY1**. Pink protons: protons irradiated during the experiment; white protons: nucleus affected by the NOE effect. Visible protons are $< 4 \text{ \AA}$ (green lines), non-visible protons are at $> 4 \text{ \AA}$ (red lines).

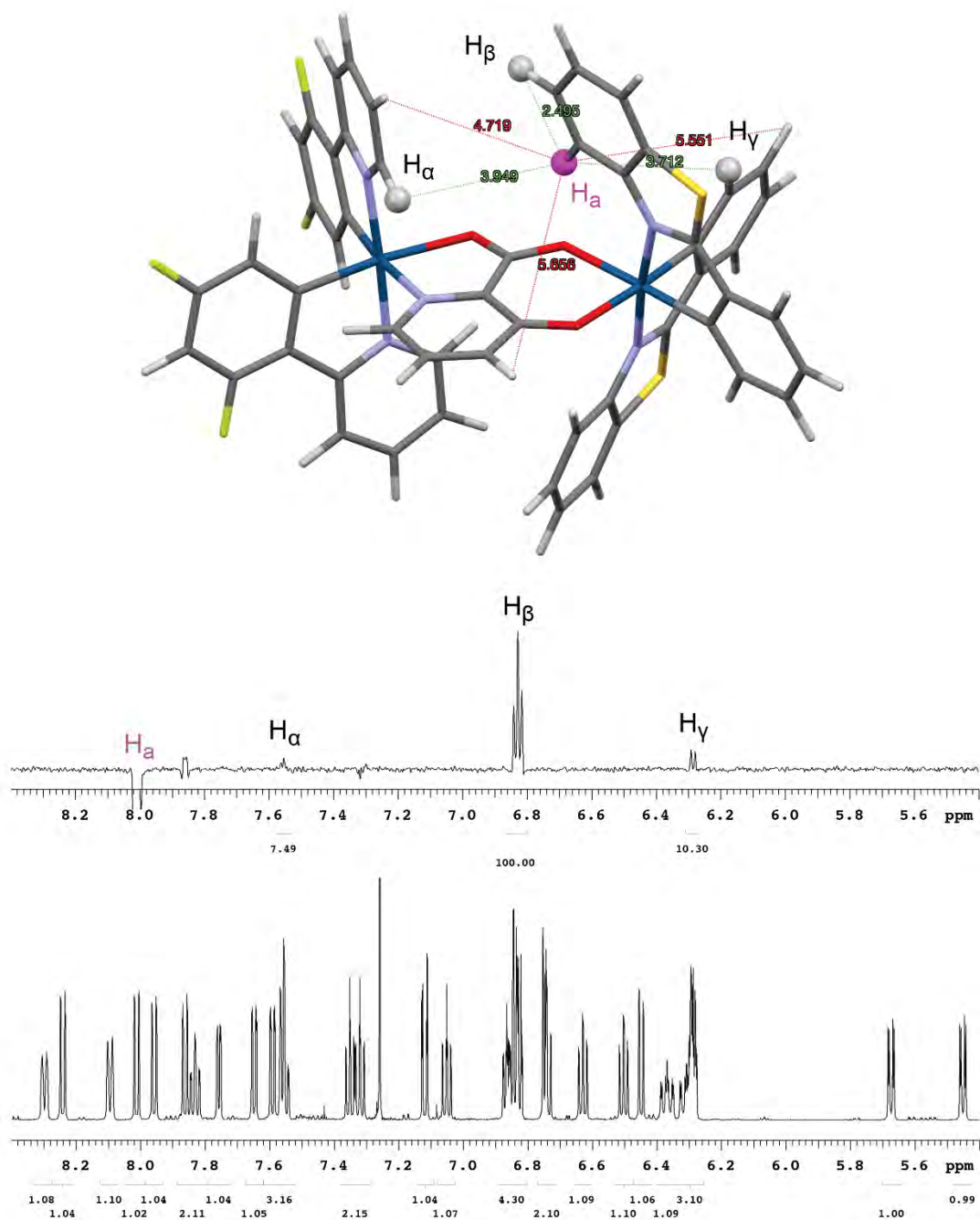


Figure S16. NOE (8.02 ppm) spectrum of complex **BY1**. Pink protons: protons irradiated during the experiment; white protons: nucleus affected by the NOE effect. Visible protons are $< 4 \text{ \AA}$ (green lines), non-visible protons are at $> 4 \text{ \AA}$ (red lines).

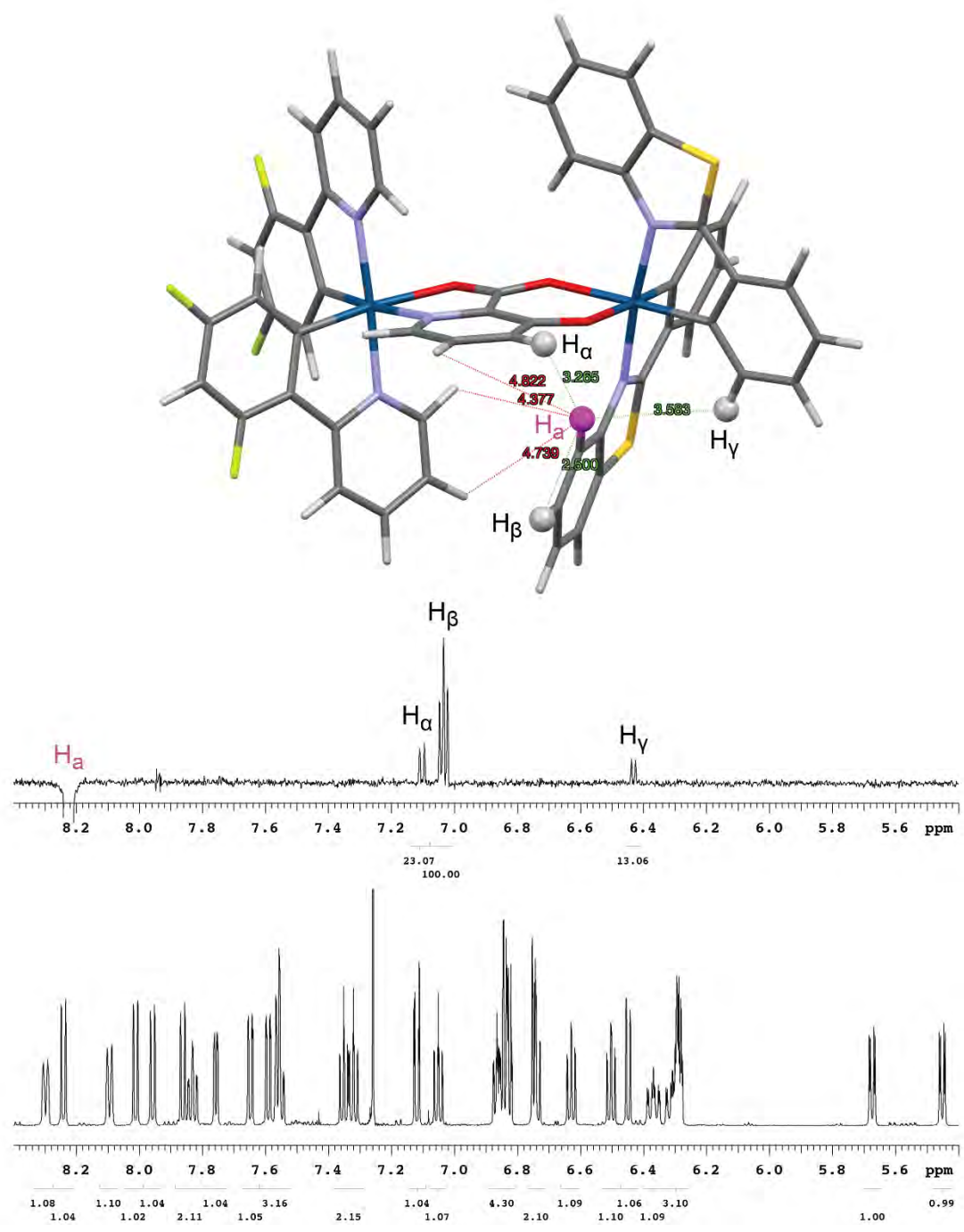


Figure S17. NOE (8.25 ppm) spectrum of complex **BY1**. Pink protons: protons irradiated during the experiment; white protons: nucleus affected by the NOE effect. Visible protons are $< 4 \text{ \AA}$ (green lines), non-visible protons are at $> 4 \text{ \AA}$ (red lines).

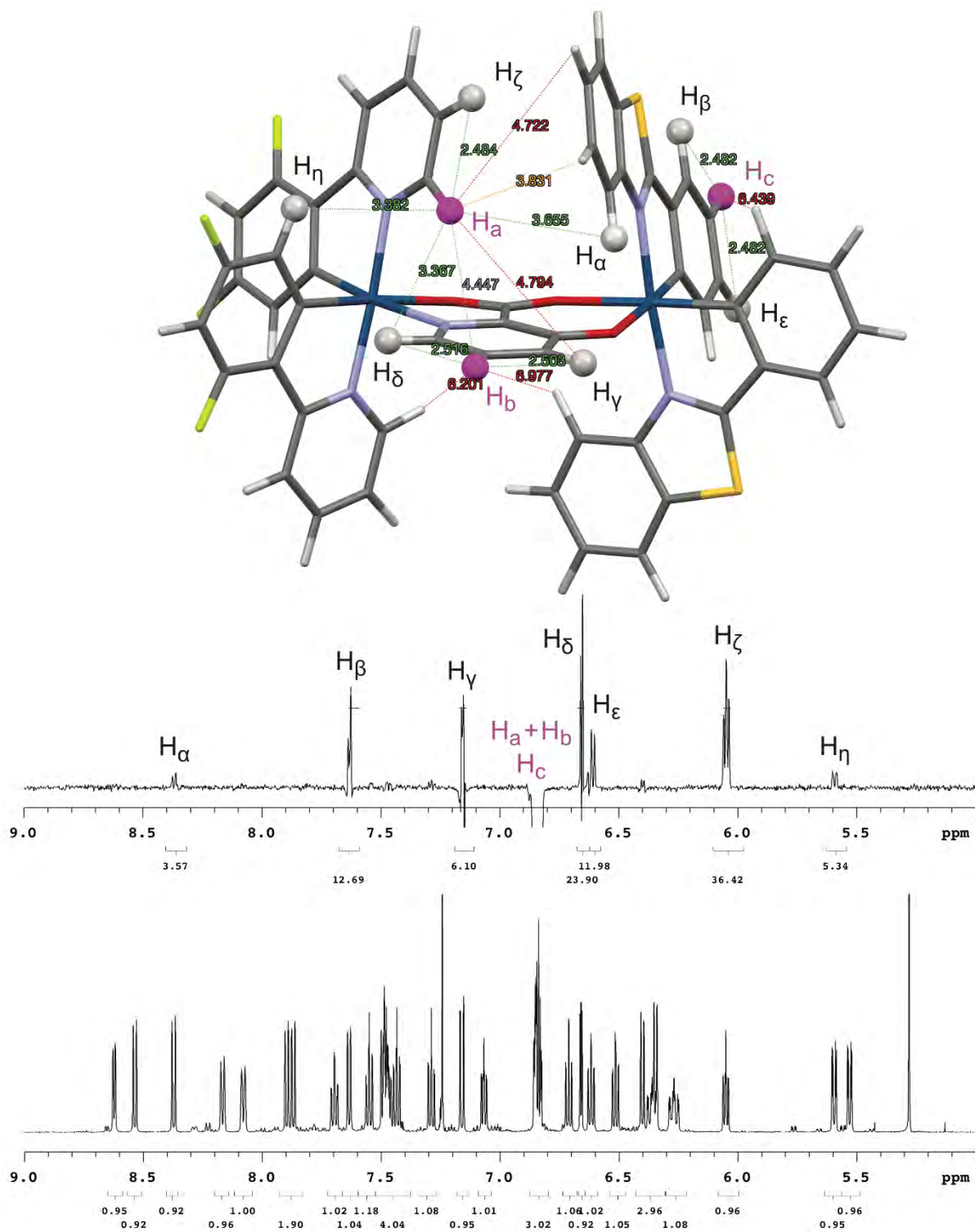


Figure S18. NOE (6.84 ppm) spectrum of complex **BY2**. Pink protons: protons irradiated during the experiment; white protons: nucleus affected by the NOE effect. Visible protons are < 4 Å (green lines), non-visible protons are at > 4 Å (red lines).

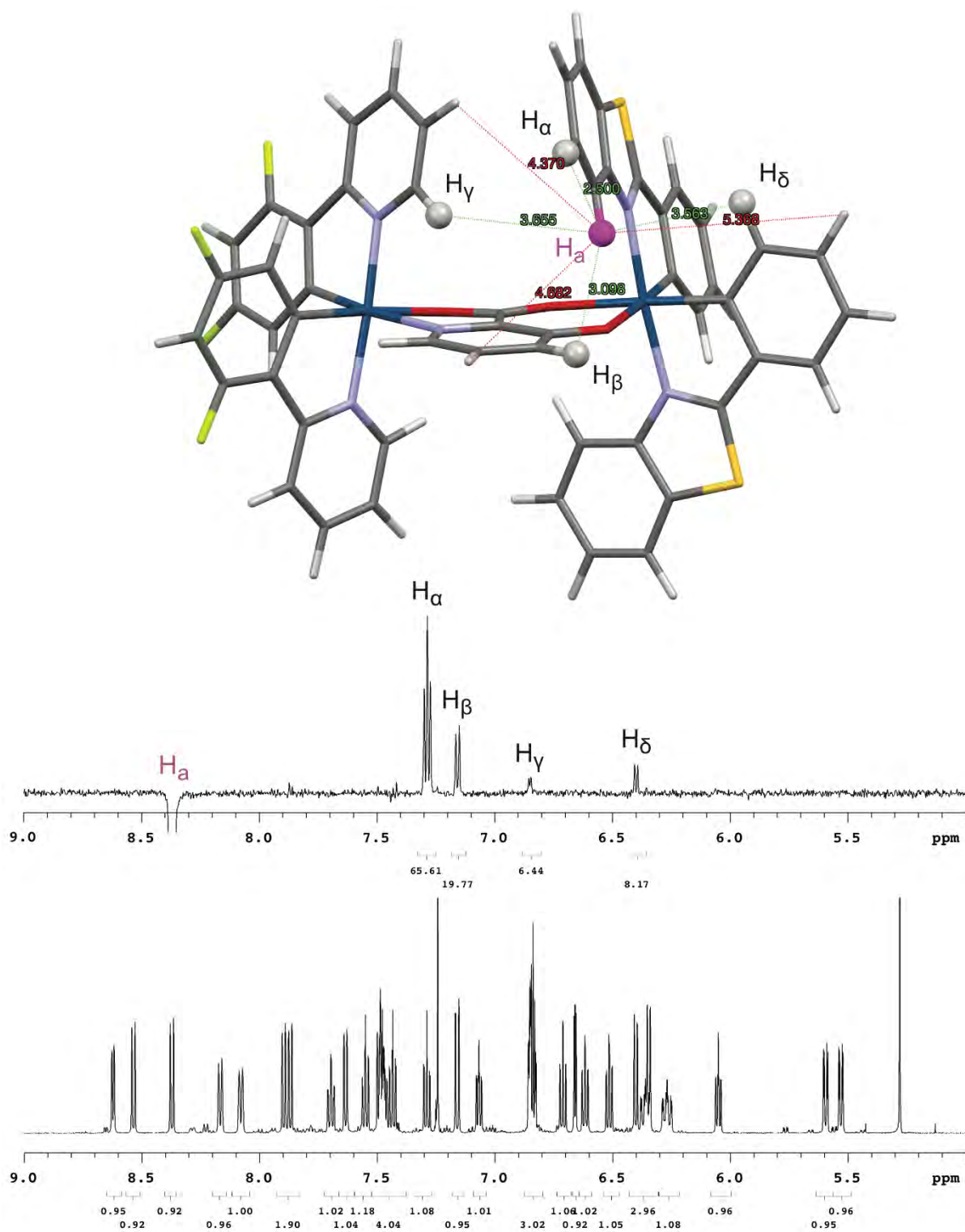


Figure S19. NOE (8.41 ppm) spectrum of complex **BY2**. Pink protons: protons irradiated during the experiment; white protons: nucleus affected by the NOE effect. Visible protons are $< 4 \text{ \AA}$ (green lines), non-visible protons are at $> 4 \text{ \AA}$ (red lines).

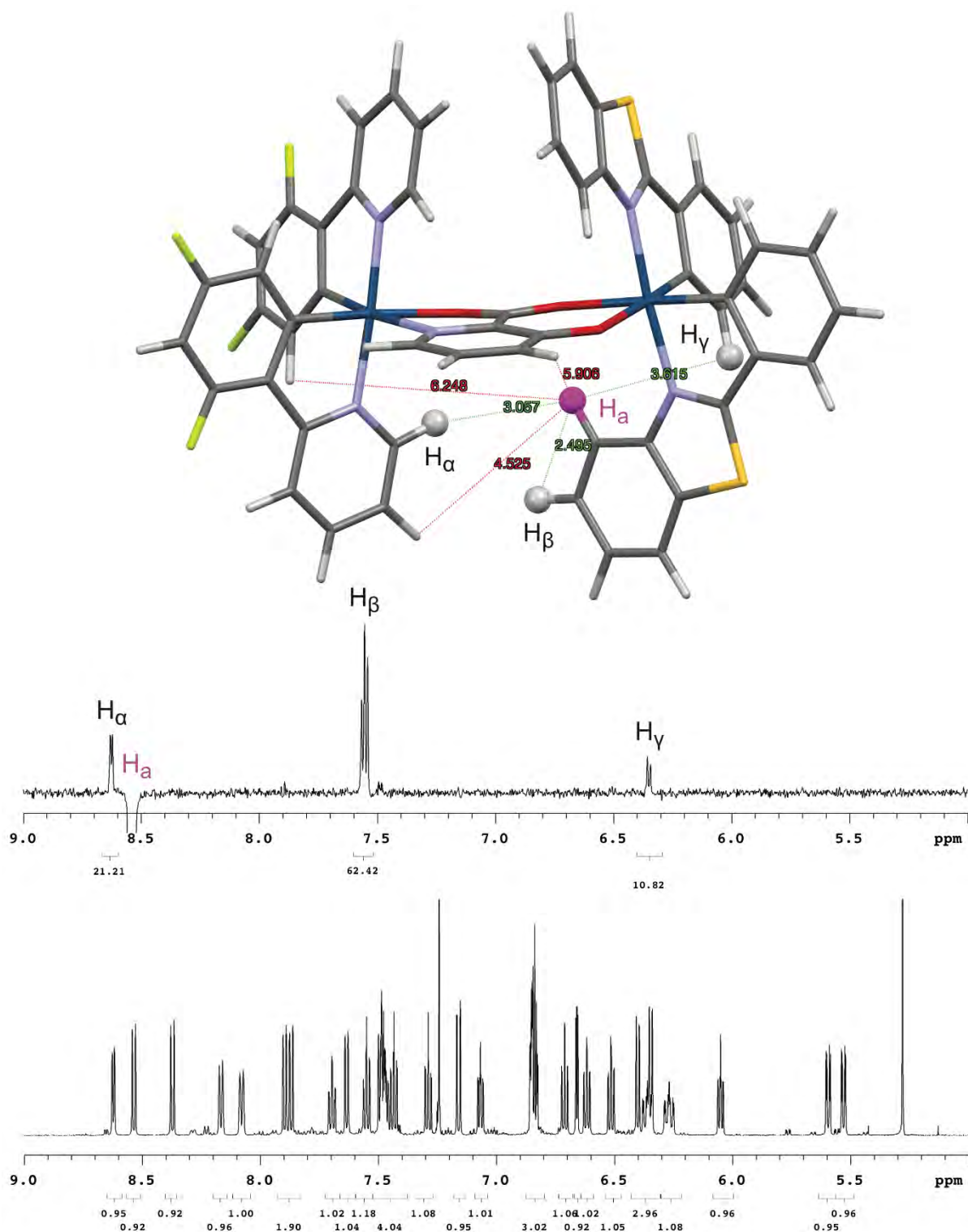


Figure S20. NOE (8.54 ppm) spectrum of complex **BY2**. Pink protons: protons irradiated during the experiment; white protons: nucleus affected by the NOE effect. Visible protons are $< 4 \text{ \AA}$ (green lines), non-visible protons are at $> 4 \text{ \AA}$ (red lines).

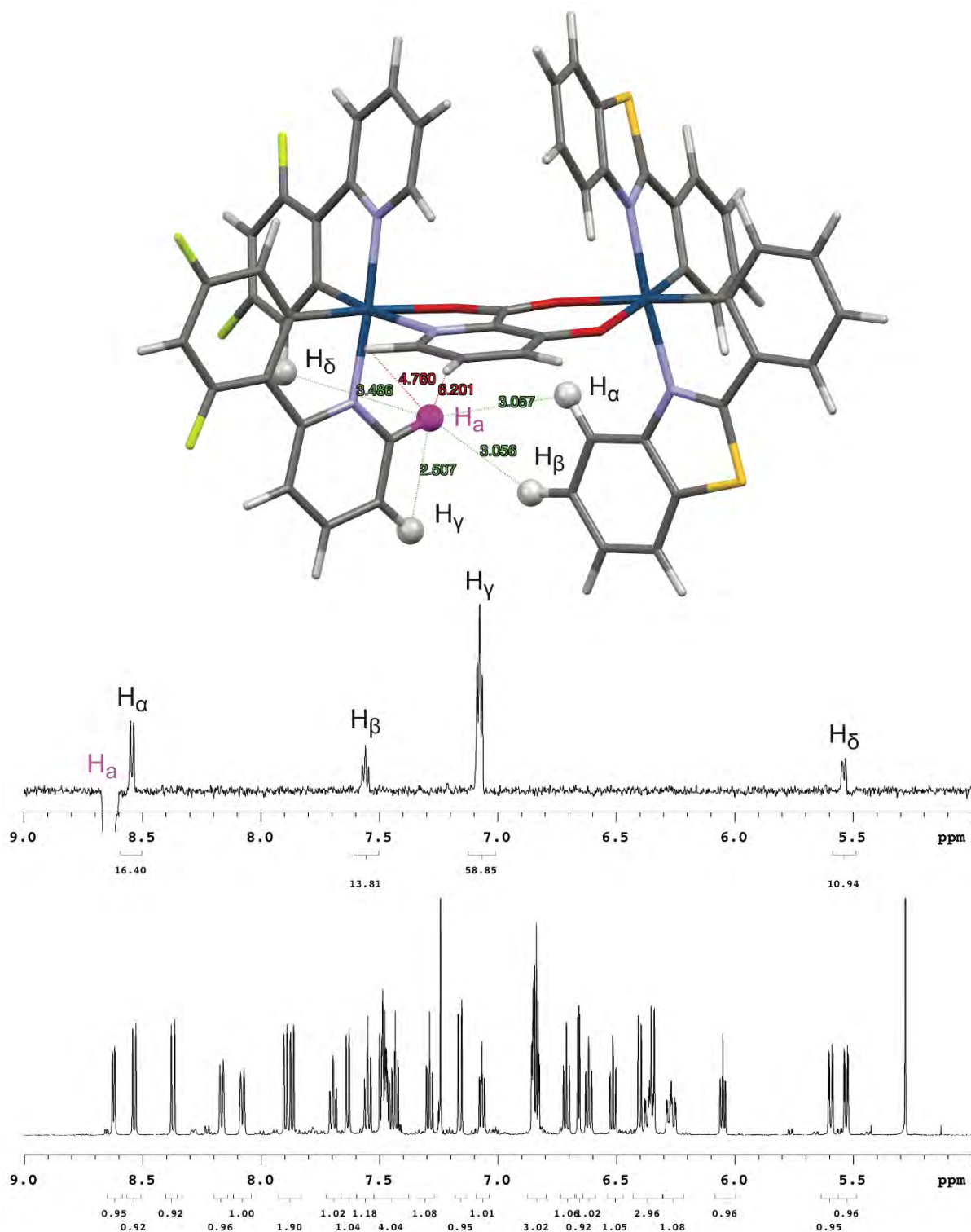


Figure S21. NOE (8.63 ppm) spectrum of complex **BY2**. Pink protons: protons irradiated during the experiment; white protons: nucleus affected by the NOE effect. Visible protons are $< 4 \text{ \AA}$ (green lines), non-visible protons are at $> 4 \text{ \AA}$ (red lines).

Table S2. Comparison between electrochemical data from cyclic voltammetry (Table 1) and square-wave voltammetry in acetonitrile solution + 0.1 M TBAPF₆ at 298 K. All potential values are reported vs. the ferrocene/ferrocenium couple, used as internal reference.

	from square-wave voltammetry		from cyclic voltammetry	
	E_{ox}^a [V]	E_{red}^a [V]	$E_{\text{ox}} (\Delta E_p)^a$ [V (mV)]	$E_{\text{red}} (\Delta E_p)^a$ [V (mV)]
BB1	+ 0.687, + 1.018	- 2.252, - 2.547	+ 0.688 (62), + 1.014 (76)	- 2.250 (69), - 2.535 (150)
BB2	+ 0.687, + 1.016	- 2.260, - 2.551	+ 0.688 (68), + 1.018 (72)	- 2.253 (67), - 2.535 (135)
BY1	+ 0.528, + 0.989	- 2.239, - 2.403, - 2.490	+ 0.526 (65), + 0.985 (98)	- 2.237 (74), - 2.430 (187)
BY2	+ 0.535, + 0.995	- 2.234, - 2.419, - 2.503	+ 0.536 (65), + 0.991 (81)	- 2.230 (73), - 2.458 (179)
YB1				
YB2	+ 0.682, + 0.837	- 2.168, - 2.422, - 2.541	+ 0.684 (66), + 0.836 (66)	- 2.168 (67), - 2.420 (76)
YY	+ 0.504, + 0.809	- 2.219, - 2.318, - 2.540	+ 0.504 (60), + 0.806 (67)	- 2.222 (73), - 2.316 (66)
B	+ 0.953	- 2.125	+ 0.954 (71)	- 2.116 (73)
Y	+ 0.782	- 2.137	+ 0.784 (67)	- 2.132 (77)

Table S3. Electrochemical data of **YB1** and **YB2** from square-wave voltammetry in dichloromethane or acetonitrile solutions + 0.1 M TBAPF₆ at 298 K. All potential values are reported vs. the ferrocene/ferrocenium couple, used as internal reference. All redox processes are reversible.

	E_{ox} [V]	E_{red} [V]
YB1 in DCM	+ 0.629, + 0.841	- 2.295
YB2 in DCM	+ 0.645, + 0.853	- 2.274
YB2 in ACN	+ 0.682, + 0.837	- 2.168, - 2.422, - 2.541

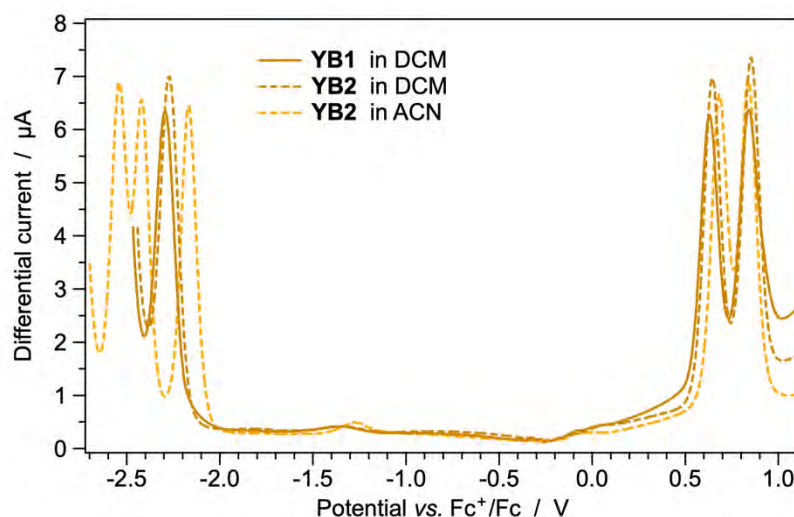


Figure S22. Comparison between the square-wave voltammograms of **YB1** and **YB2** recorded in dichloromethane or acetonitrile solutions at 298 K. The voltammogram of **YB1** in acetonitrile solution is not available due to low solubility. Solvent effects on recorded redox potentials are negligible.

Table S4. Calculated NTOs couples describing the lowest five triplet excitations (below 3.00 eV) for **BB1** in acetonitrile (see Experimental Section for details). The λ value is the natural transition orbital eigenvalue associated with each NTOs couple; orbital isovalue: $0.04 e^{-1/2} \text{ bohr}^{-3/2}$.

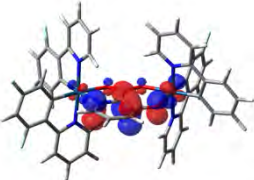
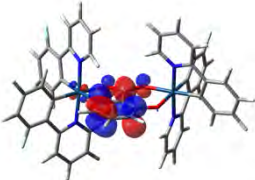
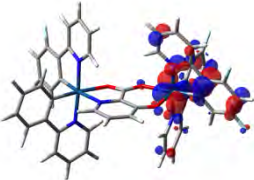
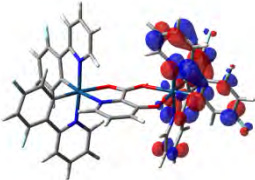
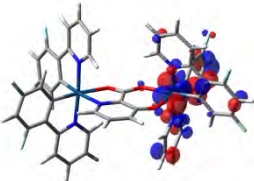
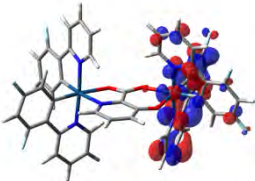
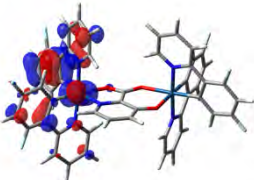
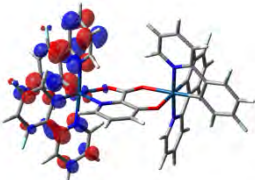
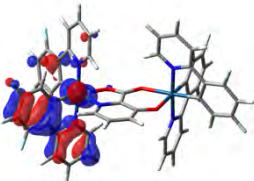
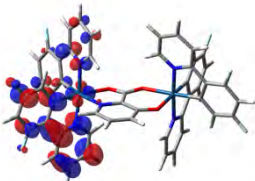
	Transition energy [eV (nm)]	NTO couple hole \rightarrow electron (λ)		Nature
$S_0 \rightarrow T_1$	2.60 (476)			π - π^* transition centered on the bridging ligand
		(99.9%)		
$S_0 \rightarrow T_2$	2.77 (448)			mainly LC on the dfppy ligands of the O \wedge O side
		(75.0%)		
$S_0 \rightarrow T_3$	2.81 (441)			mainly LC on the dfppy ligands of the O \wedge O side
		(68.1%)		
$S_0 \rightarrow T_4$	2.82 (440)			mainly LC on the dfppy ligands of the N \wedge O side
		(70.3%)		
$S_0 \rightarrow T_5$	2.87 (432)			mainly LC on the dfppy ligands of the N \wedge O side
		(59.8%)		

Table S5. Calculated NTOs couples describing the lowest five triplet excitations (below 3.00 eV) for **BB2** in acetonitrile (see Experimental Section for details). The λ value is the natural transition orbital eigenvalue associated with each NTOs couple; orbital isovalue: $0.04 \text{ e}^{-1/2} \text{ bohr}^{-3/2}$.

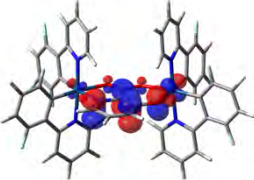
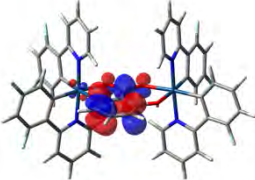
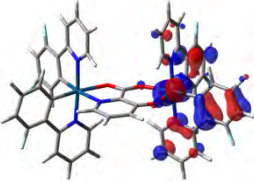
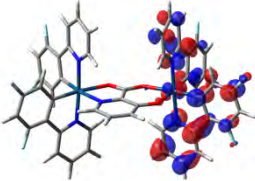
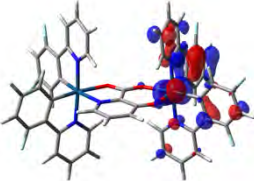
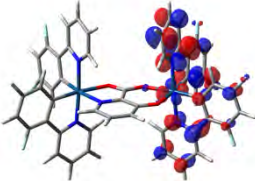
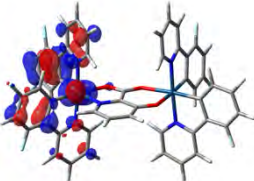
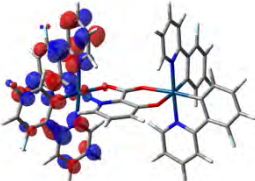
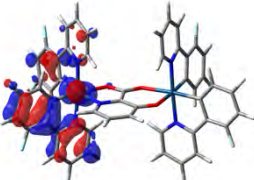
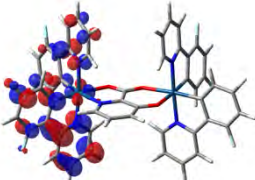
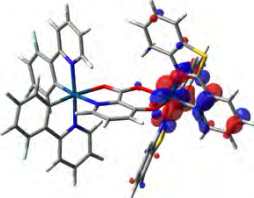
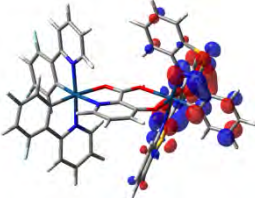
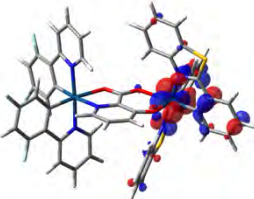
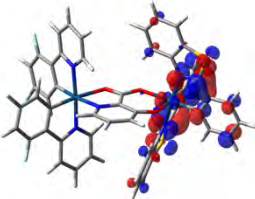
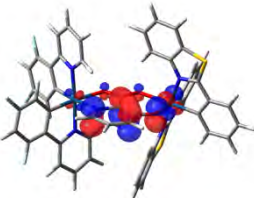
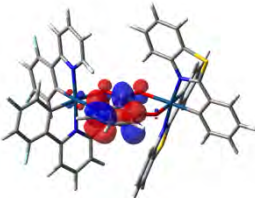
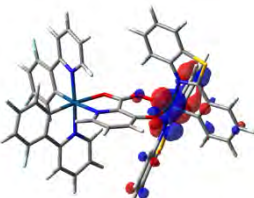
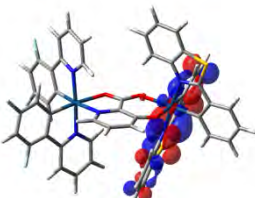
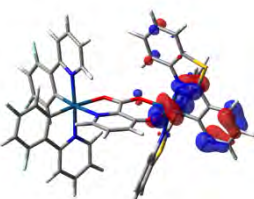
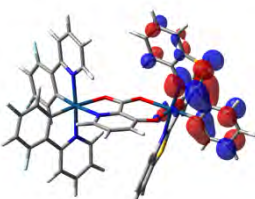
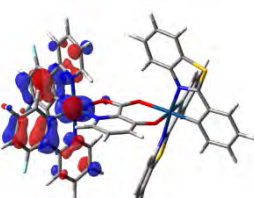
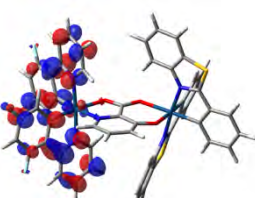
	Transition energy [eV (nm)]	NTO couple		Nature
		hole	electron (λ)	
$S_0 \rightarrow T_1$	2.60 (477)			π - π^* transition centered on the bridging ligand
		(99.9%)		
$S_0 \rightarrow T_2$	2.77 (448)			mainly LC on the dfppy ligands of the O \wedge O side
		(74.6%)		
$S_0 \rightarrow T_3$	2.81 (441)			mainly LC on the dfppy ligands of the O \wedge O side
		(68.4%)		
$S_0 \rightarrow T_4$	2.82 (439)			mainly LC on the dfppy ligands of the N \wedge O side
		(69.2%)		
$S_0 \rightarrow T_5$	2.87 (432)			mainly LC on the dfppy ligands of the N \wedge O side
		(59.0%)		

Table S6. Calculated NTOs couples describing the lowest seven triplet excitations (below 3.00 eV) for **BY1** in acetonitrile (see Experimental Section for details). The λ value is the natural transition orbital eigenvalue associated with each NTOs couple; orbital isovalue: $0.04 e^{-1/2} \text{ bohr}^{-3/2}$.

	Transition energy [eV (nm)]	NTO couple hole \rightarrow electron (λ)		Nature
$S_0 \rightarrow T_1$	2.41 (514)			mainly LC on the pbtz ligands of the O^O side
		(79.6%)		
$S_0 \rightarrow T_2$	2.44 (507)			mainly LC on the pbtz ligands of the O^O side
		(75.3%)		
$S_0 \rightarrow T_3$	2.57 (483)			π - π^* transition centered on the bridging ligand
		(99.5%)		
$S_0 \rightarrow T_4$	2.72 (455)			mainly LC on the pbtz ligands of the O^O side
		(89.8%)		
$S_0 \rightarrow T_5$	2.76 (449)			mainly LC on the pbtz ligands of the O^O side
		(89.9%)		
$S_0 \rightarrow T_6$	2.82 (440)			mainly LC on the dfppy ligands of the N^O side
		(68.7%)		

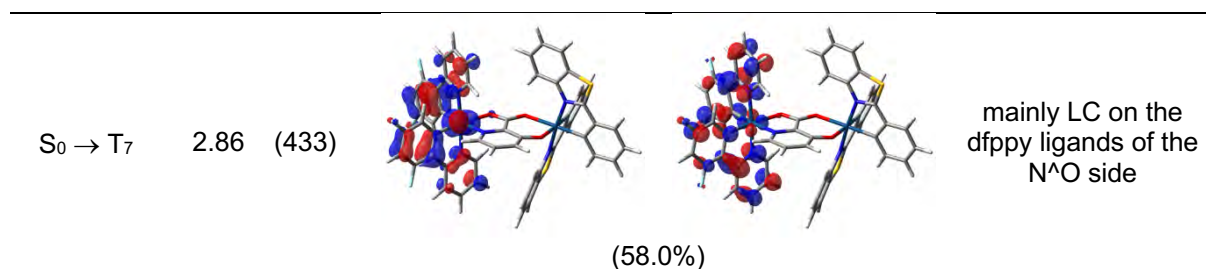
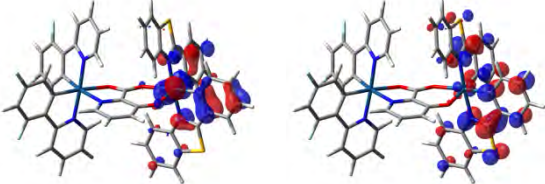
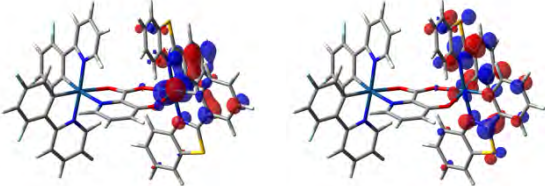
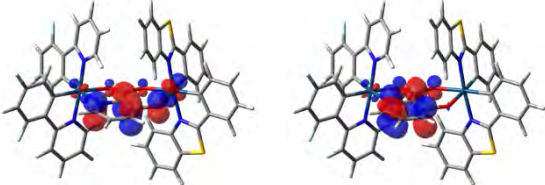
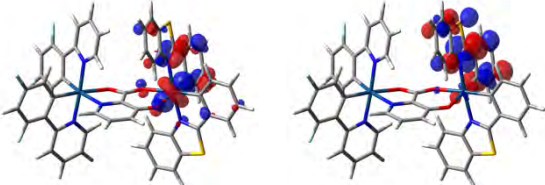


Table S7. Calculated NTOs couples describing the lowest seven triplet excitations (below 3.00 eV) for **BY2** in acetonitrile (see Experimental Section for details). The λ value is the natural transition orbital eigenvalue associated with each NTOs couple; orbital isovalue: $0.04 e^{-1/2} \text{ bohr}^{-3/2}$.

	Transition energy [eV (nm)]	NTO couple		Nature
		hole	→ electron (λ)	
$S_0 \rightarrow T_1$	2.41 (513)		mainly LC on the ptbz ligands of the O^O side	
(79.5%)				
$S_0 \rightarrow T_2$	2.44 (508)		mainly LC on the ptbz ligands of the O^O side	
(77.6%)				
$S_0 \rightarrow T_3$	2.57 (483)		π - π^* transition centered on the bridging ligand	
(99.6%)				
$S_0 \rightarrow T_4$	2.71 (458)		mainly LC on the ptbz ligands of the O^O side	
(88.8%)				

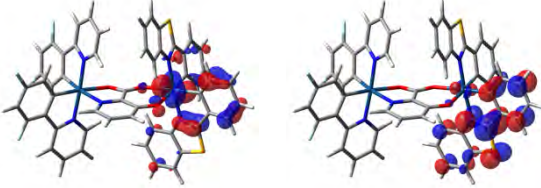
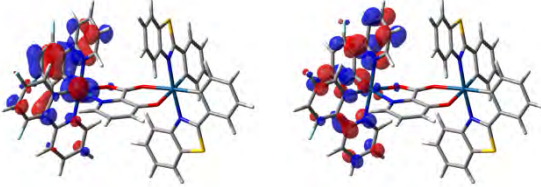
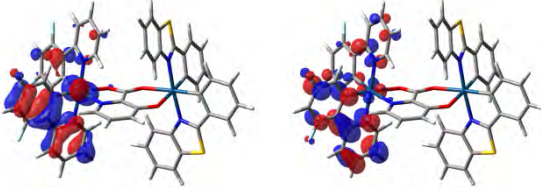
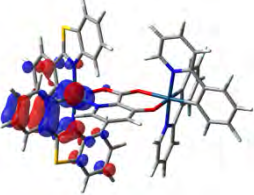
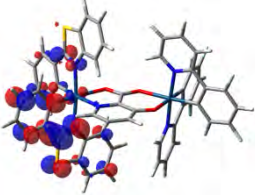
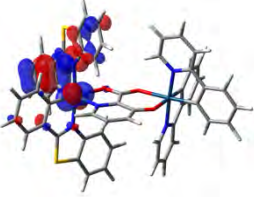
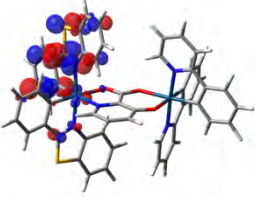
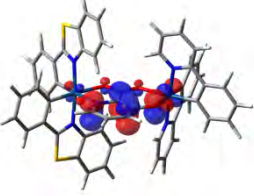
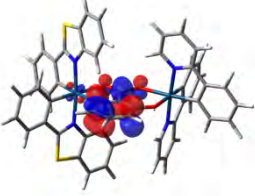
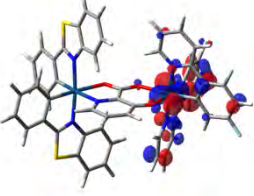
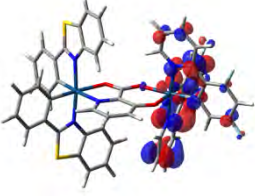
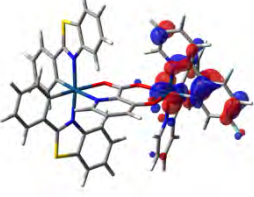
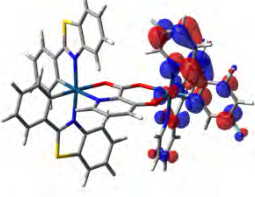
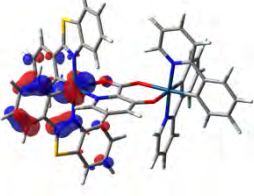
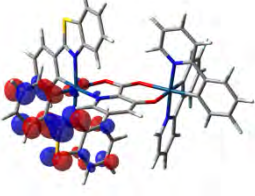
$S_0 \rightarrow T_5$	2.75	(451)		mainly LC on the ptbz ligands of the O [^] O side
(89.2%)				
$S_0 \rightarrow T_6$	2.82	(439)		mainly LC on the dfppy ligands of the N [^] O side
(70.1%)				
$S_0 \rightarrow T_7$	2.87	(432)		mainly LC on the dfppy ligands of the N [^] O side
(60.3%)				

Table S8. Calculated NTOs couples describing the lowest seven triplet excitations (below 3.00 eV) for **YB1** in acetonitrile (see Experimental Section for details). The λ value is the natural transition orbital eigenvalue associated with each NTOs couple; orbital isovalue: $0.04 e^{-1/2} \text{ bohr}^{-3/2}$.

	Transition energy [eV (nm)]	NTO couple hole \rightarrow electron (λ)		Nature
$S_0 \rightarrow T_1$	2.47 (502)			mainly LC on the pbtz ligands of the N ⁺ O side
		(79.3%)		
$S_0 \rightarrow T_2$	2.51 (493)			mainly LC on the pbtz ligands of the N ⁺ O side
		(71.5%)		
$S_0 \rightarrow T_3$	2.60 (477)			π - π^* transition centered on the bridging ligand
		(99.7%)		
$S_0 \rightarrow T_4$	2.76 (449)			mainly LC on the dfppy ligands of the O ⁺ O side
		(75.8%)		
$S_0 \rightarrow T_5$	2.80 (443)			mainly LC on the dfppy ligands of the O ⁺ O side
		(69.8%)		
$S_0 \rightarrow T_6$	2.82 (440)			mainly LC on the pbtz ligands of the N ⁺ O side
		(92.9%)		

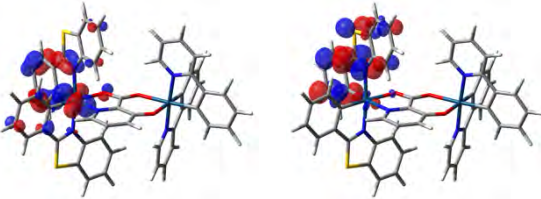
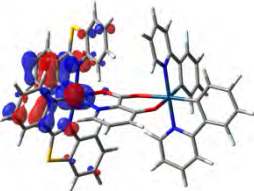
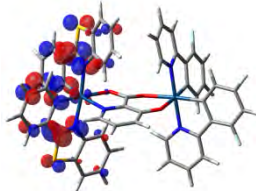
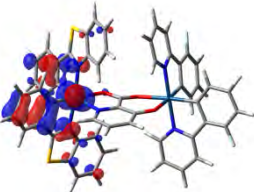
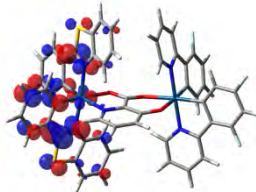
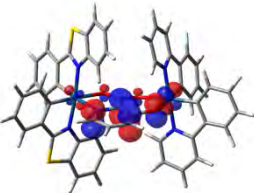
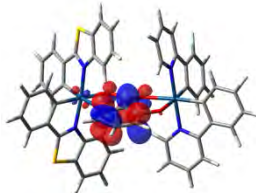
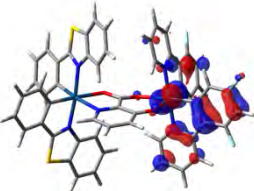
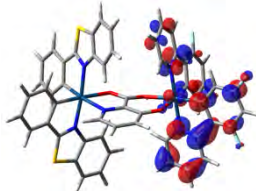
$S_0 \rightarrow T_7$	2.85 (434)		mainly LC on the pbtz ligands of the N^O side
(93.6%)			

Table S9. Calculated NTOs couples describing the lowest seven triplet excitations (below 3.00 eV) for **YB2** in acetonitrile (see Experimental Section for details). The λ value is the natural transition orbital eigenvalue associated with each NTOs couple; orbital isovalue: $0.04 e^{-1/2} \text{ bohr}^{-3/2}$.

	Transition energy [eV (nm)]	NTO couple		Nature
		hole	electron (λ)	
$S_0 \rightarrow T_1$	2.47 (501)			mainly LC on the pbtz ligands of the N^O side
(75.0%)				
$S_0 \rightarrow T_2$	2.51 (494)			mainly LC on the pbtz ligands of the N^O side
(67.4%)				
$S_0 \rightarrow T_3$	2.59 (479)			π - π^* transition centered on the bridging ligand
(99.1%)				
$S_0 \rightarrow T_4$	2.76 (449)			mainly LC on the dfppy ligands of the O^O side
(77.1%)				

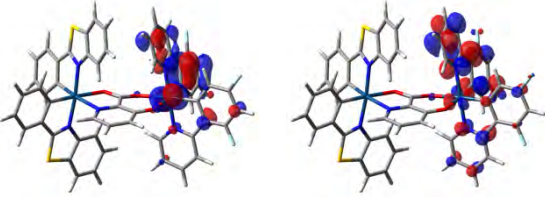
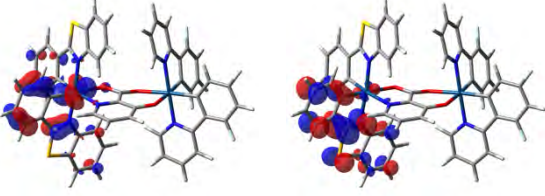
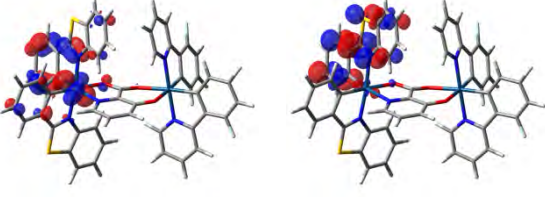
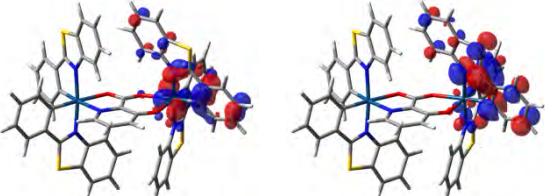
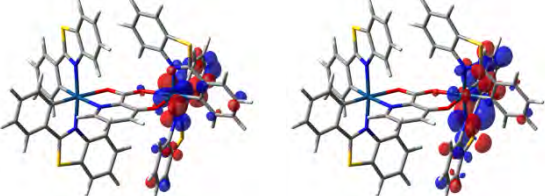
$S_0 \rightarrow T_5$	2.81	(441)		mainly LC on the dfppy ligands of the O [^] O side
(71.1%)				
$S_0 \rightarrow T_6$	2.82	(440)		mainly LC on the pbtz ligands of the N [^] O side
(93.6%)				
$S_0 \rightarrow T_7$	2.83	(438)		mainly LC on the pbtz ligands of the N [^] O side
(94.0%)				

Table S10. Calculated NTOs couples describing the lowest nine triplet excitations (below 3.00 eV) for **YY** in acetonitrile (see Experimental Section for details). The λ value is the natural transition orbital eigenvalue associated with each NTOs couple; orbital isovalue: $0.04 \text{ e}^{-1/2} \text{ bohr}^{-3/2}$.

	Transition energy [eV (nm)]	NTO couple		Nature
		hole	electron (λ)	
$S_0 \rightarrow T_1$	2.41	(513)		mainly LC on the pbtz ligands of the O [^] O side
(80.9%)				
$S_0 \rightarrow T_2$	2.44	(509)		mainly LC on the pbtz ligands of the O [^] O side
(79.6%)				

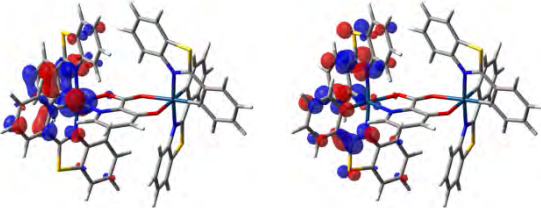
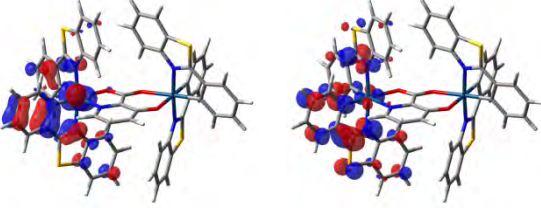
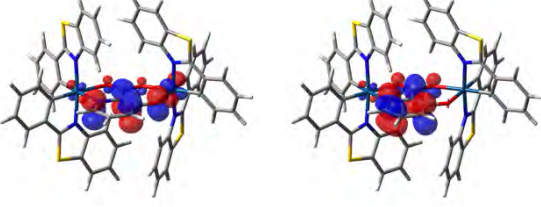
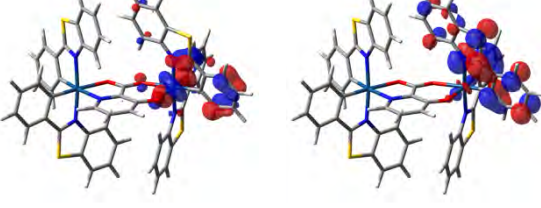
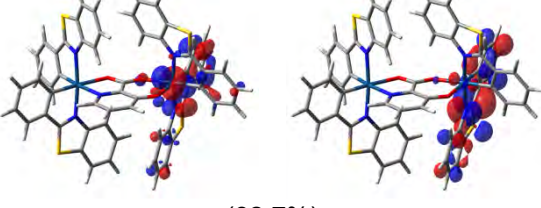
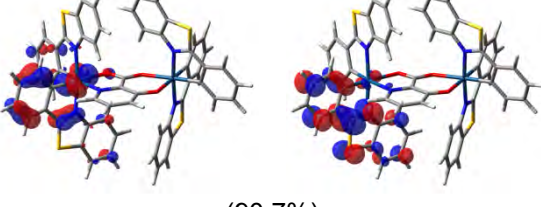
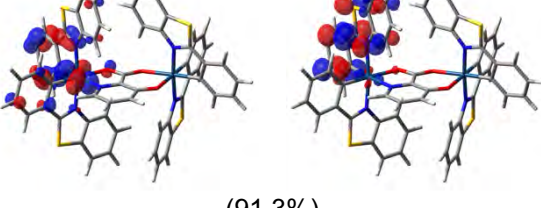
$S_0 \rightarrow T_3$	2.46	(503)		mainly LC on the pbtz ligands of the N ^{^O} side
			(74.6%)	
$S_0 \rightarrow T_4$	2.51	(495)		mainly LC on the pbtz ligands of the N ^{^O} side
			(63.8%)	
$S_0 \rightarrow T_5$	2.57	(483)		π - π^* transition centered on the bridging ligand
			(99.6%)	
$S_0 \rightarrow T_6$	2.72	(457)		mainly LC on the pbtz ligands of the O ^{^O} side
			(83.7%)	
$S_0 \rightarrow T_7$	2.74	(452)		mainly LC on the pbtz ligands of the O ^{^O} side
			(82.7%)	
$S_0 \rightarrow T_8$	2.82	(440)		mainly LC on the pbtz ligands of the N ^{^O} side
			(90.7%)	
$S_0 \rightarrow T_9$	2.84	(437)		mainly LC on the pbtz ligands of the N ^{^O} side
			(91.3%)	

Table S11. Calculated NTOs couples describing the lowest three triplet excitations for **B** in acetonitrile (see Experimental Section for details). The λ value is the natural transition orbital eigenvalue associated with each NTOs couple; orbital isovalue: $0.04 e^{-1/2} \text{ bohr}^{-3/2}$.

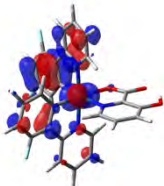
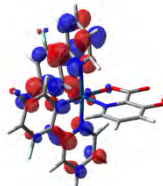
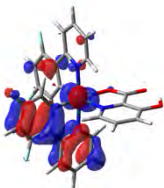
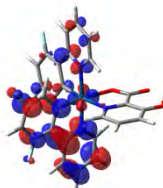
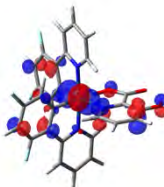
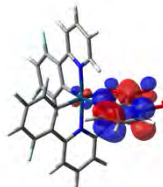

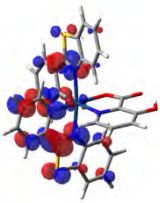
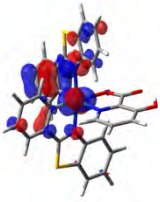
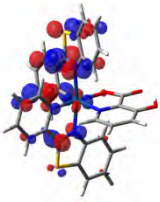

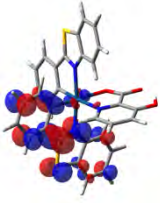
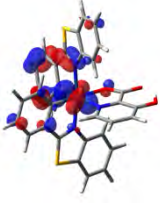
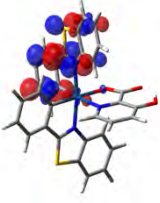
	Transition energy [eV (nm)]	NTO couple hole \rightarrow electron (λ)		Nature
$S_0 \rightarrow T_1$	2.83 (438)			mainly LC on the dfppy ligands
		(68.3%)		
$S_0 \rightarrow T_2$	2.87 (432)			mainly LC on the dfppy ligands
		(59.0%)		
$S_0 \rightarrow T_3$	3.18 (390)			mainly MLCT from the iridium(III) ion to the picolinate ligand
		(96.6%)		

Table S12. Calculated NTOs couples describing the lowest four triplet excitations (below 3.00 eV) for **Y** in acetonitrile (see Experimental Section for details). The λ value is the natural transition orbital eigenvalue associated with each NTOs couple; orbital isovalue: $0.04 \text{ e}^{-1/2} \text{ bohr}^{-3/2}$.

	Transition energy [eV (nm)]	NTO couple hole \rightarrow electron (λ)		Nature
$S_0 \rightarrow T_1$	2.48 (499)			mainly LC on the pbtz ligands
		(73.2%)		
$S_0 \rightarrow T_2$	2.52 (492)			mainly LC on the pbtz ligands
		(64.8%)		
$S_0 \rightarrow T_3$	2.83 (437)			mainly LC on the pbtz ligands
		(94.4%)		
$S_0 \rightarrow T_4$	2.86 (434)			mainly LC on the pbtz ligands
		(94.7%)		

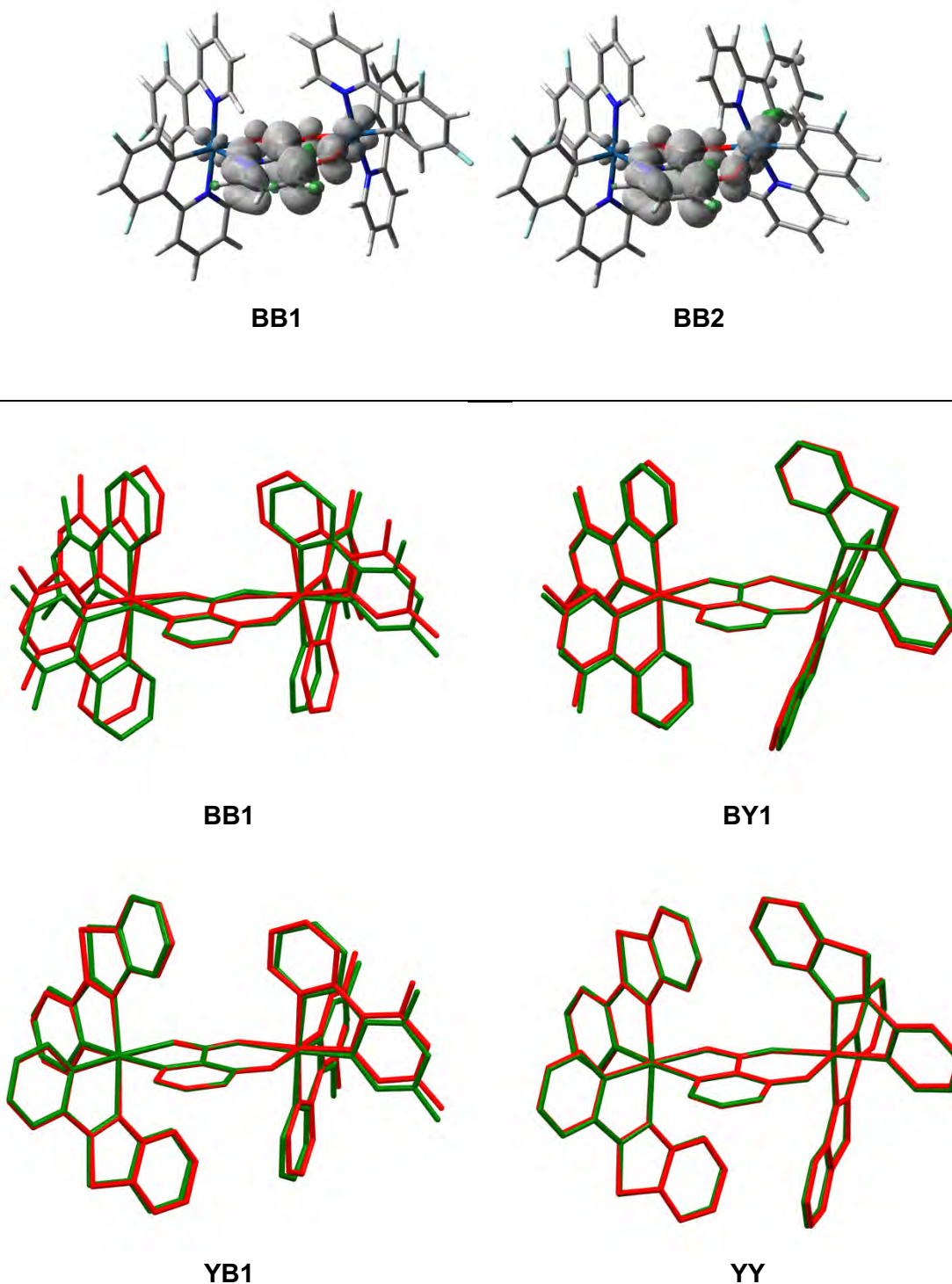


Figure S23. (Top) Unpaired-electron spin-density surfaces of the lowest triplet state (T_1) of **BB1** and **BB2** in their fully-relaxed geometries (isosurfaces: $0.002 \text{ e bohr}^{-3}$); the T_1 is a ^3LC state centred on the bridging ligand, with minor contribution from iridium ions. (Bottom) Structural overlay between the fully-relaxed geometries of the binuclear complexes in their ground state (S_0 , green) and lowest triplet excited state (T_1 , red); the overlays are obtained by maximizing the superposition of the bridge only. It is evident the much lower overlap between S_0 and T_1 geometries in the case of **BB1**, if compared to all other complexes.

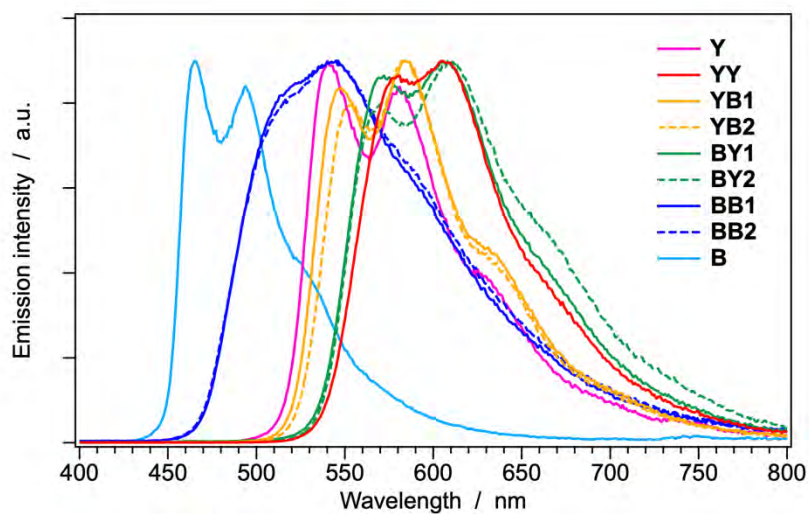


Figure S24. Normalized emission spectra of the binuclear complexes in 1% PMMA matrix at 298 K, together with their reference compounds **B** and **Y**.

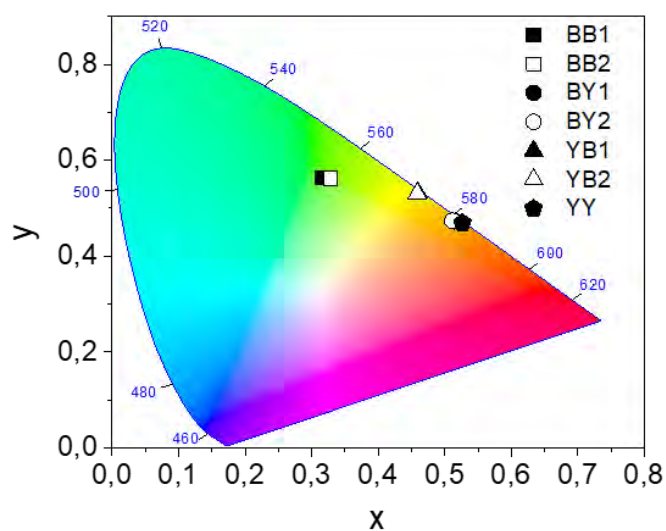


Figure S25. Commission Internationale de L'Eclairage (CIE) coordinates of OLEDs based on the binuclear iridium(III) complexes.

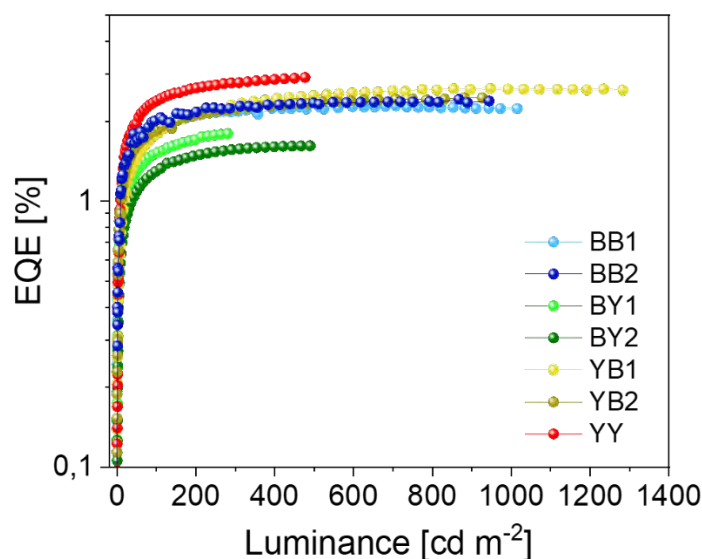


Figure S26. External quantum efficiency (EQE) as a function of the luminance of OLEDs based on binuclear complexes.

References

- 1 F. O. Garces, K. A. King and R. J. Watts, *Inorg. Chem.*, 2002, **27**, 3464-3471.
- 2 Y. J. Cho, K. R. Wee, H. J. Son, D. W. Cho and S. O. Kang, *Phys. Chem. Chem. Phys.*, 2014, **16**, 4510-4521.
- 3 M. J. Frisch, G. W. Trucks, H. B. Schlegel, G. E. Scuseria, M. A. Robb, J. R. Cheeseman, G. Scalmani, V. Barone, G. A. Petersson, H. Nakatsuji, X. Li, M. Caricato, A. V. Marenich, J. Bloino, B. G. Janesko, R. Gomperts, B. Mennucci, H. P. Hratchian, J. V. Ortiz, A. F. Izmaylov, J. L. Sonnenberg, Williams, F. Ding, F. Lipparini, F. Egidi, J. Goings, B. Peng, A. Petrone, T. Henderson, D. Ranasinghe, V. G. Zakrzewski, J. Gao, N. Rega, G. Zheng, W. Liang, M. Hada, M. Ehara, K. Toyota, R. Fukuda, J. Hasegawa, M. Ishida, T. Nakajima, Y. Honda, O. Kitao, H. Nakai, T. Vreven, K. Throssell, J. A. Montgomery Jr., J. E. Peralta, F. Ogliaro, M. J. Bearpark, J. J. Heyd, E. N. Brothers, K. N. Kudin, V. N. Staroverov, T. A. Keith, R. Kobayashi, J. Normand, K. Raghavachari, A. P. Rendell, J. C. Burant, S. S. Iyengar, J. Tomasi, M. Cossi, J. M. Millam, M. Klene, C. Adamo, R. Cammi, J. W. Ochterski, R. L. Martin, K. Morokuma, O. Farkas, J. B. Foresman and D. J. Fox, *Gaussian 16, Rev. B.01*, (2016) Gaussian Inc., Wallingford, CT, USA.
- 4 Y. Zhao and D. G. Truhlar, *Theor. Chem. Acc.*, 2008, **120**, 215-241.
- 5 Y. Zhao and D. G. Truhlar, *Acc. Chem. Res.*, 2008, **41**, 157-167.
- 6 D. Figgen, K. A. Peterson, M. Dolg and H. Stoll, *J. Chem. Phys.*, 2009, **130**, 164108.
- 7 G. A. Petersson, A. Bennett, T. G. Tensfeldt, M. A. Al-Laham, W. A. Shirley and J. Mantzaris, *J. Chem. Phys.*, 1988, **89**, 2193-2218.
- 8 G. A. Petersson and M. A. Al-Laham, *J. Chem. Phys.*, 1991, **94**, 6081-6090.
- 9 J. Tomasi and M. Persico, *Chem. Rev.*, 1994, **94**, 2027-2094.
- 10 J. Tomasi, B. Mennucci and R. Cammi, *Chem. Rev.*, 2005, **105**, 2999-3093.
- 11 C. J. Cramer and D. G. Truhlar, "Continuum Solvation Models", in *Solvent Effects and Chemical Reactivity*, eds. O. Tapia and J. Bertrán, Springer Netherlands, 2002, vol. 17, pp. 1-80.
- 12 C. Adamo and D. Jacquemin, *Chem. Soc. Rev.*, 2013, **42**, 845-856.
- 13 A. D. Laurent, C. Adamo and D. Jacquemin, *Phys. Chem. Chem. Phys.*, 2014, **16**, 14334-14356.
- 14 R. L. Martin, *J. Chem. Phys.*, 2003, **118**, 4775-4777.
- 15 R. Jain, T. Bally and P. R. Rablen, *J. Org. Chem.*, 2009, **74**, 4017-4023.

- 16 R. Dennington, T. A. Keith and J. M. Millam, *GaussView, Version 6*, (2016) Semichem Inc., Shawnee Mission, KS, USA.
- 17 G. A. Crosby and J. N. Demas, *J. Phys. Chem.*, 1971, **75**, 991-1024.
- 18 S. R. Meech and D. Phillips, *J. Photochem.*, 1983, **23**, 193-217.
- 19 C. Wurth, M. Grabolle, J. Pauli, M. Spieles and U. Resch-Genger, *Nat. Protoc.*, 2013, **8**, 1535-1550.